

**JOINT FRICTION ESTIMATION AND SLIP PREDICTION OF BIPED  
WALKING ROBOTS**

By

IYAD F.I. HASHLAMON

Submitted to the Graduate School of Engineering and Natural Sciences  
in partial fulfillment of the requirements for the degree of  
Doctor of Philosophy

Sabanci University

July 2014

**JOINT FRICTION ESTIMATION AND SLIP PREDICTION OF BIPED  
WALKING ROBOTS**

APPROVED BY:

Assoc. Prof. Dr. Kemalettin Erbatur (Thesis Advisor) .....



Prof. Dr. Mustafa Ünel



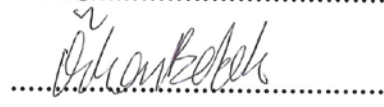
Assoc. Prof. Dr. Ahmet Onat



Assoc. Prof. Dr. Albert Levi



Assist. Prof. Dr. Özkan Bebek



DATE OF APPROVAL: 14/07/2014

© IYAD F.I. HASHLAMON

2014

All Rights Reserved

أهدئها لابئ، امئ، زوجئ وابئئ

*To my parents, wife and daughter*

## ACKNOWLEDGMENTS

My sincere appreciation and heartily thankfulness to my advisor, Kemalettin Erbatur, for his encouragement, guidance and support from the formative stages to the final level of this work. I owe him an immense debt of gratitude for his kindness, patience, and insight throughout the research.

It is an honor for me to thank my jury members Professors Mustafa Unel, Ahmet Onat, Albert Levi, and Özkan Bebek for their valuable comments.

I owe my deepest gratitude to my parents because of their love, encouragement and advice. My sincere love and thanks go to my wife whose without her encouragement and understanding this work has not been possible.

I am in debt to the team members, Mehmet Mert Gülhan, Omer Kemal Adak and Orhan Ayit for their team spirit work, help, and kindness.

My friends Yasser El-Kahlout and Basel Elthalathiny deserve special thanks for their support and encouragement when I needed them. Thanks also go to my friends Belal Amro, Ahmed Abdalal, Islam Khalil, Ahmad Al-gharib, Mus'ab Habib Husaini and Amer Fayeze, for their help and support by making my life easier and joyful. I would like to also thank my colleagues in the Mechatronics laboratory for their nice neighborhood, help and sharing the workplace.

Lastly, I offer my regards and blessings to all of those who supported me in any respect during the completion of my thesis.

# JOINT FRICTION ESTIMATION AND SLIP PREDICTION OF BIPED WALKING ROBOTS

Iyad F.I. Hashlamon

ME PhD Thesis, 2014

Thesis Supervisor Assoc. Prof. Dr. Kemalettin ERBATUR

Keywords: Friction estimation, biped, linear inverted pendulum and slip prediction.

## Abstract

Friction is a nonlinear and complex phenomenon. It is unwanted at the biped joints since it deteriorates the robot's walking performance in terms of speed and dynamic behavior. On the other hand, it is desired and required between the biped feet and the walking surface to facilitate locomotion. Further, friction forces between the feet and the ground determine the maximum acceleration and deceleration that the robot can afford without foot slip. Although several friction models are developed, there is no exact model that represents the friction behavior. This is why online friction estimation and compensation enter the picture. However, when online model-free estimation is difficult, a model-based method of online identification can prove useful.

This thesis proposes a new approach for the joint friction estimation and slip prediction of walking biped robots.

The joint friction estimation approach is based on the combination of a measurement-based strategy and a model-based method. The former is used to estimate the joint friction online when the foot is in contact with the ground, it utilizes the force and acceleration measurements in a reduced dynamical model of the biped. The latter adopts a friction model to represent the joint friction when the leg is swinging. The model parameters are identified adaptively using the estimated online friction whenever the foot is in contact. Then the estimated joint friction contributes to joint torque control signals to improve the control performance.

The slip prediction is a model-free friction-behavior-inspired approach. A measurement-based online algorithm is designed to estimate the Coulomb friction which is regarded as a slip threshold. To predict the slip, a safety margin is introduced in the negative vicinity of the estimated Coulomb friction. The estimation algorithm concludes that if the applied force is outside the safety margin, then the foot tends to slip.

The proposed estimation approaches are validated by experiments on SURALP (Sabanci University Robotics Research Laboratory Platform) and simulations on its model. The results demonstrate the effectiveness of these methods.

# İki Bacaklı Yürüyen Robotlar için Eklem Sürtünmesi ve Ayak Kayma Tahmini

Iyad F.I. Hashlamon

ME Doktora Tezi, 2014

Tez Danışmanı Doç. Dr. Kemalettin ERBATUR

## Özet

Sürtünme doğrusal olmayan ve oldukça karmaşık bir olgudur. İnsansı robotun eklemlerindeki sürtünme, robotun yürüme performansını hız ve dinamik davranış bakımından olumsuz etkilemektedir. Bu sebepten dolayı robot eklemlerindeki sürtünme istenmeyen bir durumdur. Diğer yandan robotun ayakları ile robotun üzerinde bulunduğu yüzey arasındaki sürtünme, hareketin gerçekleşebilmesi için gerekli olan ve istenilen bir durumdur. Robotun kaymadan hareket edebilmesi için gerekli olan azami hızlanma ve yavaşlama, bu sürtünme kuvveti ile belirlenir. Günümüzde bir çok sürtünme modeli geliştirilmiş olsa da, gerçek sürtünme özelliklerine tamamen sahip olan bir sürtünme modeli henüz yoktur. Bu eksiklik çevrimiçi sürtünme tahminini ve telafisinin önemini arttırmaktadır. Ancak çevrimiçi serbest model tahmini zor olsa da, online model tabanlı tanımlama yöntemleri oldukça kullanışlı olabilirler.

Bu tez, eklem sürtünmesi tahmini ve insansı robotların kayma öngörüsü üzerine yeni bir yaklaşım sunmaktadır.

Eklem sürtünmesi tahmini yaklaşımı, model tabanlı yöntem ve ölçme tabanlı stratejinin birleşimleri baz alınarak oluşturulmuştur. İlki ayak yerle temas ettiği anda eklem sürtünmesini çevrimiçi tahmin etmek için kullanılmaktadır. Biped'in küçültülmüş dinamik modelindeki yük(kuvvet) ve ivme ölçümlerini kullanmaktadır. İkincisi ayak sallanırken eklem sürtünmesini temsil etmek için bir sürtünme modeli adopte etmektedir. Robotun ayağı yerle temas ettiği anda, çevrimiçi sürtünme tahminleri yardımıyla, model parametreleri uyarlamalı olarak tanımlanmaktadır. Tanımlama işlemi sonrasında eklem sürtünmesi tahmini, eklem tork kontrol sinyaline, kontrol performansını iyileştirmek için katkıda bulunmaktadır.

Kayma öngörüsü model bazsız sürtünme davranış güdümlü bir yaklaşımdır. Ölçme tabanlı çevrimiçi algoritma, kayma eşiği olarak kabul edilen Coulomb sürtünmesini tahmin etmek için tasarlanmıştır. Kaymayı öngörmek için, güvenlik payı tahmin edilen Coulomb sürtünmesinin negatif çevresinde tanımlanmıştır. Tahmin algoritması, uygulanan kuvvetin güvenlik payının dışında olması durumunda ayağın kayma eğilimi göstereceği sonucuna varmaktadır.



Tezde sunulmuş olan tahmin yaklaşımların, SURALP (Sabancı Üniversitesi Robotik Araştırma Laboratuvarı Platformu) üzerinde yapılan deneyler ve modeli üzerinde yapılan benzetimler ile doğruluğu onaylanmıştır. Sonuçlar, kullanılan metodların geçerliliğini kanıtlamaktadır.

## TABLE OF CONTENTS

1	Introduction .....	1
1.1	Motivation .....	2
1.2	Related work .....	4
1.3	Problem definition.....	7
1.4	The proposed method .....	8
1.5	Contribution .....	10
1.6	Publications .....	11
1.7	Thesis organization .....	12
2	Preliminaries .....	13
2.1	Friction .....	13
2.1.1	Friction behavior.....	14
2.1.2	Friction models .....	15
2.2	The least squares algorithm.....	17
2.3	Integration by parts .....	19
2.4	Kalman filter .....	19
2.5	Adaptive Kalman filter.....	22
2.6	Base attitude estimation .....	24
3	Linear Inverted Pendulum Model for State Estimation.....	26
3.1	LIPM dynamics.....	27

3.2	Estimation of CoM variables .....	29
3.2.1	Form 1 .....	29
3.2.2	Form 2.....	31
3.3	The error in the $\mathbf{p}_{ZMP}$ .....	33
3.4	Results.....	34
3.4.1	Uncertain acceleration measurements due to position uncertainty (experiments).....	37
3.4.2	Uncertain acceleration measurement due to external acceleration (simulation) 41	
3.4.3	Uncertain $\mathbf{p}_{ZMP}^{F_N}$ measurements (simulation).....	42
3.4.4	Correct measurements.....	44
3.5	Conclusion.....	44
4	Joint Friction Estimation for Walking Biped.....	46
4.1	Biped dynamical model.....	47
4.2	Joint friction estimation.....	49
4.2.1	Non- slipping foot constraint .....	50
4.2.2	Reduced filtered dynamical model .....	54
4.3	Friction model parameter identification.....	57
4.4	Simulation Results .....	57
4.4.1	Walking trajectory .....	57
4.4.2	Joint friction generation in simulations .....	58
4.4.3	Joint friction estimation .....	60
4.4.4	Joint friction compensation approach .....	64
4.5	Conclusion.....	68
5	Novel Method for Slip Prediction of Walking Biped Robots .....	69

5.1	Slip definition and detection .....	70
5.1.1	Measured friction force.....	72
5.1.2	Measured foot acceleration.....	75
5.1.3	Measured friction and tangential forces.....	76
5.2	Slip prediction .....	76
5.2.1	Slip prediction approach .....	77
5.2.2	Slip prediction threshold estimation .....	78
5.3	Experimental results.....	80
5.4	Conclusion.....	84
6	Conclusion and Future work .....	85
7	References .....	88

## LIST OF FIGURES

Figure 2.1: (a) Object free body diagram (the object weight is in the normal force), (b) Friction force behavior, and (c) the friction cone. ....	14
Figure 2.2: Friction components .....	16
Figure 2.3: Attitude estimation approach .....	25
Figure 3.1: LIPM .....	27
Figure 3.2: Base frame offset, $O_b$ is the body base frame origin. ....	29
Figure 3.3: SURALP.....	35
Figure 3.4: The kinematic arrangement of SURALP .....	35
Figure 3.5: CoM position in the $x$ – direction .....	37
Figure 3.6: (a) Position error in the $x$ – direction from both forms. and (b) position RMSE in the $x$ – direction from both forms.....	38
Figure 3.7: Estimated CoM velocity in $x$ – direction .....	39
Figure 3.8: CoM position in the $y$ – direction .....	39
Figure 3.9: (a) Position error in the $y$ – direction from both forms. and (b) position RMSE in the $y$ – direction from both forms.....	40
Figure 3.10: Estimated CoM velocity in $y$ – direction .....	40
Figure 3.11: Error estimation with $\Delta\ddot{c}_x = 0.5$ .....	41
Figure 3.12: (a) Estimated velocity in $x$ – direction and (b) the corresponding RMSE.....	42
Figure 3.13: Error estimation with $x_{offset} = 0.035$ .....	43
Figure 3.14: RMSE in both directions for both forms .....	43
Figure 3.15: Estimation error.....	44
Figure 4.1. Coordinate systems. $O_w$ and $O_b$ stand for the origins of the world and body coordinate frames, respectively. The feet coordinate frames are fixed to the feet soles [8].	47

Figure 4.2: Foot walking trajectories, DS stands for the double support phase, LS stands for the left leg single support phase, and RS stands for the right leg single support phase..	58
Figure 4.3: The true generated friction for the left leg joints .....	59
Figure 4.4: The estimated friction (solid blue line) and the true generated friction (dashed red line) for the left leg joints .....	62
Figure 4.5: The estimated friction (solid blue line) and the true generated friction (dashed red line) for the left leg joints .....	64
Figure 4.6: First control structure: Friction compensation using the proposed FBSE (Foot base sensor estimation) method .....	65
Figure 4.7: First control structure response. (a) CoM trajectory in the $x$ – direction $c_x$ , (b) RSE in $c_x$ , (c) CoM trajectory in the $y$ –direction $c_y$ , and (d) RSE in $c_y$ .....	66
Figure 4.8: Second control structure: Friction compensation using the proposed FBSE method .....	67
Figure 4.9: Second control structure response. (a) CoM trajectory in the $x$ – direction $c_x$ , (b) RSE in $c_x$ , (c) CoM trajectory in the $y$ –direction $c_y$ , and (d) RSE in $c_y$ .....	67
Figure 5.1: Slip force conditions.....	71
Figure 5.2: Static and kinetic friction .....	77
Figure 5.3: Slip prediction regions .....	78
Figure 5.4: Friction parameter update in the $x$ – direction .....	81
Figure 5.5: Slip prediction test in the $x$ – direction .....	83

## List of TABLES

Table 3.1: Experimental and simulation parameters values and the initializations of AKF 35	
Table 4.1: True Friction model parameters for each joint of the leg .....	59
Table 4.2: Filter constants.....	63
Table 4: A statistical summary of Figure 5.5.....	83

## Nomenclature

Symbol	Description
IMU	Inertial measurement unit
$ZMP$	Zero Moment Point
$\mathbf{p}_{ZMP}$	Zero Moment Point
$\mathbf{p}_{ZMP}^{F_N}$	Calculated Zero Moment Point using normal reaction forces.
LIPM	Linear inverted pendulum model
BSC	Base sensor control
DO	Disturbance observer
NN	Neural networks
DS	Double support phase
SS	Single support phase
LS	Left single support
RS	Right single support
FBSE	Foot base sensor estimation
$F_f$	Friction force
$F_{f_x}$	Friction force in $x$ – direction
$F_{f_y}$	Friction force $y$ – direction
$F_{slip_y}$	Slip force $y$ – direction
$F_{slip_x}$	Slip force $y$ – direction

$\mathbf{F}_{slip}$	Slip force vector
$F_t$	Tangential force
$F_{t_x}$	Tangential force in $x$ – direction
$F_{t_y}$	Tangential force in $y$ – direction
$F_{t_{max}}$	Maximum tangential force
$F_N$	Normal reaction force
$F_s$	Maximum static friction force
$F_{fs}$	Static friction force
$F_{fd}$	Kinetic friction force
$\mu_{static}$	Coefficient of static friction
$\mu_d$	Coefficient of coulomb friction
$\mu_c$	Coefficient of kinetic friction
$F_c$	Coulomb friction
$F_{st}$	Stribeck friction
$F_v$	Viscous friction
$\bar{F}_v$	Viscous friction coefficient
$\dot{\theta}$	Angular speed
$\gamma_i, i = 1, \dots, 6$	Positive constants
$w$	Process noise
$v$	Measurement noise
$A$	State matrix
$B$	Input matrix
$u$	Input
$C$	Output matrix
$Q$	Process noise covariance
$R$	measurement noise covariance
$x$	States vector
$(\cdot)^-$	Prior estimates
$(\hat{\cdot})$	posterior estimates
KF	Kalman filter
AKF	Adaptive Kalman filter
EKF	Extended Kalman filter
$I$	Identity matrix
$O_I$	IMU frame



$O_w$	World frame
$O_b$	Base frame
$A_b^w$	Attitude of $O_b$ with respect to $O_w$
$\mathbf{A}_b$	Base attitude in $O_w$
CoM	Center of mass
$\mathbf{c}$	Center of mass position
$\dot{\mathbf{c}}$	Center of mass velocity
$\dot{\mathbf{c}}_{filtered}$	Filtered version of the CoM velocity
$\ddot{\mathbf{c}}$	Center of mass acceleration
$\Delta\ddot{\mathbf{c}}$	Center of mass acceleration error
$RMSE$	Root mean square error
$\rho$	The foot $\mathbf{p}_{ZMP}$
${}^L(\quad), or(\quad)_L$	The specified variable for the left leg or foot
${}^R(\quad), or(\quad)_R$	The specified variable for the right leg or foot
$g$	Constant gravity acceleration
$z_c$	Constant height of CoM
$\mathbf{c}_{offset}$	Error modeling in CoM position
$r_I$	IMU position
$T$	Sampling time
$\boldsymbol{\omega}_b$	Base frame angular velocity vector
$\dot{\mathbf{v}}_I$	IMU acceleration
$\dot{\boldsymbol{\omega}}_b$	Base frame angular acceleration vector
$\mathbf{p}_b$	Base frame position
$\mathbf{v}_b$	Base frame velocity
$\ddot{\mathbf{p}}$	foot frame acceleration
$\mathbf{p}_{ZMP}^{err}$	The error in Zero Moment Point
$x_{offset}$	Modeling error in the $x$ – direction
$\boldsymbol{\theta}$	Joint angles
$\boldsymbol{\omega}$	Joint angular velocity
$\mathbf{f}_b$	Force vector generated at the base link
$\mathbf{n}_b$	Torque vector generated at the base link
$\mathbf{u}_{E_1}$	Net force effect of the reaction forces on the base
$\mathbf{u}_{E_2}$	Net torque effect of the reaction forces on the base
$\mathbf{u}_F$	Joint friction forces vector

$\mathbf{b}$	Bias term
$\boldsymbol{\tau}$	Joint torque control
$\boldsymbol{\tau}^l$	link torque
$\mathbf{J}$	Jacobian
$\mathbf{F}_E$	Reaction force vector
$\bar{\mathbf{F}}_E$	Computed reaction force vector
$K_{slip}, \lambda_{slip}$	Slip estimation filter constants
$K, \sigma$	Filter constants
$\langle \eta \rangle_\lambda$	Filtered version of $\eta$ using filter $\lambda$
$k_p$	Proportional gain
$k_d$	Derivative gain
$\boldsymbol{\theta}^{ref}$	Reference angle
$\mathbf{c}^{des}$	Desired CoM position
$\boldsymbol{\tau}_{pos}$	Position control
$\boldsymbol{\tau}_{tor}$	Torque control
$m_f$	Foot mass
$F_{ms}$	Margin of safety force
$F_{suf}$	Sufficient force

---

## Chapter 1

### 1 Introduction

The interest in biped walking robots has been increased dramatically in the last three decades. The bipeds can operate in human environment [1], human assisting applications [2] and they are helpful to replace the humans in the hazardous environments [3]. Apart from its superior characteristics in obstacle avoidance and dexterity, the biped has many coupled degrees of freedom to be controlled. Further, the structure exhibits a highly nonlinear and complex to be stabilized dynamics.

An extensive research is going on about biped robots walking. Research focuses on adaptive, efficient, and robust walking [4-10, 11 ].

The mechanical structure of the biped makes the control challenge harder. In general, the structure contains transmissions or drive mechanisms to transfer the power from the actuator to the robot link through the joint [12]. Therefore friction is observed at the joints. Friction has a considerable effect on the robot behavior. It may deteriorate the robot walking performance. Typical consequences of joint friction are steady state errors, limit cycles and poor dynamic response [13-15]. Therefore, joint friction compensation received a considerable interest [16, 17].

Balance preserving of the biped robot while walking is a complicated task. It is highly desirable for the robot to adapt to the ground conditions. A walking pattern resulting in a stable gait is required. Generally, the biped walking depends on generated stable trajectories. The linear inverted pendulum model LIPM is widely used for walking trajectory generation [18]. As a stability criterion, the Zero Moment Point *ZMP* stability

criterion [19, 20 ] is widely employed. However, the foot contact with the environment poses a critical problem. The balance and locomotion ability of the biped walker is constrained by the friction forces between the foot and the contact surface [21]. If the forces or torques applied by the robot legs exceed certain thresholds, then the biped might lose its stability [22].

The friction is a complex phenomenon under research. Researchers work on mathematical models that can describe this behavior [23]. Although static and dynamic models are obtained, there is no exact model that represents the friction behavior. This poses a challenge for the friction estimation and compensation. Therefore, online model-free friction estimation based on measurements has certain virtues. It avoids the friction modeling problems by using some measurements [24, 25]. However, this approach is not always applicable.

## 1.1 Motivation

Friction forces are undesired in some applications while desired and required in other applications. Joint friction is undesired. While the friction force between the biped foot and the contact surface is required so that the robot can walk.

Joint friction is an unwanted phenomenon. It has undesirable effects on the system response which may deteriorate the biped robot performance. Joint friction becomes more significant when power transmission modules are used to transfer the actuator power to the joint. More precisely, when the transmission modules are Harmonic drive reduction gears with high reduction ratios. In this thesis, the actuation mechanisms of the considered biped are constructed with DC motors, belt -pulley system and Harmonic drive reduction gears with reduction ratios ranging between 100 and 160, depending on the joint of the leg [26].

Minimizing the effects of the joint friction through friction compensation requires information about the friction. For bipeds, a few studies are reported and can be categorized into three approaches. One approach uses friction models with offline identified parameters to compensate for the friction [27-30]. Another approach considers the friction as a

disturbance among other disturbances [31]. Or generally the joint friction is neglected [32-35].

Contrary to the joint friction, foot-ground friction is a useful phenomenon that facilitates walking. Even when stable walking trajectories (for example, once that satisfy the *ZMP* stability criterion) are employed, the robot may tend to tip over in real life. This is because of the environmental uncertainty and change. Among the parameters that affect the stable walking are the contact parameters between the robot feet and the ground. Friction forces have a significant role. They determine the maximum acceleration and deceleration that the robot can achieve, and hence the maximum forces allowed to be applied to the robot without foot slipping. By estimating the walking surface friction parameters, the biped walking can adapt its motion so that it preserves its stability.

Researchers conducted experiments on walking on arbitrary surfaces, and with arbitrary coefficients of friction. In mass of the studies, the coefficient of friction is considered to be known. In real life, however, the coefficient of friction is unknown or is only inaccurately known. Assuming a too high value of the coefficient of friction may lead to foot slipping. On the other hand, low value constrains the motion conservatively.

Therefore, this thesis is motivated to develop an online joint friction estimation method for walking bipeds. This method is based on the available force and acceleration measurements along with the reduced biped model. It is applied when the robot foot is in contact with the ground. Although it is inapplicable when the leg is swinging, it can be integrated with a friction model that works only when the leg is swinging. The model parameters are identified adaptively.

Also, this thesis is motivated to develop an online friction estimation method to estimate the friction parameters between the foot and the contact surface. In addition to the estimated friction parameters, this method will be able to predict the slip ahead.

## 1.2 Related work

Joint friction compensation is studied intensively for industrial robots. Here we will divide the compensation of the joint friction into three categories: Friction model-based, model-free and actuator fault-based.

In the first category, the friction behavior is represented by a mathematical model [36, 37]. The model parameters are identified offline. Then the model with the identified parameters is used to compensate for the joint friction [29, 38-42]. However, the friction is a complex phenomenon that depends on factors including joint position and load [16, 43]. Moreover, the friction model parameters vary due to the environmental changes. To overcome these problems, model-based adaptive methods were developed. In these methods the friction model parameters are tuned online to obtain a satisfactory compensation action [44-48]. However, friction modeling is a challenge since the friction behavior is highly nonlinear.

The second category is the model-free one. Here several strategies are used to compensate for the friction. The measurement-based friction compensation is considered one strategy [24, 25]. The transmitted torque to the manipulator's link is measured by torque sensors and used in the feedback torque control loop. Although its performance is shown to be effective in practice [24, 25], the torque sensors should be added in the design process. The drawback of mounting extra torque sensors was solved for the fixed base robots by using the base sensor control BSC method [43]. It considers that the robot base is equipped with a force/torque sensor. It projects the sensor readings on the robot links to compute the manipulator's link torque. This torque is then used in the feedback torque control law. However, the biped robot is not fixed in the ground.

Another strategy is based on the disturbance observer (DO) theory [49, 50]. In this strategy, the friction, external disturbances, system model uncertainty, gravity torque and so on are regarded as disturbance. The DO is used to eliminate the effects of this disturbance based on the frequency band [31, 51, 52]. It is assumed that the observer dynamics are faster than the disturbance. Combining the DO with the model category is reported to improve the system performance as they complement each other [53].

The Friction Approximator is a system which uses the soft computing techniques. Neural networks (NN) are characterized by the parallelism and low level learning. They are able to approximate nonlinear functions. Using this property, they are used to build compensators with friction models [54-56]. They are also used to handle the unknown dynamics including friction discontinuity [45]. However, the approximation error exists and depends on the structure of the NN. Heavy computation is the result of an overdetermined NN while low approximation accuracy will be obtained with an underdetermined NN. Approximators are locally applicable and sensitive to the NN initialization [57]. Fuzzy systems are used for friction approximation too. They are characterized by the linguistic information and the high level of logic. They are universal approximators for nonlinear functions and functionally equivalent to feed-forward NNs. This property gives them the ability to build models to represent the friction behavior [58-63]. However the approximation error exists.

The third category considered the friction as an actuator fault with time varying characteristics. The friction is compensated based on the robust fault estimation theory. To accomplish this, the fault-tolerant control (FTC) scheme is used for linear systems [64].

Although joint friction compensation is of great significance and reported intensively for the industrial robots, for bipeds it is generally neglected [32-35]. The model-based method with offline identified parameters is reported in [27-30]. In a model-free approach, the joint friction is regarded as disturbance, and the DO is used to eliminate it [31]. However, these techniques have the aforementioned drawbacks.

The friction force between the feet soles and the ground has a significant role. It determines the maximum acceleration and deceleration and hence the maximum forces allowed to be applied to the robot [22, 65]. Friction forces can be measured by sensors embedded in the feet of the humanoid robot as in [66, 67]. Or they can be computed based on other measurements like the foot ankle forces and foot acceleration. When the foot is in contact with the ground, the foot slips if the relative velocity between them is not zero. This leads to define the slipping forces as the difference between the total forces applied at the foot and the friction forces. The slipping forces are not measured directly, however they can be calculated.

Slip prediction, if can be performed successfully, can be a valuable asset [5]. It may prevent the robot from falling. Although it is significant, only a few studies were reported. In biped walking, often, the non-slipping case is assumed, In other words, the coefficient of friction is either considered to be very high such that the slip never happens [28, 68-70] or accurately known [71]. The maximum applied torque is constrained accordingly [72, 73]. For the single support phase of a biped, a method for calculating the slipping force and torque and predicting their most possible slipping direction is proposed [74]. However a known friction coefficient assumption is impractical and the environment changes a lot (the walking surface varies a lot during the walk).

For an unknown floor coefficient of friction, a method for slip detection is proposed by [75]. It depends on enlarging the walking step gradually until the biped slips, then it is used later as an upper limit for the trajectory planning. However, this requires several steps to learn the limit.

A slip observer is introduced in [76] where the slip force is calculated as the difference between the desired reaction force and the measured one. The desired force is calculated using the 3D linear inverted pendulum model with known *ZMP*. However, the desired reaction force does not include the external and inertial forces, thus it is not necessarily that the difference is due to higher desired reaction forces, and the slip may occur even the desired reaction force is less than the measured.

Sensor-based slip detection methods are reported too. Slip is detected for a quadruped during the supporting phase using the leg acceleration [77]. The slip is detected when the integration of the acceleration (obtained from an accelerometer) exceeds certain threshold. For slip-related falls, intelligent shoes were introduced for slip detection [78]. It is based on the human postural instability based on information from in-shoe pressure sensors and optional rate gyros. An insole sensor system for biped slip detection is introduced in [79]. It utilizes force and acceleration measurements for slip detection. The detection algorithm is: slipping exists when the force and acceleration readings are larger than certain threshold, otherwise there is no slip. A slip detection approach is developed in [80]. It is based on searching in the acceleration signal for high amplitudes before, during and after the slip spike. In the same contest, the acceleration and gyro readings with unscented Kalman filter



(UKF) are used for slip detection [81]. The UKF innovation is used for slip detection. However, the previous works are for slip detection not prediction.

Friction models and estimators are reported to prevent slip [82, 83]. However it is difficult to model the friction as explained before. Moreover, low velocities and the stiction friction pose more challenges. In our work, the slip is predicted without using friction models. Thus friction modeling problems are avoided.

### 1.3 Problem definition

Although joint friction compensation has considerable effect, it is generally neglected for walking bipeds [32-35]. In some cases it is regarded as a disturbance and tried to be eliminated by a DO [31], or compensated using friction model with the offline identified parameters [29, 30].

Slip may cause the robot to tip over. Therefore, it has critical importance. Although some studies are reported to compensate for the slip, they in general work when the slip occurs. Beyond this, using models for slip prevention poses problems. This is due to the discontinuity at the low speed and the stiction behavior of the friction.

Among the model-free strategies, the measurement-based strategy is fruitful. It avoids friction modeling and approximation problems. However, it can't be applied on bipeds for joint friction estimation if there are no mounted joint torque sensors. Moreover, the bipeds are not fixed in the ground, and therefore, the background developed for fixed-base industrial robots is not fully applicable for biped robot joint friction estimation. While walking, the biped switches its legs from the double support phase (DS) to the single support phase (SS) and so forth. The model-based category of joint friction estimation is characterized by having better precision friction compensation if the identified parameters have very small uncertainty [84]. High accuracy can be achieved by adaptive model parameter tuning. However, it requires information about the friction to update the model parameters. The biped dynamical model includes the body position, orientation and their

derivatives in addition to the joint angles and their derivatives. This adds more challenge to the friction estimation and compensation problem.

Therefore, for joint friction estimation, we are looking for a method that has the advantages of the measurement-based strategy and the adaptive model-based category. This method must also be able to overcome the unmeasured body velocity and joint angular accelerations in the biped dynamics model.

It is the idea of this thesis that, the measurement-based strategy, based on the available measurements, can be employed for slip prediction. It can be used to estimate the Coulomb friction between the foot and the ground, and thus it can be used to estimate allowed forces and accelerations. These can be used to predict the slip ahead. However, at least two measurements are required at the foot. The options for the two measurements are: 1) Ankle forces and foot accelerations, 2) ankle forces and the reaction forces at the foot sole, or 3) acceleration of the robot body and the reaction forces at the foot sole. For the last case, a model of the biped is required too.

Based on the above considerations, an adaptive online measurement-based algorithm is sought in the thesis. This algorithm must be able to estimate the friction and update the estimated variables when the surface changes. Also, the algorithm must predict the slip ahead, so that a control action can be executed.

#### **1.4 The proposed method**

In this paper, we are proposing two new methods. The first one is for joint friction estimation and compensation and the second one is for slip prediction.

The first method combines the model-free approach with the model-based compensation. More precisely, the measurement-based strategy is combined with the model-based approach of compensation. First, the body attitude is estimated by utilizing the IMU readings through a sensor fusion approach. Then the robot body (called the base later on) velocity is estimated using the linear inverted pendulum model LIPM [85]. This model

relates the robot base position, velocity and acceleration with the measured foot reaction forces. To accomplish this estimation, the joint accelerations are required. This challenge is solved in two ways: In the first one, walking use of the non-slipping foot assumption, the joint accelerations are estimated using a pseudo inverse. The second way is based on using a stable first order filter to obtain the robot filtered dynamic model [86]. First the biped model is reduced. Then a reduced filtered dynamic model is obtained by taking the convolution of the impulse response of the stable filter with each equation in the reduced biped model. Using this way, with integration by parts technique, the explicit calculation of the angular acceleration is avoided.

The measurement-based strategy works only when the foot is in contact with the ground without slipping. This strategy is employed for two purposes. The first one is to provide online joint friction compensation. The joint friction is estimated by using the robot link torque and the applied joint control torque. The robot link torque is computed (not measured) using a reduced dynamical model of the biped. This reduced model utilizes the ground reaction forces GRF and the IMU readings. It also utilizes the estimated base velocity and attitude and joints accelerations. However, when the foot loses the contact with the ground, the online friction compensation is no longer applicable. For this case, a friction model is adopted. The second purpose of the measurement-based strategy is to update the adopted friction model parameters. Thus the model parameters are adaptively identified whenever the foot is in contact with the ground. Hence, the proposed method is measurement-based online friction compensation when the foot is in contact and model-based adaptive method when the leg is swinging. The proposed method makes use of their advantages and overcomes their disadvantages. Since this method uses the foot and base measurements, we will call it: Foot- base sensor estimation (FBSE).

The measurement-based strategy is also used for the slip prediction. Here, based on the friction behavior, an online model-free algorithm is designed to estimate the Coulomb friction. This algorithm updates the estimated friction online adaptively. Based on the friction behavior, the Coulomb friction is the minimum friction beyond which slip will be observed. Therefore it is used to decide whether the foot is going to slip or not. This is achieved by considering the Coulomb friction as a slip threshold. To predict the slip, a

safety margin is subtracted from the Coulomb friction to define a slip risk band. Hence, whenever the applied force is below this band, we will assume that the foot will not slip. If the applied force is within the safety margin, then the foot tends to slip. Finally if the applied force is larger or equal to the Coulomb friction, we will conclude that the foot is slipping. Different measurement scenarios are discussed. The experiments are based on the foot acceleration and ankle force measurements.

## 1.5 Contribution

The estimation in this thesis is based on Kalman Filter. Therefore the first contribution is developing a Kalman Filter by adding two rules to update its process and noise covariances recursively. The result is an adaptive Kalman Filter which is summarized in the preliminaries chapter.

A new state space form for the linear inverted pendulum model to estimate the biped center of mass (CoM) position and its derivatives is proposed. This form is for the case where the measurements are the biped acceleration and the *ZMP* with modeling uncertainty in the measurement of the *ZMP*. This form estimates the modeling error in the *ZMP* and compensates for it.

A novel method for the joint friction estimation for a walking biped robot is proposed. It combines the model-free method with the adaptive model-based method. The model-free method is measurement-based and uses the acceleration and force measurements with a reduced dynamical model of the biped.

A new method for predicting the slip occurrence of walking biped is proposed. This method is measurement-based and model-free. The foot accelerations and ankle forces are used to detect the slip occurrence. Then an online algorithm is designed based on the friction behavior to estimate the Coulomb friction which in turn is used as a slip threshold. To predict the slip, a safety margin is subtracted from the estimated Coulomb friction to define a slip risk band. Hence, the foot will not slip whenever the force is below this band. If the applied force is within the safety margin, then the foot tends to slip.

## 1.6 Publications

1. I. Hashlamon and K. Erbatur, "An improved real-time adaptive Kalman filter with recursive noise covariance updating rules," *Turkish Journal of Electrical Engineering & Computer Sciences*, accepted, 2013.
2. I. Hashlamon and K. Erbatur, "Center of Mass States and Disturbance Estimation for a Walking Biped " in *IEEE International Conference on Mechatronics, ICM 2013*, Vicenza (ITALY) . 2013, pp. 248-253.
3. I. Hashlamon, Mehmet Mert Gülhan, Orhan Ayit and K. Erbatur, "Modeling errors and CoM states estimation for a walking biped." *Submitted to Measurement*.
4. I. Hashlamon and K. Erbatur, "Joint friction estimation for walking bipeds." *Robotica journal, minor revision completed, 2014*.
5. I. Hashlamon, Mehmet Mert Gülhan and Orhan Ayit and K. Erbatur, "A novel method for slip prediction of walking biped robots." *Submitted to Robotica*.
6. İyad Hashlamon, Ömer Kemal Adak and Kemallettin Erbatur, "Kalman filtresi ve hata durumu ile insansı robot gövde durumu tahmini" In: Otomatik Kontrol Ulusal Toplantısı 2012 (TOK'12), Niğde, Türkiye.
7. I. Hashlamon and K. Erbatur , "Ground reaction force sensor fault detection and recovery method based on virtual force sensor for walking biped robots", in *Control Conference (ASCC)*, 2013 9th Asian, 2013, pp. 1-6.
8. I. Hashlamon and K. Erbatur , "Simple Virtual Slip Force Sensor for walking biped robots," in *Control Conference (ASCC)*, 2013 9th Asian, 2013, pp. 1-5.
9. I. Hashlamon and K. Erbatur , "An optimal estimation of feet contact distributed normal reaction forces of walking bipeds," in *IEEE 23rd International Symposium on Industrial Electronics (ISIE)*, accepted, 2014.
10. I. Hashlamon and K. Erbatur , "Joint sensor fault detection and recovery based on virtual sensor for walking legged robots," in *IEEE 23rd International Symposium on Industrial Electronics (ISIE)*, accepted, 2014.

## 1.7 Thesis organization

This thesis is organized as follows.

In Chapter 2, preliminary concepts are introduced. The friction phenomenon, least squares algorithm, Kalman and adaptive Kalman filter equations are reviewed.

In Chapter 3, the biped CoM position and velocity are estimated in the presence of disturbance. The linear inverted pendulum model is written in two forms. These forms are discussed and tested for disturbance rejection and estimation.

In Chapter 4, the joint friction is estimated and compensated. The estimation is measurement-based when the foot is in contact with the ground and adaptive model-based when it is swinging. Since the joint angular accelerations are required, two methods are used: While the first one uses the foot non-slipping constraint to calculate the joint angular acceleration, the second method uses a low-pass filtering technique with the biped model to avoid the explicit calculation of the angular accelerations.

In Chapter 5, the slip occurrence is predicted. An online algorithm is designed based on the friction behavior to estimate the Coulomb friction which is used for slip prediction.

Finally Chapter 6 contains the conclusion and future research.

## **Chapter 2**

### **2 Preliminaries**

This thesis is about friction estimation. Therefore the friction phenomenon is explored and discussed in this chapter first. Then, the least squares algorithm and integration by parts are listed as system identification and mathematical tools. After that, Kalman filter (KF) and adaptive Kalman filter (AKF) are reviewed. Finally, a summary of attitude estimation approach is discussed.

#### **2.1 Friction**

Friction is the motion resistance phenomenon that appears between two surfaces in contact. The friction appears also when there are mechanical systems such as gears, transmissions and wheels.

The friction is required and useful in such applications such as brakes, cars and walking robots. For example, the friction force between the biped foot and the contact surface determines the maximum allowable acceleration the robot can have. On the other hand, the friction forces at the robot joints have undesirable effects on the robot performance.

Therefore, for control purposes, it is important to understand the friction behavior and its effects on the closed loop control system.

### 2.1.1 Friction behavior

Consider the object in Figure 2.1.a, the friction force is the tangential reaction force  $F_f$  in the opposite direction of motion. The applied tangential force is  $F_t$  and the normal reaction force is  $F_N \geq 0$ . The Friction force  $F_f$  can be either a static force, denoted by  $F_{fs}$ , or kinetic one, denoted by  $F_{fd}$  as in. Figure 2.1.b. These forces are respectively defined by

$$F_{fs} \leq \mu_{static} F_N, \quad (2.1)$$

and

$$F_{fd} = \mu_d F_N, \quad (2.2)$$

where  $\mu_{static}$  is the static coefficient of friction and  $\mu_d$  the kinetic coefficient of friction.

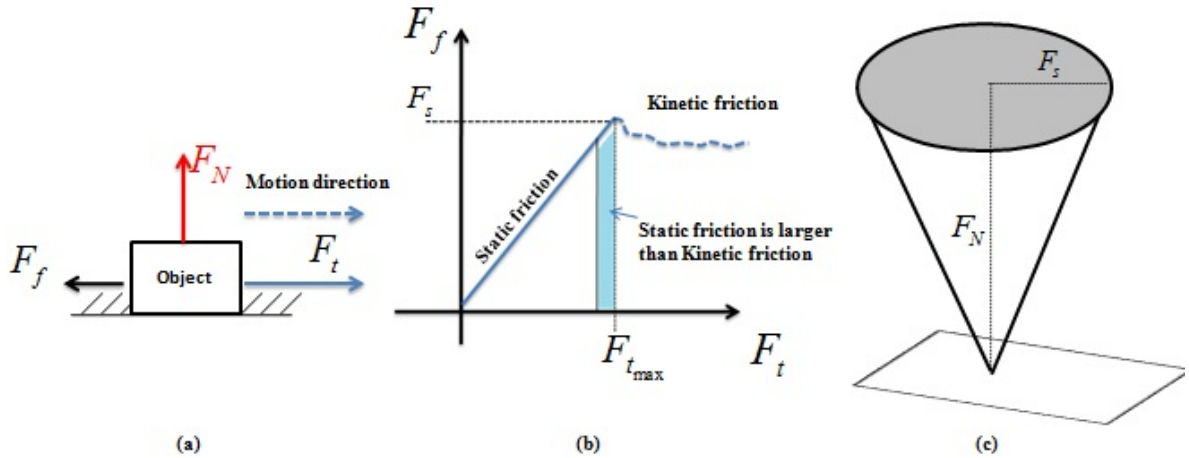


Figure 2.1: (a) Object free body diagram (the object weight is in the normal force), (b) Friction force behavior, and (c) the friction cone.

When the object is at rest, it resists the initial motion with a larger frictional force than it does when the motion starts. This can be stated by the coefficients of friction as  $\mu_{static} \geq \mu_d$ . As shown in Figure 2.2.b, the value of  $F_{fs}$  is at its maximum when the relative motion starts, and then the friction force decreases. We denote the maximum value of  $F_{fs}$  by  $F_s$ . At  $F_s$ , the maximum applied force called  $F_{t_{max}}$  is observed. The region where the object is in static condition of no motion is referred to as the static region. In this region



$F_t < F_s$ . The phase of motion with nonzero velocity is called the kinetic region. In the kinetic region  $F_t > F_s$ . Equivalently, the allowable force  $F_t$  such that the object is in no motion must be inside a cone with radius  $F_s$  and height  $F_N$  as shown in Figure 2.1.c.

### 2.1.2 Friction models

There is no exact model that represents the friction force. In general, the dominant friction components are the Coulomb friction  $F_c$ , Stribeck friction  $F_{st}$ ,  $F_s$  and viscous friction  $F_v$  as illustrated in Figure 2.2. Several friction models to represent the friction behavior were developed [36]. The models are either dynamic or static. In a typical static model, the basic structure contains the Coulomb and viscous friction components and the friction effect is expressed by

$$F_f = F_c \operatorname{sgn}(v) + F_v, \quad (2.3)$$

with

$$F_c = \mu_c F_N, \quad (2.4)$$

and

$$F_v = \bar{F}_v v. \quad (2.5)$$

Here,  $\mu_c$  and  $\bar{F}_v$  are the coefficients of coulomb and viscous friction respectively, and  $v$  is the velocity of the moving object.

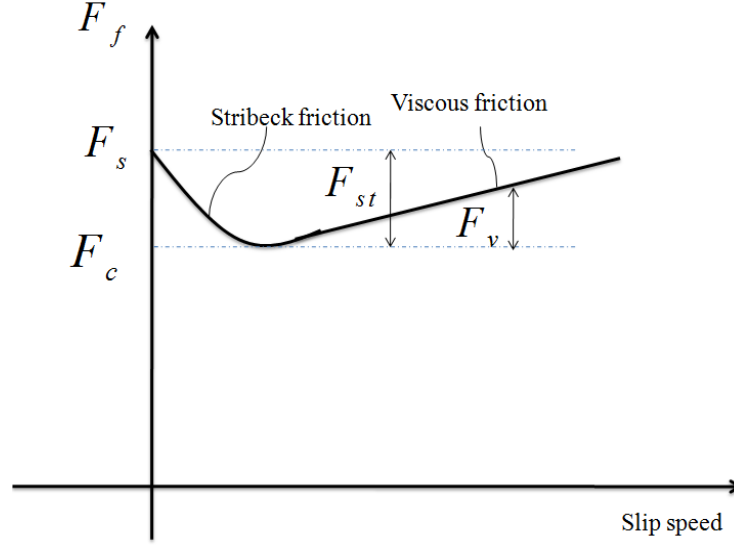


Figure 2.2: Friction components

An early dynamic model is the Dahl model [87]. It was inspired by the stress-strain curves to explain the friction behavior. This formulation does not model the velocity dependent terms or the Stribeck friction behavior. However, it was the basis for LuGre model [88] which modified the Dahl model by adding the velocity dependent terms. Also LuGre model is further modified to the Leuven model [89] by using a stack mechanism to implement the pre-sliding hysteresis. [89] is also modified in [90] by replacing the stack mechanism by the Maxwell slip model. A recent continuous model is proposed in [23]. The friction expression in [23] is

$$F_f = \gamma_1 \left( \tanh(\gamma_2 \dot{\theta}) - \tanh(\gamma_3 \dot{\theta}) \right) + \gamma_4 \tanh(\gamma_5 \dot{\theta}) + \gamma_6 \dot{\theta}, \quad (2.6)$$

where  $\gamma_i, i=1, \dots, 6$  are positive constants. The model has the viscous dissipation term  $\gamma_6 \dot{\theta}$  and the coulomb friction term  $\gamma_4 \tanh(\gamma_5 \dot{\theta})$ . It captures the Stribeck effect by the term  $\tanh(\gamma_2 \dot{\theta}) - \tanh(\gamma_3 \dot{\theta})$ . The static coefficient of friction can be approximated by  $\gamma_1 + \gamma_4$ .

In this thesis, the model in (2.6) will be used as a friction generator, while the model in (2.3) will be used for friction estimation.

## 2.2 The least squares algorithm

In an identification problem, where the model parameters are to be identified, a cost function is introduced. This cost function measures how the model fits the experimental data. The least squares method minimizes the sum of the square of the errors. Lets consider the linear model

$$y(k) = a_1 \mathcal{G}_1(k) + \dots + a_n \mathcal{G}_n(k) = \mathcal{G}^T(k) \phi, \quad (2.7)$$

where

$$\phi = \begin{bmatrix} a_1 \\ \vdots \\ a_n \end{bmatrix}, \quad (2.8)$$

and

$$\mathcal{G} = \begin{bmatrix} \mathcal{G}_1(k) \\ \vdots \\ \mathcal{G}_n(k) \end{bmatrix}. \quad (2.9)$$

Here,  $y$  is the observed or measured data,  $\phi$  the unknown parameter vector,  $\mathcal{G}$  the known regression variable vector and  $i \in \{1, \dots, n\}$ .  $n$  is the number of unknown scalar parameters.

Then, for a number of samples  $N_s$ , the estimated parameters vector  $\hat{\phi}$  is

$$\hat{\phi} = \arg \min_{\phi} \frac{1}{2} (Y - \psi \phi) (Y - \psi \phi)^T \quad (2.10)$$

where

$$Y = \begin{bmatrix} y(1) \\ \vdots \\ y(N_s) \end{bmatrix}, \quad (2.11)$$

and

$$\psi = \begin{bmatrix} \mathcal{G}^T(1) \\ \vdots \\ \mathcal{G}^T(N_s) \end{bmatrix} \quad (2.12)$$

The dimensions of the above vectors and matrices are:  $Y: N_s \times 1$ ,  $\mathcal{G}: n \times 1$ ,  $\psi: N_s \times n$  and  $\phi: n \times 1$ . Then the parameters vector is calculated by

$$\hat{\phi} = (\psi^T \psi)^{-1} \psi^T Y . \quad (2.13)$$

The term  $(\psi^T \psi)^{-1} \psi^T$  is called the pseudo inverse of  $\psi$  .

The above discussion is for one model with  $n$  parameters and  $N_s$  samples. For  $N$  models, combined matrices can be expressed as

$$\Phi = \begin{bmatrix} \phi_1 \\ \vdots \\ \phi_N \end{bmatrix} \quad (2.14)$$

$$\mathbf{Y} = \begin{bmatrix} Y_1 \\ \vdots \\ Y_N \end{bmatrix} , \quad (2.15)$$

and

$$\Psi = \text{diag} \left( \begin{bmatrix} \psi_1 \\ \vdots \\ \psi_N \end{bmatrix} \right) . \quad (2.16)$$

Then the estimated models parameters vector  $\hat{\Phi}$  is then obtained by

$$\hat{\Phi} = (\Psi^T \Psi)^{-1} \Psi^T \mathbf{Y} \quad (2.17)$$

For real time applications, the recursive least squares (RLS) is more preferable than (2.17). Here with  $N_s = 1$  , the RLS algorithm [91] is

$$\hat{\Phi}(k) = \hat{\Phi}(k-1) + K_{RLS}(k) e_{RLS}(k) , \quad (2.18)$$

$$e_{RLS}(k) = \mathbf{Y}(k) - \Psi(k)\hat{\Phi}(k-1), \quad (2.19)$$

$$K_{RLS}(k) = P_{RLS}(k-1)\Psi^T(k)(I + \Psi(k)P_{RLS}(k-1)\Psi^T(k))^{-1}, \quad (2.20)$$

$$P_{RLS}(k) = (I - K_{RLS}(k)\Psi(k))P_{RLS}(k-1). \quad (2.21)$$

where the matrix  $P_{RLS}$  can be interpreted as the covariance of the parameter vector.

### 2.3 Integration by parts

Integration by parts will be used to avoid the explicit calculation of the joint angular acceleration. Given two continuous functions  $f(r)$  and  $g(r)$ , then the integral

$\int_a^b f(r)\dot{g}(r)dr$  can be evaluated using the integration by parts technique as

$$\begin{aligned} \int_a^b f(r)\dot{g}(r)dr &= f(r)g(r)\Big|_a^b - \int_a^b \dot{f}(r)g(r)dr \\ &= f(b)g(b) - f(a)g(a) - \int_a^b \dot{f}(r)g(r)dr \end{aligned}, \quad (2.22)$$

where the dot notation represents the derivative of the function [92].

### 2.4 Kalman filter

Kalman filter KF is among the most popular and famous estimation techniques. That is because it merges the observer theory and the Bayesian approach. It is a statistically optimal estimator that estimates the instantaneous state of a dynamic system perturbed by noise using noisy observation that are related to the state [93]. Basically, KF depends on two models: The plant dynamic model which describes the system behavior over time and

the stochastic models which describe the process and observation noise properties [94, 95]. Consider the discrete-time linear state space model

$$\begin{aligned} x_k &= Ax_{k-1} + Bu_{k-1} + w_{k-1}, \\ y_k &= Cx_k + v_k \end{aligned} \quad (2.23)$$

where  $x_k \in \mathbb{R}^n$  is an  $n$ -dimensional state vector with initial state value  $x_0$  that has Gaussian distribution of mean  $m_0$  and covariance  $P_0$  (i.e.  $x_0 \sim N(m_0, P_0)$ ),  $A \in \mathbb{R}^{n \times n}$  is the state matrix,  $B \in \mathbb{R}^{n \times m}$  is the input matrix,  $u \in \mathbb{R}^m$  is the system input,  $w \in \mathbb{R}^n$  is the Gaussian process noise with zero mean and constant covariance  $Q$  (i.e.  $w \sim N(0, Q)$ ),  $v \in \mathbb{R}^d$  is the Gaussian measurement noise with zero mean and constant covariance  $R$  (i.e.  $v \sim N(0, R)$ ),  $y \in \mathbb{R}^d$  is a  $d$ -dimensional measurement vector,  $C \in \mathbb{R}^{d \times n}$  is the output matrix, and  $k$  is the time index. For this system, the matrices  $A, B$ , and  $C$  are considered to be known at the time instant  $k$ , and a random initial state mean  $m_0$  and covariance  $P_0$  are given before applying KF. The state estimation is carried out under the following assumptions:

**Assumption 1:** The process and measurement noises are assumed to be independent and mutually uncorrelated with the given means and covariances

$$\begin{aligned} E(w_k) &= E(v_k) = E(w_k v_k^T) = 0 \\ Q &= \delta_{ki} E(w_k w_k^T); R = \delta_{ki} E(v_k v_k^T) \end{aligned} \quad (2.24)$$

with

$$\delta_{ki} = \begin{cases} 1 & i=k \\ 0 & i \neq k \end{cases}, \quad (2.25)$$

where  $E(\cdot)$  stands for the expectation of  $(\cdot)$ .

**Assumption 2:** The inputs are considered to be piecewise constant over the sampling time interval  $T$ , i.e.  $u(t) = u_{k-1}$ ,  $t_{k-1} \leq t < t_k = t_{k-1} + T$ .

**Assumption 3:** The noise covariances are considered to be constant.

**Assumption 4:** The process and measurements have the same sampling time.

Under these assumptions for the system in (2.23), the conventional KF algorithm is composed of the prediction step

$$\begin{aligned}\hat{x}_k^- &= A \hat{x}_{k-1} + B u_{k-1} \\ P_k^- &= A P_{k-1} A^T + Q_{k-1}\end{aligned}\quad (2.26)$$

and the measurement update step

$$\begin{aligned}K_k &= P_k^- C^T (C P_k^- C^T + R_k)^{-1} \\ \hat{x}_k &= \hat{x}_k^- + K_k (z_k - C \hat{x}_k^-) \\ P_k &= (I - K_k C) P_k^-\end{aligned}\quad (2.27)$$

In (2.26) and (2.27), the following notation is employed:  $(\cdot)^-$  and  $(\hat{\cdot})$  stand for the prior and posterior estimates, respectively.  $P$  is the estimation error covariance matrix and  $K$  is the Kalman gain.  $I$  is the identity matrix,  $\hat{x}$  is the estimated state and  $z$  is the measurement vector with the same dimension as  $y$ .

For the best performance of KF, both the system dynamic model and the noise statistic model parameters must be known. However, in many applications, the stochastic model parameters may be unknown or partially known. As a result, KF performance degrades or may even diverge [96, 97].

The values of  $Q$  and  $R$  have an important effect on Kalman filter estimates, the estimated state  $\hat{x}_k$  will be biased if the value of  $Q$  is too small with respect to the correct value, and  $\hat{x}_k$  will oscillate around the true value if the value of  $Q$  is too large with respect to the correct value [98]. The KF algorithm uses the noise statistics to influence the KF gain that is applied on the error between the available process information and the most recent obtained measurements. The filter gain projects this error to the process information to get the best estimate. Thus, noise characteristics have a significant importance on KF performance. This motivates the research of developing and improving KF such that it can adapt itself to the uncertainty in the noise statistical parameters, thus reduce their effects. This type of KF is well known as Adaptive Kalman Filter AKF.

An AKF is developed in the framework of this Ph.D. study [99]. It uses the idea of the recursive estimation of KF to develop two recursive updating rules for the process and observation covariances respectively. The design is based on the covariance matching principles. Each rule has a tuning parameter which enhances its flexibility for noise adaptation. The proposed AKF proved itself to have an improved performance over the conventional KF and in the worst case, it converges to the KF.

## 2.5 Adaptive Kalman filter

In this section the proposed AKF is briefed. It is based on developing two recursive updating rules R1 and R2 for noise covariances  $R$  and  $Q$ , respectively. Consider that the assumptions 1 - 4 hold for the discrete-time linear state space model given in (2.23), then for a given initial value matrices  $R_0$  and  $Q_0$ , there are constants  $0 < \alpha_1 < 1$  and  $0 < \alpha_2 < 1$ , positive constants  $N_R$  and  $N_Q$ , and noise covariance errors  $\Delta Q$  and  $\Delta R$  such that the KF performance is improved by updating the observation and the process covariance matrices.

The adaptive Kalman filter algorithm is summarized in (2.28) - (2.38). For given initial values  $\bar{\omega}_0, \bar{e}_0, \hat{x}_0, P_0, N_R, N_Q, Q_0$  and  $R_0$ , the priori estimate of the state vector  $\hat{x}_k^-$  is given by

$$\hat{x}_k^- = A \hat{x}_{k-1} + B u_{k-1}, \quad (2.28)$$

with a priori estimated covariance  $P^-$

$$P_k^- = A P_{k-1} A^T + Q_{k-1}. \quad (2.29)$$

The measurement residual  $e$  and its mean  $\bar{e}$  are defined as

$$e_k = z_k - C \hat{x}_k^-, \quad (2.30)$$

and

$$\bar{e}_k = \alpha_1 \bar{e}_{k-1} + \frac{1}{N_R} e_k, \quad (2.31)$$



respectively, where  $N_R$  is a positive tuning constant and

$$\alpha_1 = \frac{N_R - 1}{N_R}. \quad (2.32)$$

The measurement noise covariance matrix  $R$  is updated as

$$R_k = \left| \text{diag} \left( \alpha_1 R_{k-1} + \Delta R_k \right) \right|, \quad (2.33)$$

where  $\text{diag}$  stands for the diagonal matrix.  $\Delta R$  is given by

$$\Delta R_k = \frac{1}{N_R - 1} (e_k - \bar{e}_k)(e_k - \bar{e}_k)^T - \frac{1}{N_R} (C P^- C^T)_k. \quad (2.34)$$

The posteriori estimate  $\hat{x}$  is obtained using the update rule

$$\hat{x}_k = \hat{x}_k^- + K_k e_k, \quad (2.35)$$

where  $K$  is Kaman filter gain and expressed by

$$K_k = P_k^- C^T \left( C P_k^- C^T + R_k \right)^{-1}, \quad (2.36)$$

The posteriori covariance  $P$  is updated by

$$P_k = (I - K_k C) P_k^-, \quad (2.37)$$

where  $I$  is the identity matrix. The process covariance matrix  $Q$  is updated by the expression

$$Q_k = \left| \text{diag} \left( \alpha_2 Q_{k-1} + \Delta Q_k \right) \right|. \quad (2.38)$$

Here  $\Delta Q$  is defined by

$$\Delta Q_k = \frac{1}{N_Q} \left( P_k - A P_{k-1} A^T \right) + \frac{1}{N_Q - 1} \left( \hat{\Lambda}_k - \bar{\Lambda}_k \right) \left( \hat{\Lambda}_k - \bar{\Lambda}_k \right)^T, \quad (2.39)$$

where  $N_Q$  is a positive tuning constant and

$$\alpha_2 = \frac{N_Q - 1}{N_Q}, \quad (2.40)$$

$\hat{\Lambda}$  and  $\bar{\Lambda}$  are the state error and its mean respectively. They are defined by

$$\hat{\Lambda}_k = \hat{x}_k - \hat{x}_k^-, \quad (2.41)$$

and

$$\bar{\Lambda}_k = \alpha_2 \bar{\Lambda}_{k-1} + \frac{1}{N_Q} \hat{\Lambda}_k, \quad (2.42)$$

respectively. This AKF is used throughout this thesis for estimation purposes.

## 2.6 Base attitude estimation

In a previous work of the author a sensor fusion approach to estimate the attitude of robots by utilizing the IMU readings was developed [100]. This approach is independent of the robot model and it can be applied for the bipeds too. It employs two sequential estimators. The first one is for the gravity estimation and uses KF. The second one is for the attitude estimation and uses an Extended Kalman Filter EKF (Figure 2.3).

KF is employed for the gravity estimation mainly based on acceleration readings. KF states are the gravity acceleration, linear acceleration and the acceleration bias. The accelerometer output consists of the gravity acceleration, linear acceleration, bias and noise. The gravity acceleration vector contains information about the roll and pitch angles of the body. To initialize KF states, the accelerometer output signal has to be decomposed. By ignoring the noise, the values of the accelerometer signal terms are predicted using the pseudo inverse matrix multiplication. The predicted values are used as initial values for KF. The gravity acceleration estimate from KF is used for the computation of the x- and y-Euler angles. The computed Euler angles are transformed into quaternion representation to be considered as a “measured quaternion” for the correction stage in the EKF. To accomplish this transformation, the z-Euler angle is also required. It is borrowed from the quaternion estimate of the EKF and initially it is considered to be zero.

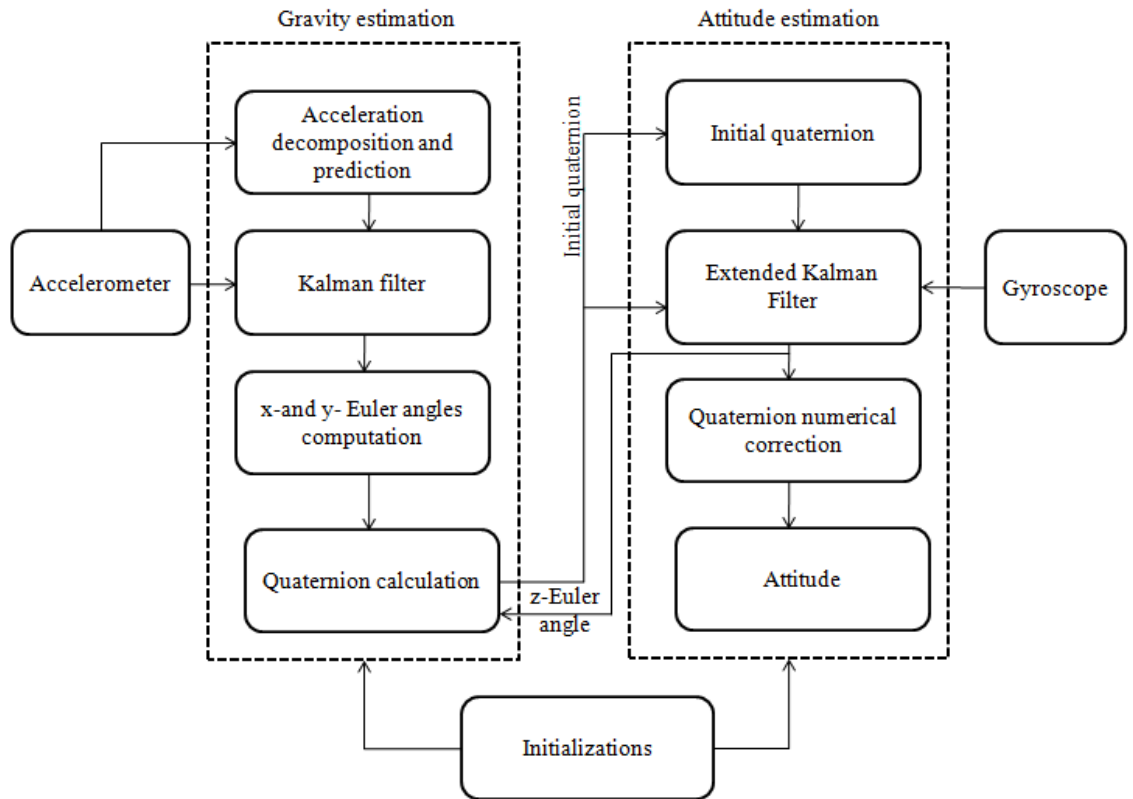


Figure 2.3: Attitude estimation approach

The EKF uses the measured quaternion and the gyroscope readings to produce the correct quaternion vector. Since the quaternion has the unity norm constraint, this correction is followed by a numerical norm correction to keep the unity magnitude of the quaternion. Then the normalized estimated quaternion is converted to represent the attitude. The two estimators feed each other cyclically: The EKF provides the z-Euler angle for the gravity estimator, whereas the gravity estimator produces the measured quaternion for the attitude estimator. The noise covariances initializations are provided for both estimators.

The resulting attitude matrix  $A_l^w$  represents the attitude of the IMU frame  $O_l$  with respect to the world frame  $O_w$

## Chapter 3

### 3 Linear Inverted Pendulum Model for State Estimation

An on-line assessment of the balance of the robot requires information of the state variables of the robot dynamics. However, modeling errors, external forces and hard to measure states pose difficulties to the control systems. This chapter presents a method of using the motion and force information to estimate the center of mass CoM position and its derivative and the disturbance effects on a walking biped robot. The motion (acceleration and angular velocity of the robot body) is acquired from the inertial measurement unit IMU and the force is measured from force sensors at the robot feet. An AKF is employed for the states estimation based on the Linear Inverted Pendulum Model LIPM. Two types of disturbances are estimated, the modeling errors and external accelerations. To estimate these disturbances, the LIPM is written in two forms, which we call form 1 and form 2, and each form has its own advantages. The former is well known and has better performance when external accelerations exist, however it fails in case of modeling errors. Therefore, we introduce the latter, its performance is better when modeling errors exist. Both forms are equivalent when no disturbance exists.

This chapter introduces the LIPM, estimation methodology and the results of estimation.

### 3.1 LIPM dynamics

In this model, the biped base is modeled as a point mass concentrated at the CoM. This mass is connected to a stable contact point on the ground using a massless rod which is an idealized model of the supporting leg [101] as in Figure 3.1. The swinging leg is assumed to be massless too. The CoM has fixed height  $z_c$  and position coordinates in the three dimensional space  $\mathbf{c} = [c_x \quad c_y \quad z_c]^T$ .

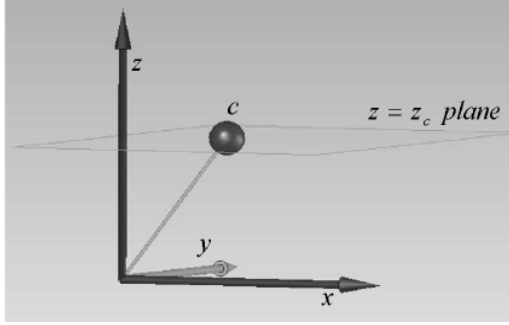


Figure 3.1: LIPM

The LIPM is frequently used to generate walking trajectories [18]. Yet another requirement is that the walking trajectories must be stable. As a stability criterion, the Zero Moment Point stability criterion [19, 20] is widely used. Referring to Figure 3.1, the *ZMP*,  $\mathbf{p}_{\text{ZMP}}$  is the point on the sole ( $x-y$  plane) where the moments  $M$  around the  $x$ - and  $y$ -axes are equal to zero. In other words  $M_x = M_y = 0$ . These moments are due to the ground reaction forces. For the biped to be stable, the  $\mathbf{p}_{\text{ZMP}}$  must lie in the supporting polygon. The  $\mathbf{p}_{\text{ZMP}}$  can be calculated using the normal reaction force measurements  $F_N$  to form  $\mathbf{p}_{\text{ZMP}}^{F_N}$  as [102]

$$\mathbf{p}_{\text{ZMP}}^{F_N} = \frac{{}^L F_N \rho_L + {}^R F_N \rho_R}{{}^L F_N + {}^R F_N}, \quad (3.1)$$

where  ${}^m F_N$  and  $\rho_m$  are the normal force and the  $\mathbf{p}_{\text{ZMP}}$  position vector for the foot  $\mathbf{m}$  with

$$\mathbf{m} = \begin{cases} \mathbf{L} & \text{for the left foot} \\ \mathbf{R} & \text{for the right foot} \end{cases}. \quad (3.2)$$

The LIPM relates the  $\mathbf{p}_{\text{ZMP}}$  with the CoM dynamics as

$$\ddot{\mathbf{c}} = \frac{g}{z_c} (\mathbf{c} - \mathbf{p}_{\text{ZMP}}), \quad (3.3)$$

where  $g$  is the constant gravity acceleration and  $\ddot{\mathbf{c}}$  the CoM acceleration. This model is convenient since it can be written in a discrete state space representation. Also, linear methods of estimation can be implemented on it.

The biped base is assigned the frame  $O_b$  as in Figure 3.2. The IMU consisting of triaxial accelerometer and a triaxial gyro unit has the frame  $O_I$  and located at a position  $r_I$  and attitude  $A_I^b$  with respect to  $O_b$ . Bearing in mind these frames, the acceleration of  $O_b$  can be calculated using the IMU readings. And hence the CoM acceleration can be calculated if it is at  $O_b$ . However, the CoM frame origin is not necessarily to be the same as the base frame. The CoM may have an offset  $\mathbf{c}_{\text{offset}}$ . An example of this offset is shown in Figure 3.2, the CoM has  $x_{\text{offset}}$  from the base frame which has to be considered. Note that  $O_I$  and  $O_b$  are two points on the same rigid body, thus their angular velocities are the same. Accordingly, the IMU output acceleration  $\dot{\mathbf{v}}_I$  and angular velocity  $\boldsymbol{\omega}_I$  are utilized to compute  $\ddot{\mathbf{c}}$  in the world frame  $O_w$  as

$$\ddot{\mathbf{c}}^w = A_I^w \dot{\mathbf{v}}_I + A_I^w \boldsymbol{\omega}_I \times \left( A_I^w \boldsymbol{\omega}_I \times \left( r_I^w + \mathbf{c}_{\text{offset}}^w \right) \right) + A_I^w \dot{\boldsymbol{\omega}}_I \times \left( r_I^w + \mathbf{c}_{\text{offset}}^w \right), \quad (3.4)$$

where  $r_I^w$  and  $\mathbf{c}_{\text{offset}}^w$  are respectively  $r_I$  and  $\mathbf{c}_{\text{offset}}$  as expressed in the world frame.

**Assumption:**  $\mathbf{c}_{\text{offset}}$  is assumed to be constant in the body frame.

The computed acceleration from (3.4) is expressed in the body frame as

$$\ddot{\mathbf{c}} = \mathbf{A}_b^T \ddot{\mathbf{c}}^w, \quad (3.5)$$

Here  $\mathbf{A}_b$  is the attitude of the frame  $O_b$  with respect to world frame  $O_w$  and defined by

$$\mathbf{A}_b = A_I^w A_b^I. \quad (3.6)$$

The acceleration expression  $\ddot{\mathbf{c}}$  is utilized for the state estimation in the next subsection

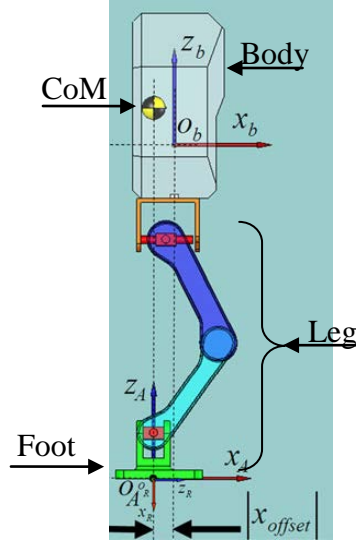


Figure 3.2: Base frame offset,  $O_b$  is the body base frame origin.

### 3.2 Estimation of CoM variables

The CoM position, velocity and acceleration are estimated using (3.3). The LIPM can be written in several discrete state space models depending on the considered states, inputs and measurements [69, 103, 104]. Here, the available data are the IMU acceleration and  $\mathbf{p}_{ZMP}^{F_N}$ , then (3.3) can be written in two state space forms: Form 1 and Form 2. Each has its own characteristics and conditions. The former is known in the literature; however the latter is introduced in this thesis work to be used in cases where the former fails.

#### 3.2.1 Form 1

This form considers the states as  $\mathbf{x} = [\mathbf{c}^T \quad \dot{\mathbf{c}}^T \quad \ddot{\mathbf{c}}^T]^T$ . With this state description, (3.3) can be written [69] as

$$\frac{d}{dt} \begin{bmatrix} \mathbf{c} \\ \dot{\mathbf{c}} \\ \ddot{\mathbf{c}} \end{bmatrix} = \begin{bmatrix} 0_3 & I_3 & 0_3 \\ 0_3 & 0_3 & I_3 \\ 0_3 & 0_3 & 0_3 \end{bmatrix} \begin{bmatrix} \mathbf{c} \\ \dot{\mathbf{c}} \\ \ddot{\mathbf{c}} \end{bmatrix} + \begin{bmatrix} 0_3 \\ 0_3 \\ I_3 \end{bmatrix} \ddot{\mathbf{c}}, \quad (3.7)$$

and

$$\mathbf{Y} = \begin{bmatrix} I_3 & 0_3 & -\frac{z_c}{g} I_3 \end{bmatrix} \begin{bmatrix} \mathbf{c} \\ \dot{\mathbf{c}} \\ \ddot{\mathbf{c}} \end{bmatrix}. \quad (3.8)$$

In discrete from, (3.7) and (3.8) correspond to

$$\begin{bmatrix} \mathbf{c} \\ \dot{\mathbf{c}} \\ \ddot{\mathbf{c}} \end{bmatrix}_k = \underbrace{\begin{bmatrix} I_3 & I_3 T & I_3 0.5 T^2 \\ 0_3 & I_3 & I_3 T \\ 0_3 & 0_3 & I_3 \end{bmatrix}}_A \begin{bmatrix} \mathbf{c} \\ \dot{\mathbf{c}} \\ \ddot{\mathbf{c}} \end{bmatrix}_{k-1} + \underbrace{\begin{bmatrix} 0_3 \\ 0_3 \\ T I_3 \end{bmatrix}}_B \ddot{\mathbf{c}}_k + \mathbf{w}_{k-1}, \quad (3.9)$$

and

$$\mathbf{Y}_k = \underbrace{\begin{bmatrix} I_3 & 0_3 & -\frac{z_c}{g} I_3 \end{bmatrix}}_C \begin{bmatrix} \mathbf{c} \\ \dot{\mathbf{c}} \\ \ddot{\mathbf{c}} \end{bmatrix}_k + \mathbf{v}_k, \quad (3.10)$$

with

$$\ddot{\mathbf{c}}_k = \frac{\ddot{\mathbf{c}}_k - \ddot{\mathbf{c}}_{k-1}}{T}. \quad (3.11)$$

Here  $k$  is the time index,  $\mathbf{Y}$  the measurement vector and  $\dot{\mathbf{c}}$  the CoM velocity. The input  $\ddot{\mathbf{c}}$  is piecewise constant over the sampling time interval  $T$ , i.e.  $\ddot{\mathbf{c}}(t) = \ddot{\mathbf{c}}_k$ ,  $t_k \leq t < t_{k+1} = t_k + T$ .  $\mathbf{w}$  and  $\mathbf{v}$  are the process and measurements noises respectively and they are defined as in (2.24). This form is observable one and preferred when:

- $\mathbf{c}_{offset}$  is known and the IMU location is known too. Thus the  $\mathbf{p}_{ZMP}^{F_N}$  is correctly measured. Then, the model (3.9) and (3.10) along with (3.11) are used directly in the stable AKF (2.28) - (2.38) with the state vector  $\mathbf{x} = [\mathbf{c}^T \quad \dot{\mathbf{c}}^T \quad \ddot{\mathbf{c}}^T]^T$  to estimate the states. After



that, the base frame position  $\mathbf{p}_b$  and velocity  $\mathbf{v}_b$ , as expressed in the world frame  $O_w$ , are calculated using the estimated states  $\hat{\mathbf{c}}$  and  $\hat{\dot{\mathbf{c}}}$  as:

$$\mathbf{p}_b = \mathbf{A}_b \left( \hat{\mathbf{c}} + \mathbf{c}_{offset} \right), \quad (3.12)$$

and

$$\mathbf{v}_b = \mathbf{A}_b \left( \hat{\dot{\mathbf{c}}} + \left( \mathbf{A}_I^b \boldsymbol{\omega}_I \right) \times \mathbf{c}_{offset} \right), \quad (3.13)$$

respectively.

- $\mathbf{p}_{ZMP}^{F_N}$  is correctly measured while the accelerometer position has some uncertainty. This leads to an error in the  $\mathbf{p}_{ZMP}$  called  $\mathbf{p}_{ZMP}^{err}$ . This error is used to estimate this uncertainty as shown later. If there is no position error or uncertainty, the  $\mathbf{p}_{ZMP}^{err}$  represents the external force applied on the biped.

### 3.2.2 Form 2

This form differs from form 1 in terms of inputs, outputs and states. Here the measured time derivative  $\dot{\mathbf{p}}_{ZMP}^{F_N}$  is the input and the output is the CoM acceleration.  $\mathbf{p}_{ZMP}^{F_N}$  is included in the states. This model is used when the measured acceleration is correct while the measured  $\mathbf{p}_{ZMP}^{F_N}$  has uncertainty. One advantage of this form is that the uncertainty is reduced when using  $\dot{\mathbf{p}}_{ZMP}^{F_N}$ . This can be explained as follows: the measured  $\mathbf{p}_{ZMP}^{F_N}$  has position and acceleration errors, since the position error is constant in the body frame, i.e.  $\mathbf{c}_{offset}(k) = \mathbf{c}_{offset}(k-1)$ , then this error is canceled by using the derivative. The form is built first by taking the time derivative of (3.3) as

$$\ddot{\mathbf{c}} = \frac{\mathbf{g}}{z_c} \left( \dot{\mathbf{c}} - \dot{\mathbf{p}}_{ZMP}^{F_N} \right), \quad (3.14)$$

then, by using the backward Euler method with sampling time  $T$ , the acceleration at the current time instant  $k$  for the discrete form of (3.14) is

$$\ddot{\mathbf{c}}(k) = T \frac{g}{z_c} (\dot{\mathbf{c}}(k-1) - \dot{\mathbf{p}}_{\text{ZMP}}^{F_N}(k-1)) + \ddot{\mathbf{c}}(k-1), \quad (3.15)$$

where

$$\dot{\mathbf{p}}_{\text{ZMP}}^{F_N}(k-1) = \frac{\mathbf{p}_{\text{ZMP}}^{F_N}(k) - \mathbf{p}_{\text{ZMP}}^{F_N}(k-1)}{T} \quad (3.16)$$

Let  $(\mathbf{c}^T \quad \dot{\mathbf{c}}^T \quad \ddot{\mathbf{c}}^T \quad (\mathbf{p}_{\text{ZMP}}^{F_N})^T)^T$  be the states, then the discrete state space is

$$\begin{pmatrix} \mathbf{c} \\ \dot{\mathbf{c}} \\ \ddot{\mathbf{c}} \\ \mathbf{p}_{\text{ZMP}}^{F_N} \end{pmatrix} (k) = \begin{bmatrix} 1 & T & 0.5T^2 & 0 \\ 0 & 1 & T & 0 \\ 0 & \frac{g}{z_c}T & 1 & 0 \\ 0 & 0 & 0 & 1 \end{bmatrix} \begin{pmatrix} \mathbf{c} \\ \dot{\mathbf{c}} \\ \ddot{\mathbf{c}} \\ \mathbf{p}_{\text{ZMP}}^{F_N} \end{pmatrix} (k-1) + \begin{bmatrix} 0 \\ 0 \\ -\frac{g}{z_c}T \\ T \end{bmatrix} \dot{\mathbf{p}}_{\text{ZMP}}^{F_N}(k-1) + \mathbf{w}(k-1), \quad (3.17)$$

and

$$\mathbf{Y} = [0 \quad 0 \quad 1 \quad 0] \begin{pmatrix} \mathbf{c} \\ \dot{\mathbf{c}} \\ \ddot{\mathbf{c}} \\ \mathbf{p}_{\text{ZMP}}^{F_N} \end{pmatrix} (k) + v_k. \quad (3.18)$$

Then, the model (3.17) and (3.18) along with (3.16) and (3.1) are used directly in the stable AKF (2.28) - (2.38) with the states vector  $\mathbf{x} = (\mathbf{c}^T \quad \dot{\mathbf{c}}^T \quad \ddot{\mathbf{c}}^T \quad (\mathbf{p}_{\text{ZMP}}^{F_N})^T)^T$  to estimate the states.

However, the estimated velocity state  $\hat{\mathbf{c}}$  requires post processing due to the noise and peaks that show up. It is filtered with a filter constant  $g_3 \in (0,1)$ . Calling the filtered version  $\hat{\mathbf{c}}_{\text{filtered}}$ , then it can be expressed as

$$\hat{\mathbf{c}}_{\text{filtered}}(k) = g_3 \hat{\mathbf{c}}(k) + (1 - g_3) \hat{\mathbf{c}}_{\text{filtered}}(k-1), \quad (3.19)$$

after that, the velocity  $\mathbf{v}_b$ , as expressed in the world frame, is calculated using  $\hat{\mathbf{c}}_{\text{filtered}}$  as

$$\mathbf{v}_b(k) = \mathbf{A}_b(k) \left( \hat{\mathbf{c}}_{filtered}(k) + \left( \mathbf{A}_I^b \boldsymbol{\omega}_I(k) \right) \times \mathbf{c}_{offset}(k) \right) \quad (3.20)$$

This form is preferred when the measured  $\mathbf{p}_{ZMP}^{F_N}$  has modeling error. This is because the modeling error is constant and its time derivative is equal to zero. Thus its effect is canceled.

### 3.3 The error in the $\mathbf{p}_{ZMP}$

The  $\mathbf{p}_{ZMP}$  trajectory can be measured using the force sensors as in (3.1). Also, it can be calculated from (3.3) as

$$\mathbf{p}_{ZMP} = \mathbf{c} - \frac{z_c}{g} \ddot{\mathbf{c}}, \quad (3.21)$$

In the ideal case the results of both (3.1) and (3.21) are the same. However, modeling and acceleration errors lead to  $\mathbf{p}_{ZMP}^{err}$ . Two errors are possible, position modeling error like  $\mathbf{c}_{offset}$  and acceleration error  $\Delta \ddot{\mathbf{c}}$ . The position error  $\mathbf{c}_{offset}$  exists if the body frame position  $\mathbf{p}_b$  is considered without including  $x_{offset}$  as in Figure 3.2. The acceleration error  $\Delta \ddot{\mathbf{c}}$  exists if the accelerometer has uncertainty in its position with respect to the CoM or an external acceleration is applied. Considering the frame  $O_b$  as the origin of the body, then  $\mathbf{p}_{ZMP}$  is stated mathematically as

$$\mathbf{p}_{ZMP} = \left( \mathbf{A}_b^T \mathbf{p}_b - \mathbf{c}_{offset} \right) - \frac{z_c}{g} \left( \mathbf{A}_b^T \ddot{\mathbf{p}}_b - \Delta \ddot{\mathbf{c}} \right). \quad (3.22)$$

Accordingly,  $\mathbf{p}_{ZMP}^{err}$  is expressed as

$$\mathbf{p}_{ZMP}^{err} = \mathbf{p}_{ZMP}^{F_N} - \left( \left( \mathbf{A}_b^T \mathbf{p}_b - \mathbf{c}_{offset} \right) - \frac{z_c}{g} \left( \mathbf{A}_b^T \ddot{\mathbf{p}}_b - \Delta \ddot{\mathbf{c}} \right) \right). \quad (3.23)$$

This error has both the position and acceleration errors. In terms of estimated states, the error can be written as ,

$$\mathbf{p}_{\text{ZMP}}^{\text{err}}(k) = \underbrace{\mathbf{p}_{\text{ZMP}}^{F_N}(k)}_{\text{measured}} - \left( \hat{\mathbf{c}}(k) - \frac{z_c}{g} \hat{\mathbf{c}}(k) \right), \quad (3.24)$$

where the  $\mathbf{p}_{\text{ZMP}}^{F_N}$  in (3.24) is the measured one from (3.1). This equation can be interpreted as follows: The error  $\mathbf{p}_{\text{ZMP}}^{\text{err}}$  is the difference between the measured  $\mathbf{p}_{\text{ZMP}}^{F_N}$  based on force sensor readings and the measured  $\mathbf{p}_{\text{ZMP}}$  based on acceleration sensor measurements. As clear from (3.23) and (3.24), the error signal  $\mathbf{p}_{\text{ZMP}}^{\text{err}}$  is composed of modeling and acceleration errors. In this thesis the modeling error is assumed to be the low frequency component of  $\mathbf{p}_{\text{ZMP}}^{\text{err}}$ . Therefore, a low pass filtering approach is used to estimate the modeling error and then the estimated error is used to correct the estimated states.

### 3.4 Results

Experimental and simulation tests are conducted on SURALP ( Sabanci University Robotics Research Laboratory Platform (Figure 3.3)) [26] and its model while walking. SURALP is equipped by force/torque sensors located at the feet ankles and a three-axes accelerometer located at the base frame. The force/torque sensors are used to calculate  $\mathbf{p}_{\text{ZMP}}^{F_N}$ . While walking, the biped was not subjected to external forces. The simulation model is a 12 degrees of freedom DOF biped model. It consists of two legs, each has 6 DOF, and a trunk connecting them. The hip has three joint axes, the ankle has two joints and the knee has one joint (Figure 3.4). The dimensions are taken to match SURALP. The details of contact modeling and simulation algorithm are in [105]. The body frame has an offset  $(x_{\text{offset}})$  of 35 mm. The IMU is located with attitude  $A_b^l = I_3$ , where  $I_3$  is a  $3 \times 3$  identity matrix. In the simulations, the three-axes IMU which is available in MATLAB simulink is used. It is composed of three-axes accelerometer and three -axes gyroscope with contaminated noise. Each foot has four triaxial force sensors. These sensors are located at known positions with respect to the foot frame [26]. The experimental and simulation parameter values and the initialization of AKF for the  $x$ - and  $y$ - directions are identical. They are presented for one direction in Table 3.1.



Figure 3.3: SURALP

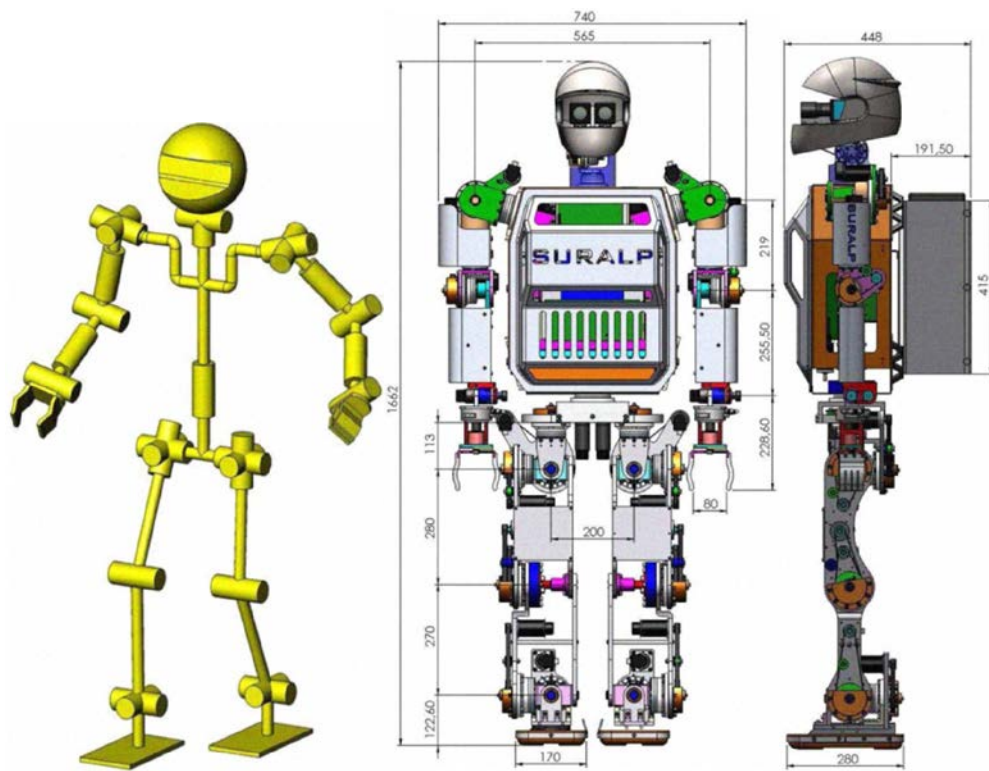


Figure 3.4: The kinematic arrangement of SURALP

Table 3.1: Experimental and simulation parameters values and the initializations of AKF

Parameter	Form 2		Form1	
	Value		Value	
	Experimental	Simulation	Experimental	Simulation
$T$	0.001 sec	0.001 sec	0.001 sec	0.001 sec
$N_Q$	2000	2000	2000	2000
$N_R$	1000	1000	1000	1000
$x_0$	$[0 \ 0 \ 0 \ 0]^T$	$[0 \ 0 \ 0 \ 0]^T$	$[0 \ 0 \ 0]^T$	$[0 \ 0 \ 0]^T$
$Q_0$	$I_4$	$I_4$	$I_3$	$I_3$
$R_0$	1	1	1	1
$P_0$	$100I_4$	$100I_4$	$100I_3$	$100I_3$
$\bar{\Lambda}_0$	$[0 \ 0 \ 0 \ 0]^T$	$[0 \ 0 \ 0 \ 0]^T$	$[0 \ 0 \ 0]^T$	$[0 \ 0 \ 0]^T$
$\bar{e}_0$	0	0	0	0
$g_3$	0.0025	0.002	-	-

To measure the performance, the root mean square error (*RMSE*) is used. It is defined as

$$RMSE = \sqrt{\frac{\sum_{i=1}^{i=N_s} (\hat{\Xi}(i) - \Xi(i))^2}{N_s}}, \quad (3.25)$$

where  $\hat{\Xi}$  and  $\Xi$  are the estimated and true variables respectively.

The tests are conducted to examine four conditions: Uncertain acceleration measurements due to position uncertainty with correct  $\mathbf{p}_{ZMP}^{F_N}$  measurement; uncertain acceleration measurement due to external acceleration with correct  $\mathbf{p}_{ZMP}^{F_N}$  measurement; correct acceleration measurements with uncertain  $\mathbf{p}_{ZMP}^{F_N}$  measurements; and correct acceleration and  $\mathbf{p}_{ZMP}^{F_N}$  measurements.

### 3.4.1 Uncertain acceleration measurements due to position uncertainty (experiments)

In this experiment, the accelerometer position has uncertainty while the measured  $\mathbf{p}_{ZMP}^{F_N}$  is correct. The CoM position must follow the  $\mathbf{p}_{ZMP}^{F_N}$ . Therefore, the estimated CoM position is compared with the  $\mathbf{p}_{ZMP}^{F_N}$ . Figure 3.5 shows the  $\mathbf{p}_{ZMP}^{F_N}$  and the estimated position in the  $x$ -direction using the two forms introduced in the previous sections. Initially, the biped is not walking as observed from the constant  $\mathbf{p}_{ZMP}^{F_N} \equiv \mathbf{p}_{ZMP}$  trajectory. After that the biped starts walking, the measured  $\mathbf{p}_{ZMP}^{F_N} \equiv \mathbf{p}_{ZMP}$  trajectory is shown as the blue dashed line. Form 1 tracks the  $\mathbf{p}_{ZMP}^{F_N}$ . This is expected since it uses the correct  $\mathbf{p}_{ZMP}^{F_N}$  in the correction stage of the AKF. Form 2 estimation has a constant offset, this offset is due taking the first derivative of  $\mathbf{p}_{ZMP}^{F_N}$ . The value of the offset is estimated as in Figure 3.6.a using form 2. Accordingly, the true state  $\hat{\mathbf{c}}_{true}$  of Form 2 is

$$\hat{\mathbf{c}}_{true}(k) = \hat{\mathbf{c}}(k) + \hat{\mathbf{c}}_{offset}(k), \quad (3.26)$$

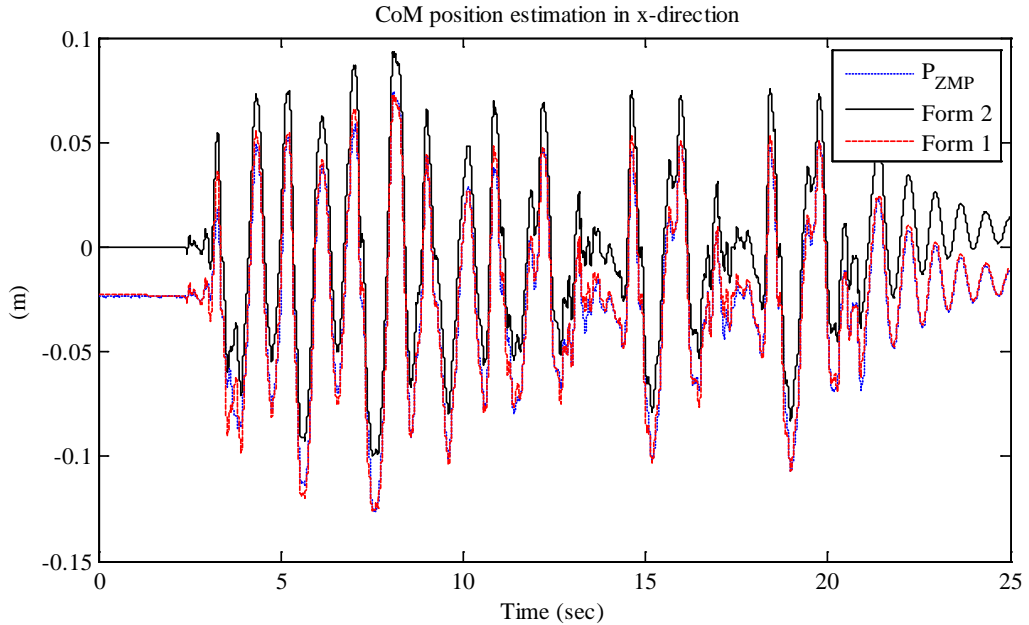


Figure 3.5: CoM position in the  $x$ -direction

The offset estimation converges exponentially and starts even though the biped is not walking. This is due to that the measured  $\mathbf{p}_{ZMP}^{F_N}$  depends on the force measurements not the

body acceleration. Furthermore, the measured  $\mathbf{p}_{ZMP}^{F_N}$  is used directly to calculate the  $\mathbf{p}_{ZMP}^{err}$  and hence to estimate the offset.

Figure 3.6.b shows that when the offset is compensated as in (3.26), both forms have similar position estimation behavior. One observation is that when the biped starts walking, the RMSE of Form 1 increased dramatically while the RMSE of Form 2 has much less increment. The estimated CoM velocity using the two forms is shown in Figure 3.7. As observed, Form 2 has zero estimated velocity while the biped is not walking. Further, at the end of the walking period (25 sec), the velocity converges to zero. However, Form 1 has a nonzero velocity value even the biped is not walking and the velocity converges to a nonzero value at the end of the walk. While walking both forms have similar behavior.

It can be conclude that Form 1 and form 2 have similar behavior for this case.

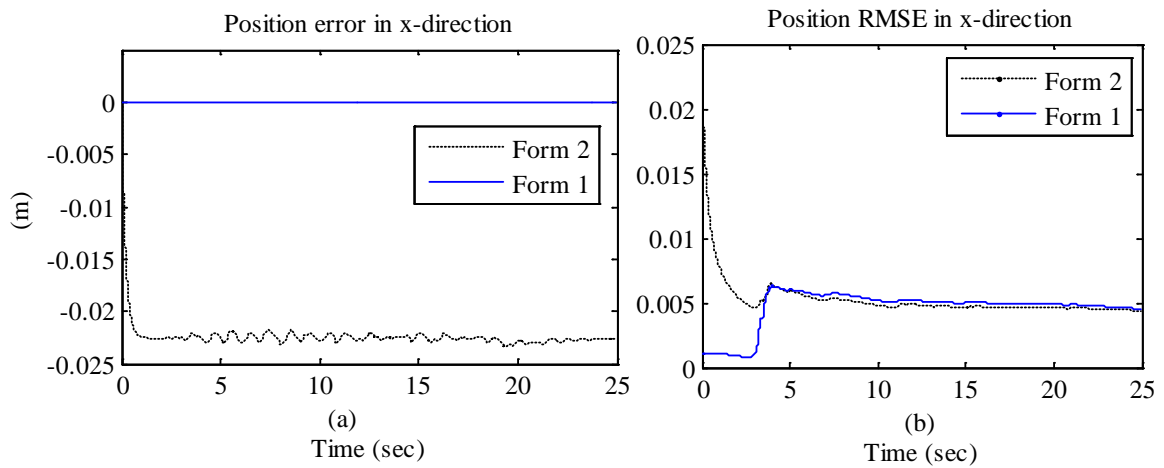


Figure 3.6: (a) Position error in the  $x$ – direction from both forms. and (b) position RMSE in the  $x$ – direction from both forms



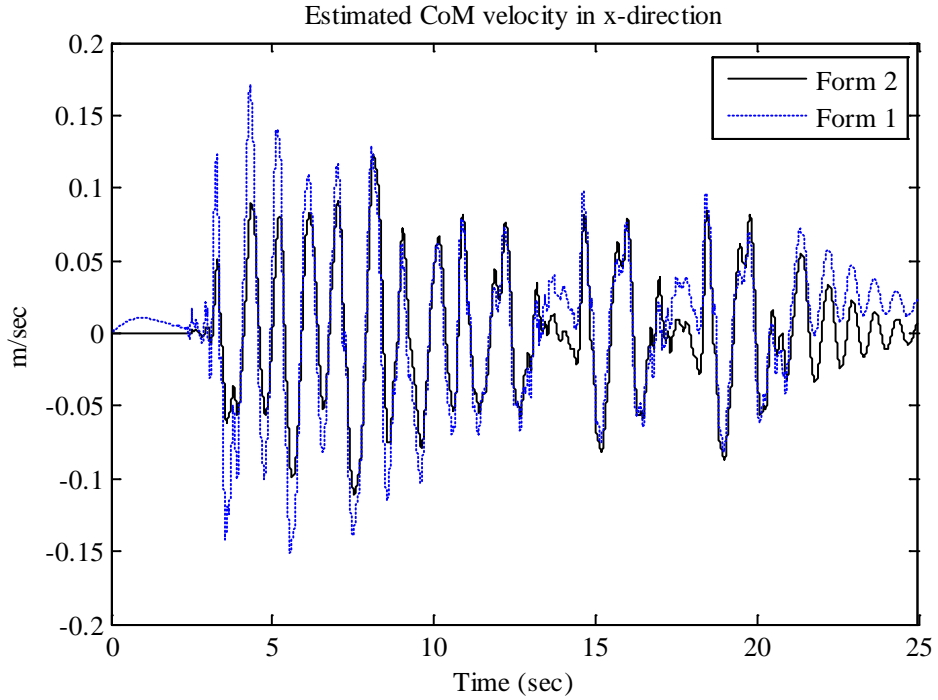


Figure 3.7: Estimated CoM velocity in  $x$  – direction

The same discussion is valid for the estimation in the  $y$  – direction. The position estimate is shown in Figure 3.8, the error performance in Figure 3.9 and the estimated velocity in Figure 3.10.

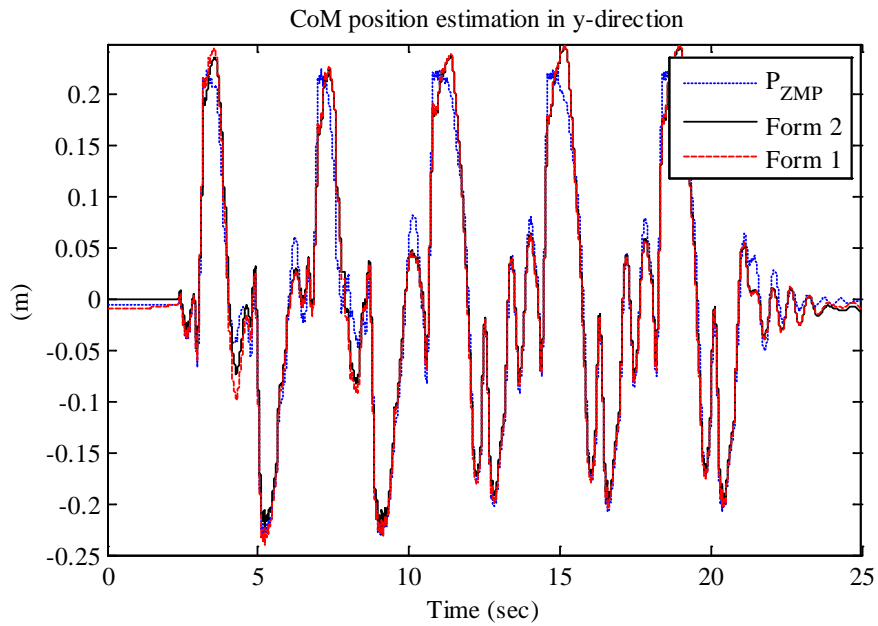


Figure 3.8: CoM position in the  $y$  – direction

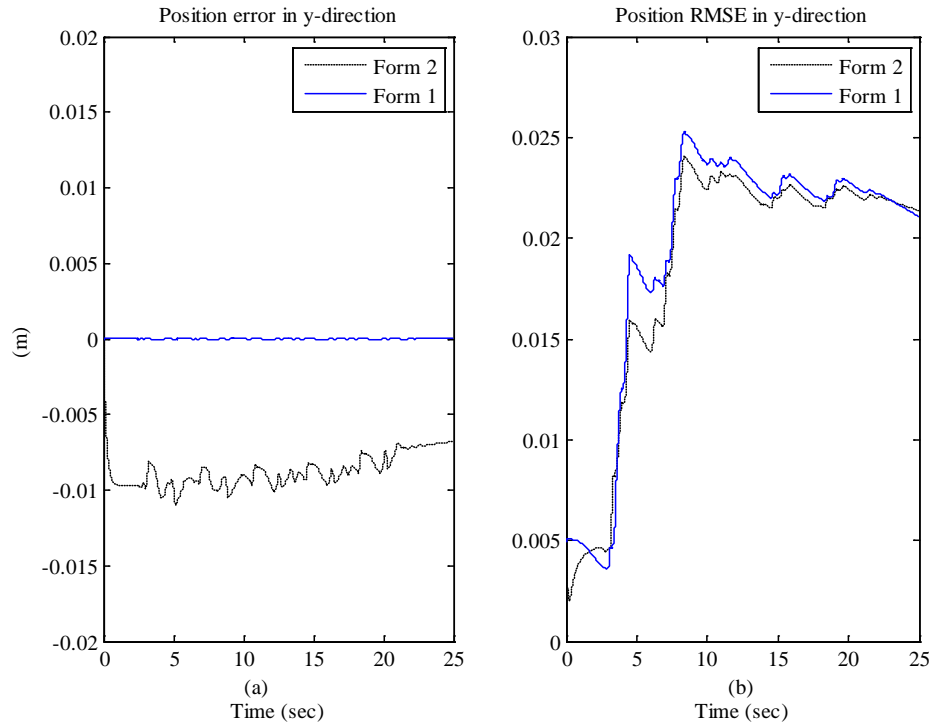


Figure 3.9: (a) Position error in the  $y$  – direction from both forms. and (b) position RMSE in the  $y$  – direction from both forms

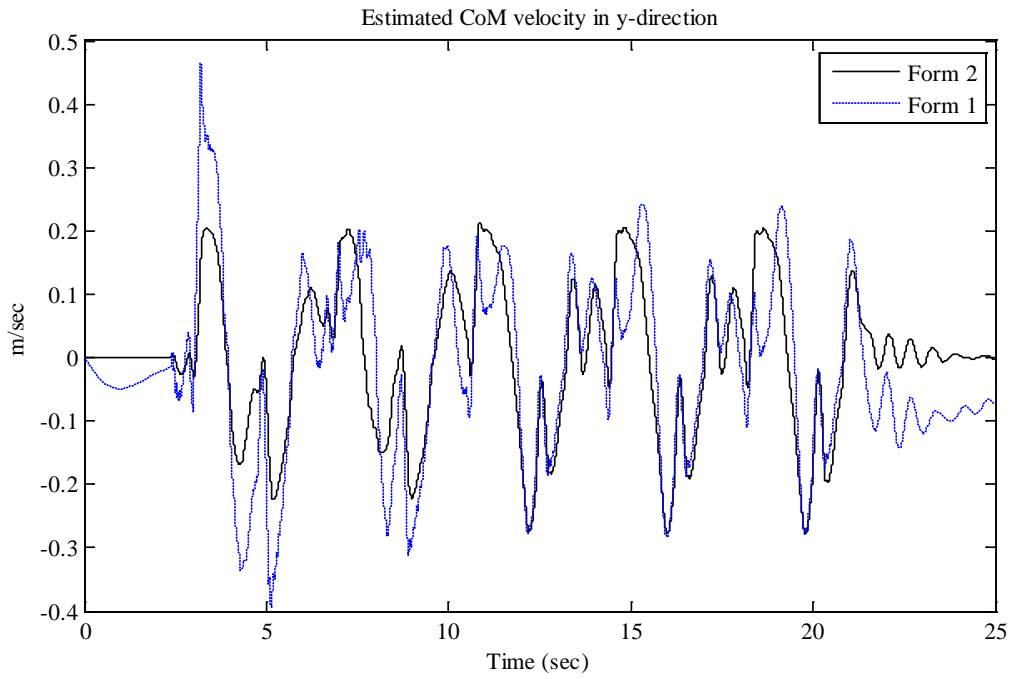


Figure 3.10: Estimated CoM velocity in  $y$  – direction

### 3.4.2 Uncertain acceleration measurement due to external acceleration (simulation)

In this simulation, a constant acceleration error  $\Delta\ddot{c} = 0.5\text{ m/sec}^2$  is considered in the  $x$ -direction. Since Form 1 has the input  $\ddot{c}$ , then the constant acceleration error is canceled. Hence it will not affect the estimation. Furthermore, Form 1 can estimate it (Figure 3.11), the estimated acceleration error  $\Delta\hat{c} = 0.45$ . Form 2 fails in this case. This is expected since the wrongly measured acceleration is used in correcting the final states in the AKF. The estimated  $\Delta\hat{c}$  diverges with time as observed in Figure 3.11. Since no offset errors are introduced, the estimated error converges to zero. The velocity estimation performance is shown in Figure 3.12. Although the RMSE of form 1 is larger, it decreases with time. However, the RMSE of Form 2 increases.

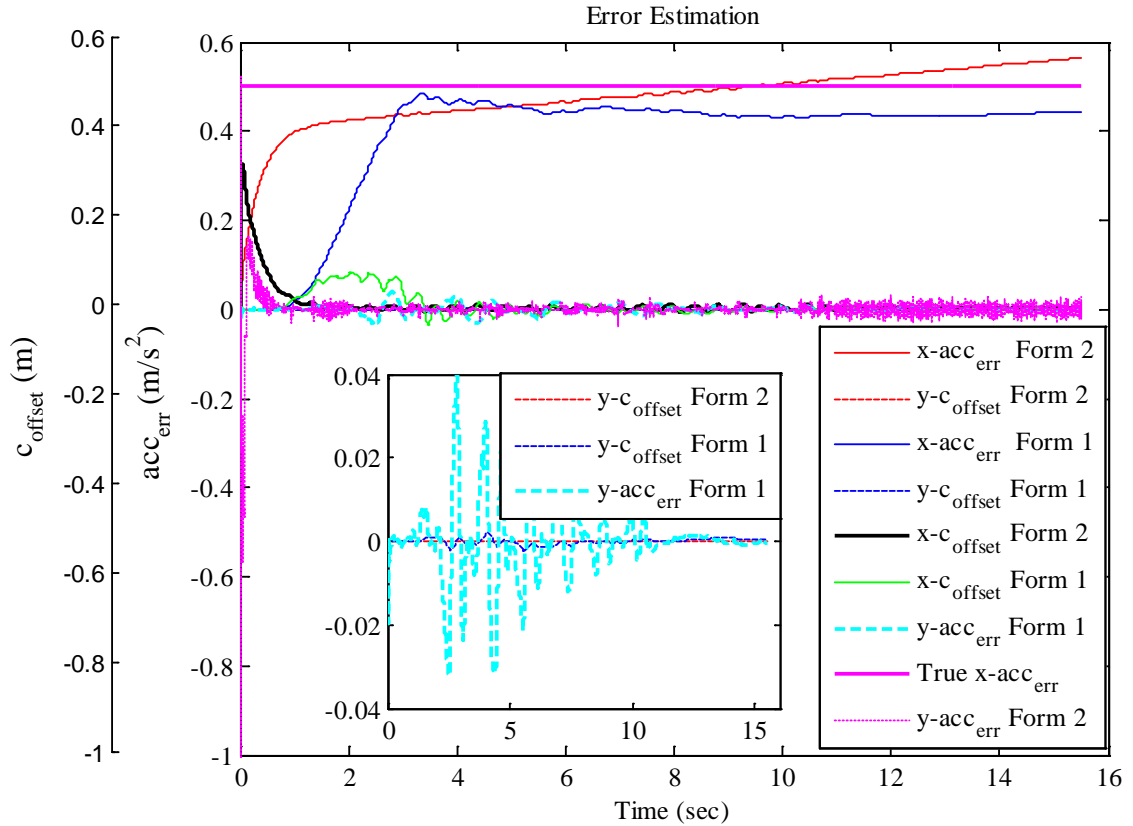


Figure 3.11: Error estimation with  $\Delta\ddot{c}_x = 0.5$ .

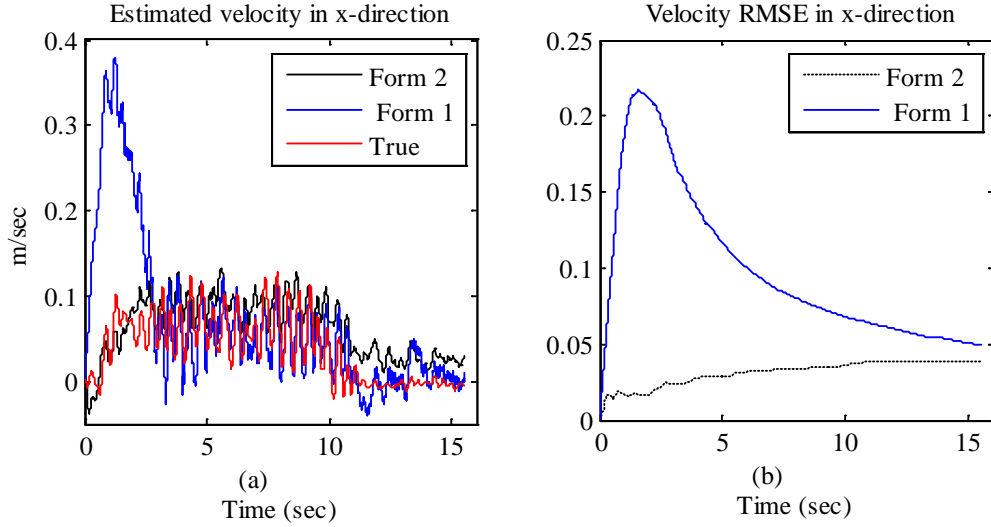


Figure 3.12: (a) Estimated velocity in  $x$  – direction and (b) the corresponding RMSE

### 3.4.3 Uncertain $\mathbf{p}_{ZMP}^{F_N}$ measurements (simulation)

In this simulation, the accelerometer has a known position and no external acceleration. The measured  $\mathbf{p}_{ZMP}^{F_N}$  has position uncertainty. In these tests, a modeling error in the  $x$ -direction of 0.035m is added. It is expected that this error will not affect Form 2 since  $\dot{\mathbf{p}}_{ZMP}^{F_N}$  is considered as an input and thus the constant modeling error is canceled. Form 1 is affected since it uses  $\mathbf{p}_{ZMP}^{F_N}$  with the error in the correction stage of the AKF. This is confirmed in Figure 3.13; form 2 compensated for this modeling error and estimated it, while Form 1 failed. This modeling error has limited effect on the velocity estimation and both forms have similar estimated velocity behavior (Figure 3.14).

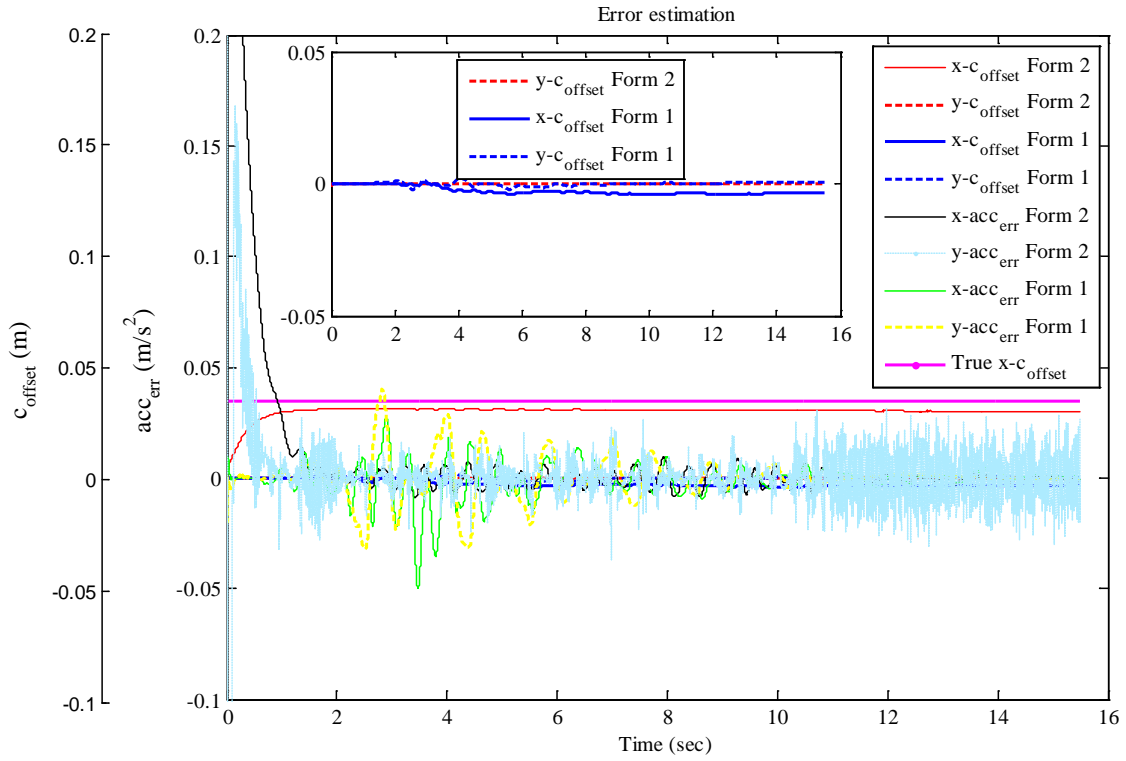


Figure 3.13: Error estimation with  $x_{offset} = 0.035$

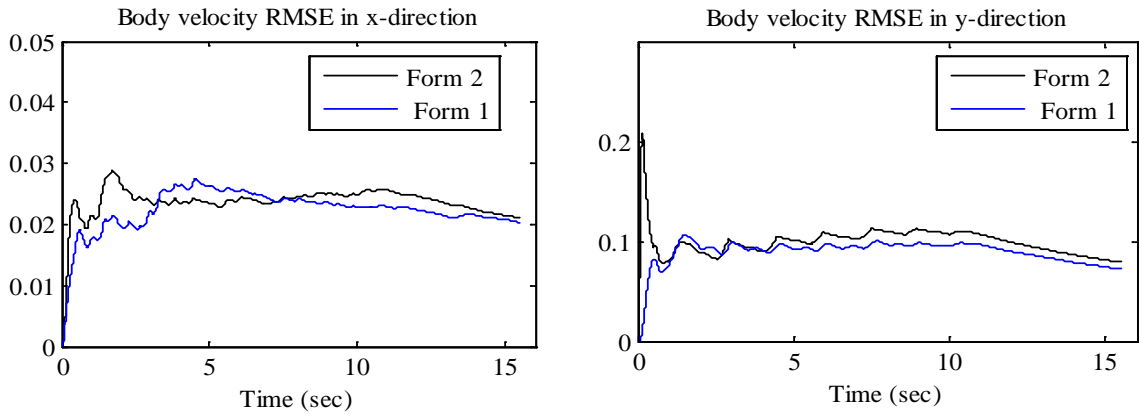


Figure 3.14: RMSE in both directions for both forms

### 3.4.4 Correct measurements

Here, neither modeling errors nor external accelerations are added and both the accelerometer and the measured  $\mathbf{p}_{ZMP}^{F_N}$  are assumed accurate. Both of the forms have the same performance as shown in the error plot in Figure 3.15. The estimated offset and acceleration error converge to zero.

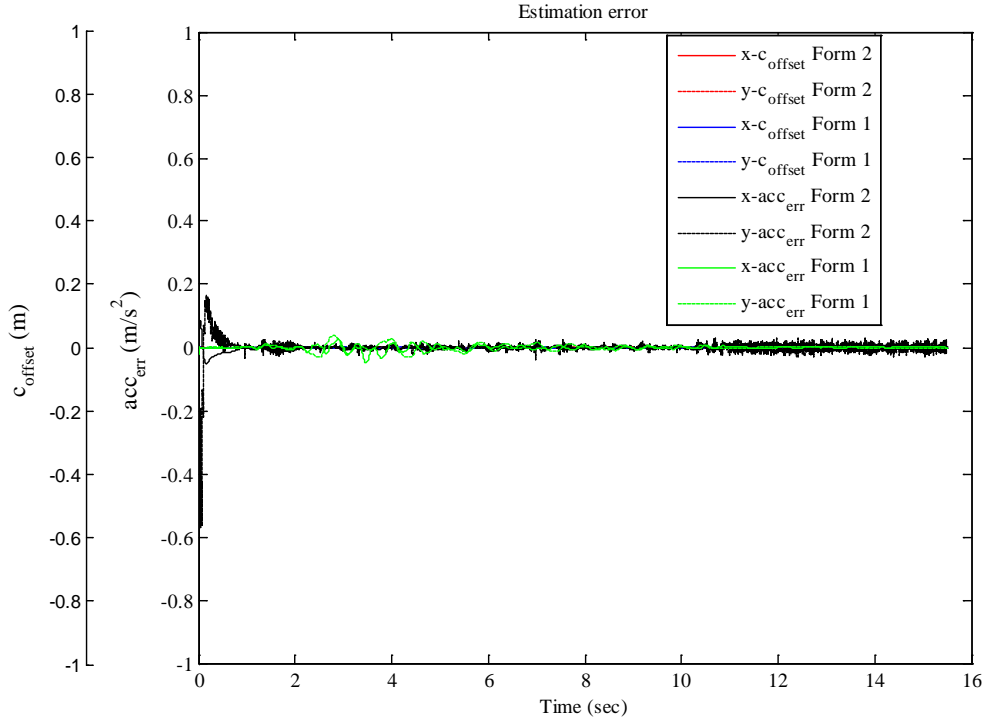


Figure 3.15: Estimation error

### 3.5 Conclusion

A method to estimate the center of mass CoM position and its derivative and the disturbance effects on a walking biped robot is proposed. The method utilizes the robot body acceleration and the reactions forces at the robot feet. An AKF is employed for the states estimation based on the Linear Inverted Pendulum Model LIPM.

The LIPM is written in two state space forms: Form 1 and form 2. The former is well known and considers the CoM position and its first and second derivatives as the states. The input to this form is the CoM jerk and the output is the  $\mathbf{p}_{ZMP}$ . The latter is introduced

in this thesis, it considers the CoM position and its first and second derivatives and  $\mathbf{p}_{ZMP}^{F_N}$  as the states. The input to the form is  $\dot{\mathbf{p}}_{ZMP}^{F_N}$  and the output is the acceleration.

Two types of disturbances are estimated, modeling errors and external accelerations. The results demonstrate that both forms are equivalent when the measurements are correct and no disturbance exists. Also there are equivalent when the accelerometer has position uncertainty. However, Form 2 fails when there exists an external acceleration. On the other hand, form 1 fails when there are modeling errors in the measured  $\mathbf{p}_{ZMP}^{F_N}$ .

## Chapter 4

### 4 Joint Friction Estimation for Walking Bipeds

The joint friction of a non-slipping walking biped is estimated. A measurement-based strategy is used to estimate the joint friction online when the foot is in contact with the ground. This strategy does not necessitate a friction model. To estimate the friction, it employs a reduced dynamical model of the biped and utilizes the measured ground reaction forces and the IMU readings. It uses the estimated body attitude, body velocity and joint angular accelerations. However, when the leg is swinging, this strategy is inapplicable. Therefore, a friction model is adopted to represent the joint friction. Its parameters are identified adaptively using the estimated online friction whenever the foot is in contact. The estimated joint friction is used in the feedback torque control signal.

Joint angular accelerations have a significant role in the joint friction estimation. Therefore, two methods of joint angular acceleration estimation are employed: The first one uses the constraint of non-slipping walking and the other one uses a filtered dynamics model.

The method depends on the robot foot and base measurements, so we call it: Foot base sensor estimation FBSE. This chapter introduces the biped model, joint angular acceleration estimation methods, joint friction estimation methodology and the results.



#### 4.1 Biped dynamical model

The biped, which is considered here, consists of a body and two legs which are connected to it as in Figure 4.1. Its motion is defined in the fixed world frame  $O_w$ . The body is considered as the base link with the base coordinate system  $O_b$ . The hips and feet soles have coordinate frames too.

For this work, it is assumed that the biped is equipped with contact force sensors with frame origin  $O_F$  assembled at the feet soles [7], joint encoders attached to the joint actuators and an IMU with a frame origin  $O_I$ . The IMU is composed of a 3-axes accelerometer and a 3-axes gyroscope.

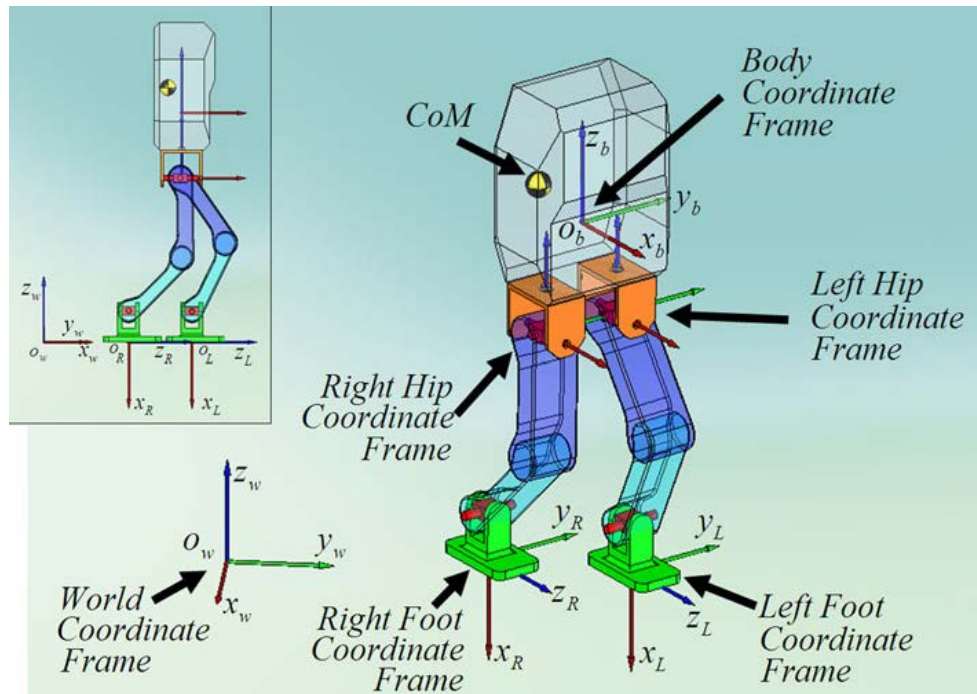


Figure 4.1. Coordinate systems.  $O_w$  and  $O_b$  stand for the origins of the world and body coordinate frames, respectively. The feet coordinate frames are fixed to the feet soles [8].

The biped interacts with the ground and is modeled as a free-fall manipulator. For a biped with  $N$  joints, and the defined generalized coordinates

$\mathbf{x}^T = [\mathbf{p}_b^T, \mathbf{A}_b^T, \boldsymbol{\theta}^T] \in R^3 \times SO(3) \times R^N$ , generalized velocities  $\mathbf{v}^T = [\mathbf{v}_b^T, \boldsymbol{\omega}_b^T, \boldsymbol{\omega}^T] \in R^3 \times R^3 \times R^N$  and generalized forces  $\mathbf{u}^T = [\mathbf{f}_b^T, \mathbf{n}_b^T, \boldsymbol{\tau}^T] \in R^3 \times R^3 \times R^N$ , the robot model is

$$\mathbf{H}(\mathbf{x})\dot{\mathbf{v}} + \mathbf{C}(\mathbf{x}, \mathbf{v})\mathbf{v} + \mathbf{g}(\mathbf{x}) + \mathbf{u}_F = \mathbf{u} + \mathbf{u}_E, \quad (4.1)$$

where  $\boldsymbol{\theta} \in R^N$  and  $\dot{\boldsymbol{\theta}} = \boldsymbol{\omega} \in R^N$  are the joint displacement and angular velocity vectors, respectively.  $\mathbf{A}_b \in SO(3)$  is the transformation matrix describing the orientation of body frame axes relative to the world axes.  $\mathbf{p}_b$  and  $\dot{\mathbf{p}}_b = \mathbf{v}_b$  are the position and linear velocity of the robot base-link coordinate frame center.  $\boldsymbol{\omega}_b$  is the angular velocity of the robot body coordinate frame.  $\mathbf{f}_b \in R^3$  and  $\mathbf{n}_b \in R^3$  are the force and torque vectors generated in the base-link by the legs, and  $\boldsymbol{\tau}$  is the generalized joint control vector.  $\mathbf{u}_F$  is the joint frictional forces vector. The matrix  $H$  represents the inertia, the  $\mathbf{C}(\mathbf{x}, \mathbf{v})$  matrix specifies the centrifugal and Coriolis effects and the  $\mathbf{g}(\mathbf{x})$  vector stands for the gravity effect. For simplification, let's use the term  $\mathbf{b}$  as  $\mathbf{b} = \mathbf{C}(\mathbf{x}, \mathbf{v})\mathbf{v} + \mathbf{g}(\mathbf{x})$  and rewrite (4.1) as

$$\mathbf{H} \begin{pmatrix} \dot{\mathbf{v}}_b \\ \dot{\boldsymbol{\omega}}_b \\ \ddot{\boldsymbol{\theta}}_L \\ \ddot{\boldsymbol{\theta}}_R \end{pmatrix} + \begin{pmatrix} \mathbf{b}_1 \\ \mathbf{b}_2 \\ \mathbf{b}_L \\ \mathbf{b}_R \end{pmatrix} + \begin{pmatrix} \mathbf{u}_{F_1} \\ \mathbf{u}_{F_2} \\ \mathbf{u}_{F_L} \\ \mathbf{u}_{F_R} \end{pmatrix} = \begin{pmatrix} \mathbf{f}_b \\ \mathbf{n}_b \\ \boldsymbol{\tau}_L \\ \boldsymbol{\tau}_R \end{pmatrix} + \begin{pmatrix} \mathbf{u}_{E_1} \\ \mathbf{u}_{E_2} \\ \mathbf{u}_{E_L} \\ \mathbf{u}_{E_R} \end{pmatrix}, \quad (4.2)$$

with

$$\mathbf{H} = \begin{pmatrix} H_{11} & H_{12} & H_{13} & H_{14} \\ H_{21} & H_{22} & H_{23} & H_{24} \\ H_{31} & H_{32} & H_{33} & 0 \\ H_{41} & H_{42} & 0 & H_{44} \end{pmatrix},$$

where  $H_{ij}$  for  $(i, j) \in \{1, 2, 3, 4\}$  are sub-matrices of the robot inertia matrix.  $\mathbf{u}_{E_1}$  is the net force effect and  $\mathbf{u}_{E_2}$  the net torque effect of the reaction forces on the base.  $\mathbf{u}_{E_L}$  and  $\mathbf{u}_{E_R}$  stand for the effect of reaction forces generated by environmental interaction on the robot joints for the left and right legs respectively. The subscripts  $(\ )_L$  and  $(\ )_R$  stand for the left and right legs respectively.

For joint friction estimation, (4.2) can be reduced as

$$\begin{pmatrix} H_{31} & H_{32} & H_{33} & 0 \\ H_{41} & H_{42} & 0 & H_{44} \end{pmatrix} \begin{pmatrix} \dot{\mathbf{v}}_b \\ \ddot{\boldsymbol{\theta}}_L \\ \ddot{\boldsymbol{\theta}}_R \end{pmatrix} + \begin{pmatrix} \mathbf{b}_L \\ \mathbf{b}_R \end{pmatrix} + \begin{pmatrix} \mathbf{u}_{F_L} \\ \mathbf{u}_{F_R} \end{pmatrix} = \begin{pmatrix} \boldsymbol{\tau}_L \\ \boldsymbol{\tau}_R \end{pmatrix} + \begin{pmatrix} \mathbf{u}_{E_L} \\ \mathbf{u}_{E_R} \end{pmatrix}, \quad (4.3)$$

which will be used as the basic equation for the joint friction estimation.

## 4.2 Joint friction estimation

In the proposed approach, the joint friction estimation depends on the knowledge of the applied joint control torque  $\boldsymbol{\tau}$  and the transmitted torque to the link  $\boldsymbol{\tau}^l$ . It can be stated mathematically as

$$\begin{pmatrix} \boldsymbol{\tau}_L \\ \boldsymbol{\tau}_R \end{pmatrix} = \begin{pmatrix} \mathbf{u}_{F_L} \\ \mathbf{u}_{F_R} \end{pmatrix} + \begin{pmatrix} \boldsymbol{\tau}_L^l \\ \boldsymbol{\tau}_R^l \end{pmatrix}, \quad (4.4)$$

where  $\boldsymbol{\tau}_L^l$  and  $\boldsymbol{\tau}_R^l$  are the transmitted torque to the manipulator's left and right leg links respectively. Referring to (4.2), the links torque vector can be represented by the reduced biped model as

$$\begin{pmatrix} \boldsymbol{\tau}_L^l \\ \boldsymbol{\tau}_R^l \end{pmatrix} = \bar{\mathbf{H}} \begin{pmatrix} \dot{\mathbf{v}}_b \\ \ddot{\boldsymbol{\theta}}_L \\ \ddot{\boldsymbol{\theta}}_R \end{pmatrix} + \begin{pmatrix} \mathbf{b}_L \\ \mathbf{b}_R \end{pmatrix} - \begin{pmatrix} \mathbf{u}_{E_L} \\ \mathbf{u}_{E_R} \end{pmatrix}, \quad (4.5)$$

with

$$\bar{\mathbf{H}} = \begin{pmatrix} H_{31} & H_{32} & H_{33} & 0 \\ H_{41} & H_{42} & 0 & H_{44} \end{pmatrix}. \quad (4.6)$$

In (4.5), the right hand-side is the response due to the vectors  $\boldsymbol{\tau}_L^l$  and  $\boldsymbol{\tau}_R^l$  from the total applied joint control torque vector. Moreover, it explains that the reaction forces are the net transmitted forces and torques to the robot's links.

The basic idea of the friction estimation is to compute the right hand-side of (4.5). The bias term components  $\mathbf{b}_L$  and  $\mathbf{b}_R$  contain the gravity and coriolis effects. Hence, the bias term can be formulated as

$$\mathbf{b}_m = \mathbf{f}_m(\mathbf{A}_b, \boldsymbol{\theta}_m, \boldsymbol{\omega}_m, \boldsymbol{\omega}_b, \mathbf{v}_b) . \quad (4.7)$$

$\mathbf{m}$  represents here either  $\mathbf{L}$  or  $\mathbf{R}$ , for the left and right feet, respectively. All of the variables required to compute  $\mathbf{b}_m$  are known either by direct measurements or estimation explained in Sections 3.2 and 2.6.

The effect of the reaction forces  $\mathbf{u}_{E_m}$  can be calculated based on the contact force sensors readings  $\mathbf{F}_{E_R}$  and  $\mathbf{F}_{E_L}$ . These forces  $\mathbf{F}_{E_m}$  are mapped to the links by using the Jacobian  $\mathbf{J}_{F_m}$  as

$$\mathbf{u}_{E_m} = \mathbf{J}_{F_m}^T(\mathbf{x})\mathbf{F}_{E_m} . \quad (4.8)$$

The Jacobian  $\mathbf{J}_{F_m}$  computation depends on the robot geometry which is known. The matrices  $H_{ij}$  for  $j \in \{1, 2, 3, 4\}, i \in \{3, 4\}$  depend on  $\boldsymbol{\theta}$  and  $\mathbf{A}_b$  only and they are both known too. The main difficulty is the existence of the angular acceleration terms which are in most cases not measured directly. One solution is using offline numerical differentiation [12]. However, it is inapplicable in the real time applications. This thesis proposes two methods: The application of the foot non-slipping constraint; and the application of the filtered dynamic model [86, 106].

#### 4.2.1 Non- slipping foot constraint

The non-slipping foot constraint is used to calculate the angular accelerations. Bipedes are not fixed to the ground, while walking they are switching from the double support (DS) phase to the single support (SS) phase and so forth. The acceleration of the foot frame  $\ddot{\mathbf{p}}_m$  can be obtained by double differentiating the position of the foot frame  $\mathbf{p}_m$  as

$$\mathbf{J}_m(\mathbf{x}) \begin{bmatrix} \dot{\mathbf{v}}_b \\ \dot{\boldsymbol{\omega}}_b \\ \dot{\boldsymbol{\theta}}_m \end{bmatrix} + \dot{\mathbf{J}}_m(\mathbf{x}) \begin{bmatrix} \mathbf{v}_b \\ \boldsymbol{\omega}_b \\ \boldsymbol{\theta}_m \end{bmatrix} = \ddot{\mathbf{p}}_m, \quad (4.9)$$

where  $\mathbf{J}_m$  is the Jacobian of the foot frame origin and it can be expressed in terms of its sub matrices  $\mathbf{J}_{m_i}, i = 1, 2, 3$  as

$$\mathbf{J}_m = \begin{bmatrix} \mathbf{J}_{m_1} & \mathbf{J}_{m_2} & \mathbf{J}_{m_3} \end{bmatrix}, \quad (4.10)$$

$\dot{\mathbf{J}}_m$  is the first derivative of  $\mathbf{J}_m$ . The base acceleration is measured, therefore (4.9) can be written as

$$\begin{bmatrix} \mathbf{J}_{m_2} & \mathbf{J}_{m_3} \end{bmatrix} \begin{bmatrix} \dot{\boldsymbol{\omega}}_b \\ \dot{\boldsymbol{\theta}}_m \end{bmatrix} = \ddot{\mathbf{p}}_m - \dot{\mathbf{J}}_m(\mathbf{x}) \begin{bmatrix} \mathbf{v}_b \\ \boldsymbol{\omega}_b \\ \boldsymbol{\theta}_m \end{bmatrix} - \mathbf{J}_{m_1} \dot{\mathbf{v}}_b. \quad (4.11)$$

The biped has two different phases. The estimation formulations for these phases are as follows:

#### 4.2.1.1 DS phase

In the DS phase, bearing in mind that there are neither feet accelerations nor slipping, i.e.  $\ddot{\mathbf{p}}_L = \ddot{\mathbf{p}}_R \approx 0$ , then (4.11) can be written for the left and right feet as

$$\begin{bmatrix} \mathbf{J}_{L_2} & \mathbf{J}_{L_3} \end{bmatrix} \begin{bmatrix} \dot{\boldsymbol{\omega}}_b \\ \dot{\boldsymbol{\theta}}_L \end{bmatrix} = -\dot{\mathbf{J}}_L(\mathbf{x}) \begin{bmatrix} \mathbf{v}_b \\ \boldsymbol{\omega}_b \\ \boldsymbol{\theta}_L \end{bmatrix} - \mathbf{J}_{L_1} \dot{\mathbf{v}}_b, \quad (4.12)$$

and

$$\begin{bmatrix} \mathbf{J}_{R_2} & \mathbf{J}_{R_3} \end{bmatrix} \begin{bmatrix} \dot{\boldsymbol{\omega}}_b \\ \dot{\boldsymbol{\theta}}_R \end{bmatrix} = -\dot{\mathbf{J}}_R(\mathbf{x}) \begin{bmatrix} \mathbf{v}_b \\ \boldsymbol{\omega}_b \\ \boldsymbol{\theta}_R \end{bmatrix} - \mathbf{J}_{R_1} \dot{\mathbf{v}}_b, \quad (4.13)$$

respectively. The above two equations i.e. (4.12) and (4.13) are written as

$$\begin{bmatrix} \mathbf{J}_{L_2} & \mathbf{J}_{L_3} & 0 \\ \mathbf{J}_{R_2} & 0 & \mathbf{J}_{R_3} \end{bmatrix} \begin{bmatrix} \dot{\boldsymbol{\omega}}_b \\ \ddot{\boldsymbol{\theta}}_L \\ \ddot{\boldsymbol{\theta}}_R \end{bmatrix} = \begin{bmatrix} -\dot{\mathbf{J}}_L(\mathbf{x}) \begin{bmatrix} \mathbf{v}_b \\ \boldsymbol{\omega}_b \\ \dot{\boldsymbol{\theta}}_L \end{bmatrix} - \mathbf{J}_{L_1} \dot{\mathbf{v}}_b \\ -\dot{\mathbf{J}}_R(\mathbf{x}) \begin{bmatrix} \mathbf{v}_b \\ \boldsymbol{\omega}_b \\ \dot{\boldsymbol{\theta}}_R \end{bmatrix} - \mathbf{J}_{R_1} \dot{\mathbf{v}}_b \end{bmatrix}. \quad (4.14)$$

Then the angular accelerations can be calculated as

$$\begin{bmatrix} \dot{\boldsymbol{\omega}}_b \\ \ddot{\boldsymbol{\theta}}_L \\ \ddot{\boldsymbol{\theta}}_R \end{bmatrix} = \mathbf{J}_{DS}^T (\mathbf{J}_{DS} \mathbf{J}_{DS}^T)^{-1} \Upsilon_{DS}, \quad (4.15)$$

where

$$\Upsilon_{DS} = \begin{bmatrix} -\dot{\mathbf{J}}_L(\mathbf{x}) \begin{bmatrix} \mathbf{v}_b \\ \boldsymbol{\omega}_b \\ \dot{\boldsymbol{\theta}}_L \end{bmatrix} - \mathbf{J}_{L_1} \dot{\mathbf{v}}_b \\ -\dot{\mathbf{J}}_R(\mathbf{x}) \begin{bmatrix} \mathbf{v}_b \\ \boldsymbol{\omega}_b \\ \dot{\boldsymbol{\theta}}_R \end{bmatrix} - \mathbf{J}_{R_1} \dot{\mathbf{v}}_b \end{bmatrix}, \quad (4.16)$$

and

$$\mathbf{J}_{DS} = \begin{bmatrix} \mathbf{J}_{L_2} & \mathbf{J}_{L_3} & 0 \\ \mathbf{J}_{R_2} & 0 & \mathbf{J}_{R_3} \end{bmatrix}. \quad (4.17)$$

This fulfills the requirements to calculate the link torque in (4.5). Then the friction is estimated from (4.4) as

$$\hat{\mathbf{u}}_{F_m} = \boldsymbol{\tau}_m - \boldsymbol{\tau}_m^l, \quad (4.18)$$

where  $\hat{\mathbf{u}}_F$  is the estimated friction vector.

The estimated friction torque can be used in the control loop to compensate for the friction. However for the SS phase, the friction for the swinging leg can not be estimated in this strategy. For this reason, it is necessary to use models for the friction and identify their parameters while the leg is in contact as in Section 4.3.

#### 4.2.1.2 SS phase

For the SS phase, assuming that there is no foot acceleration nor slipping for the foot which is in contact, i.e.  $\ddot{\mathbf{p}}_{\mathbf{m}} \approx \mathbf{0}$ , then (4.11) is written as

$$\begin{bmatrix} \mathbf{J}_{m_2} & \mathbf{J}_{m_3} \end{bmatrix} \begin{bmatrix} \dot{\boldsymbol{\omega}}_b \\ \ddot{\boldsymbol{\theta}}_m \end{bmatrix} = -\dot{\mathbf{J}}_m(\mathbf{x}) \begin{bmatrix} \mathbf{v}_b \\ \boldsymbol{\omega}_b \\ \dot{\boldsymbol{\theta}}_m \end{bmatrix} - \mathbf{J}_{m_1} \dot{\mathbf{v}}_b. \quad (4.19)$$

Then, the angular accelerations can be calculated from (4.19) as

$$\begin{bmatrix} \dot{\boldsymbol{\omega}}_b \\ \ddot{\boldsymbol{\theta}}_m \end{bmatrix} = \mathbf{J}_{SS}^T (\mathbf{J}_{SS} \mathbf{J}_{SS}^T)^{-1} \Upsilon_{SS}, \quad (4.20)$$

where

$$\Upsilon_{SS} = -\dot{\mathbf{J}}_m(\mathbf{x}) \begin{bmatrix} \mathbf{v}_b \\ \boldsymbol{\omega}_b \\ \dot{\boldsymbol{\theta}}_m \end{bmatrix} - \mathbf{J}_{m_1} \dot{\mathbf{v}}_b, \quad (4.21)$$

and

$$\mathbf{J}_{SS} = \begin{bmatrix} \mathbf{J}_{m_2} & \mathbf{J}_{m_3} \end{bmatrix}. \quad (4.22)$$

Then the link torque is

$$\boldsymbol{\tau}_m^l = \bar{\mathbf{H}}_m \begin{pmatrix} \dot{\mathbf{v}}_b \\ \dot{\boldsymbol{\omega}}_b \\ \ddot{\boldsymbol{\theta}}_m \end{pmatrix} + \mathbf{b}_m - \mathbf{u}_{E_m}, \quad (4.23)$$

where

$$\bar{\mathbf{H}}_m = \begin{cases} (H_{31} & H_{32} & H_{33}), \mathbf{m} = \mathbf{L} \\ (H_{41} & H_{42} & H_{44}), \mathbf{m} = \mathbf{R} \end{cases}.$$

The calculated  $\boldsymbol{\tau}_m^l$  is substituted in (4.18) to estimate the joint friction vector for the leg  $\mathbf{m}$ . Then the estimated joint friction is used for joint friction compensation and friction model parameter identification.

## 4.2.2 Reduced filtered dynamical model

Equation (4.3) can be reshaped in terms of friction as

$$\begin{pmatrix} \mathbf{u}_{F_L} \\ \mathbf{u}_{F_R} \end{pmatrix} = \begin{pmatrix} \boldsymbol{\tau}_L \\ \boldsymbol{\tau}_R \end{pmatrix} + \begin{pmatrix} \mathbf{u}_{E_L} \\ \mathbf{u}_{E_R} \end{pmatrix} - \bar{\mathbf{H}} \begin{pmatrix} \dot{\boldsymbol{\omega}}_b \\ \ddot{\boldsymbol{\theta}}_L \\ \ddot{\boldsymbol{\theta}}_R \end{pmatrix} - \begin{pmatrix} H_{31} \\ H_{41} \end{pmatrix} \dot{\mathbf{v}}_b - \begin{pmatrix} \mathbf{b}_L \\ \mathbf{b}_R \end{pmatrix}, \quad (4.24)$$

with

$$\bar{\mathbf{H}} = \begin{pmatrix} H_{32} & H_{33} & 0 \\ H_{42} & 0 & H_{44} \end{pmatrix}. \quad (4.25)$$

By using the filtered dynamic model approach below [86], the explicit calculation of the angular accelerations is avoided. This is accomplished by filtering both sides of (4.24) using a proper stable filter. A first order filter transfer function is considered with parameters  $K$  and  $\sigma$  as

$$Z(s) = K \frac{1}{s + \sigma}, \quad (4.26)$$

its impulse response is

$$z(t) = \ell^{-1}(Z(s)) = Ke^{-\sigma t}, \quad (4.27)$$

where  $\ell^{-1}(\cdot)$  is the inverse Laplace transform. The multiplication in the frequency domain is equivalent to the convolution in time domain, and since there are  $N$  joint equations in (4.24), each of them can be filtered by (4.26). Therefore, there will be  $N$  filters with impulse responses which can be organized into a matrix as

$$\mathbf{z}(t) = \begin{bmatrix} K_1 e^{-\sigma_1 t} & & 0 \\ & \ddots & \\ 0 & & K_N e^{-\sigma_N t} \end{bmatrix}, \quad (4.28)$$

where  $K_i$  and  $\sigma_i$   $i=1,2,\dots,N$  are the  $i^{\text{th}}$  joint filter constants. The filtered version of (4.24) can be obtained as



$$\begin{aligned}
\int_0^t \mathbf{z}(t-\tau) \begin{pmatrix} \mathbf{u}_{F_L} \\ \mathbf{u}_{F_R} \end{pmatrix} d\tau &= \int_0^t \mathbf{z}(t-\tau) \left( \begin{pmatrix} \boldsymbol{\tau}_L \\ \boldsymbol{\tau}_R \end{pmatrix} + \begin{pmatrix} \mathbf{u}_{E_L} \\ \mathbf{u}_{E_R} \end{pmatrix} \right) d\tau \\
&\quad - \int_0^t \mathbf{z}(t-\tau) \left( \bar{\mathbf{H}} \begin{pmatrix} \dot{\boldsymbol{\omega}}_b \\ \ddot{\boldsymbol{\theta}}_L \\ \ddot{\boldsymbol{\theta}}_R \end{pmatrix} \right) d\tau \\
&\quad - \int_0^t \mathbf{z}(t-\tau) \left( \begin{pmatrix} H_{31} \\ H_{41} \end{pmatrix} \dot{\mathbf{v}}_b + \begin{pmatrix} \mathbf{b}_L \\ \mathbf{b}_R \end{pmatrix} \right) d\tau
\end{aligned} \tag{4.29}$$

The term  $\int_0^t \mathbf{z}(t-\tau) \left( \bar{\mathbf{H}} \begin{pmatrix} \dot{\boldsymbol{\omega}}_b \\ \ddot{\boldsymbol{\theta}}_L \\ \ddot{\boldsymbol{\theta}}_R \end{pmatrix} \right) d\tau$  can be integrated by parts with

$$\dot{\boldsymbol{\theta}}_L(0) = \dot{\boldsymbol{\theta}}_R(0) = \dot{\boldsymbol{\omega}}_b(0) = 0 \text{ and } \mathbf{z}(0) = K = \begin{bmatrix} K_1 & 0 \\ & \ddots \\ 0 & K_N \end{bmatrix} \text{ as}$$

$$\int_0^t \mathbf{z}(t-\tau) \left( \bar{\mathbf{H}} \begin{pmatrix} \dot{\boldsymbol{\omega}}_b \\ \ddot{\boldsymbol{\theta}}_L \\ \ddot{\boldsymbol{\theta}}_R \end{pmatrix} \right) d\tau = K \bar{\mathbf{H}} \begin{pmatrix} \boldsymbol{\omega}_b \\ \dot{\boldsymbol{\theta}}_L \\ \dot{\boldsymbol{\theta}}_R \end{pmatrix} - \int_0^t \mathbf{z}(t-\tau) \dot{\bar{\mathbf{H}}} \begin{pmatrix} \boldsymbol{\omega}_b \\ \dot{\boldsymbol{\theta}}_L \\ \dot{\boldsymbol{\theta}}_R \end{pmatrix} - \dot{\mathbf{z}}(t-\tau) \bar{\mathbf{H}} \begin{pmatrix} \boldsymbol{\omega}_b \\ \dot{\boldsymbol{\theta}}_L \\ \dot{\boldsymbol{\theta}}_R \end{pmatrix} d\tau, \tag{4.30}$$

then (4.29) can be rewritten as

$$\begin{aligned}
\int_0^t \mathbf{z}(t-\tau) \begin{pmatrix} \mathbf{u}_{F_L} \\ \mathbf{u}_{F_R} \end{pmatrix} d\tau &= -K \bar{\mathbf{H}} \begin{pmatrix} \boldsymbol{\omega}_b \\ \dot{\boldsymbol{\theta}}_L \\ \dot{\boldsymbol{\theta}}_R \end{pmatrix} \\
&\quad + \int_0^t \mathbf{z}(t-\tau) \left( \begin{pmatrix} \boldsymbol{\tau}_L \\ \boldsymbol{\tau}_R \end{pmatrix} + \begin{pmatrix} \mathbf{u}_{E_L} \\ \mathbf{u}_{E_R} \end{pmatrix} + \dot{\bar{\mathbf{H}}} \begin{pmatrix} \boldsymbol{\omega}_b \\ \dot{\boldsymbol{\theta}}_L \\ \dot{\boldsymbol{\theta}}_R \end{pmatrix} - \begin{pmatrix} H_{31} \\ H_{41} \end{pmatrix} \dot{\mathbf{v}}_b - \begin{pmatrix} \mathbf{b}_L \\ \mathbf{b}_R \end{pmatrix} \right) d\tau \\
&\quad + \int_0^t \dot{\mathbf{z}}(t-\tau) \bar{\mathbf{H}} \begin{pmatrix} \boldsymbol{\omega}_b \\ \dot{\boldsymbol{\theta}}_L \\ \dot{\boldsymbol{\theta}}_R \end{pmatrix} d\tau
\end{aligned} \tag{4.31}$$

All the terms are filtered using (4.26) except the last term

$$\int_0^t \dot{\mathbf{z}}(t-\tau) \bar{\mathbf{H}} \begin{pmatrix} \boldsymbol{\omega}_b \\ \dot{\boldsymbol{\theta}}_L \\ \dot{\boldsymbol{\theta}}_R \end{pmatrix} d\tau$$

which is filtered using

$$Z_2(s) = \ell\{\dot{\mathbf{z}}(t)\} = \ell\{-K\sigma e^{-\sigma t}\} = -K \frac{\sigma}{s+\sigma}, \quad (4.32)$$

or in matrix form

$$\mathbf{z}_2(t) = - \begin{bmatrix} K_1 \sigma_1 e^{-\sigma_1 t} & & 0 \\ & \ddots & \\ 0 & & K_N \sigma_N e^{-\sigma_N t} \end{bmatrix} \quad (4.33)$$

By introducing the notation  $\langle \eta \rangle_\lambda$  to indicate that the term  $\eta$  is filtered using the filter  $\lambda$ , then the filtered dynamic equation is

$$\left\langle \begin{pmatrix} \mathbf{u}_{F_L} \\ \mathbf{u}_{F_R} \end{pmatrix} \right\rangle_{Z(s)} = K \xi_1 + \langle \xi_2 \rangle_{Z(s)} + \langle -\xi_1 \rangle_{Z_2(s)}, \quad (4.34)$$

where

$$\xi_1 = -\bar{\mathbf{H}} \begin{pmatrix} \boldsymbol{\omega}_b \\ \dot{\boldsymbol{\theta}}_L \\ \dot{\boldsymbol{\theta}}_R \end{pmatrix}, \quad (4.35)$$

and

$$\xi_2 = \begin{pmatrix} \boldsymbol{\tau}_L \\ \boldsymbol{\tau}_R \end{pmatrix} + \begin{pmatrix} \mathbf{u}_{E_L} \\ \mathbf{u}_{E_R} \end{pmatrix} + \dot{\bar{\mathbf{H}}} \begin{pmatrix} \boldsymbol{\omega}_b \\ \dot{\boldsymbol{\theta}}_L \\ \dot{\boldsymbol{\theta}}_R \end{pmatrix} - \begin{pmatrix} H_{31} \\ H_{41} \end{pmatrix} \dot{\mathbf{v}}_b - \begin{pmatrix} \mathbf{b}_L \\ \mathbf{b}_R \end{pmatrix}, \quad (4.36)$$

Then the estimated filtered joint friction is used for joint friction compensation and friction model parameter identification.

### 4.3 Friction model parameter identification

The estimated friction in (4.18) or (4.34) uses the measurement based strategy. It works only when the foot is in contact with the ground. Therefore, for the swinging leg, a friction model is adopted to represent the frictional forces at the leg joints [107]. The estimated friction is used to identify the adopted model parameters. Thus the model parameters are adaptively identified in every step the biped walks using the RLS algorithm (2.18)-(2.21).

### 4.4 Simulation Results

A 12-degrees-of-freedom (DOF) biped model as in Figure 3.4 is used for the simulations. All measurements and calculations are performed in the world frame. The IMU is located with a position  $r_l = [0.01 \quad -0.01 \quad 0.02]^T$  with respect to the CoM position in the body frame and attitude  $A_b^l = I_3$ , where  $I_3$  is a  $3 \times 3$  identity matrix. In the simulations we used the three-axes IMU which is available in MATLAB simulink.

#### 4.4.1 Walking trajectory

The foot walking trajectories are shown in

Figure 4.2. The biped has a single support period of 0.6 sec and a double support period of 0.9 sec. It starts walking after 0.5 sec, left single support (LS) then DS then right single support (RS) and so forth. The robot stops at the time instant 10.1 sec.

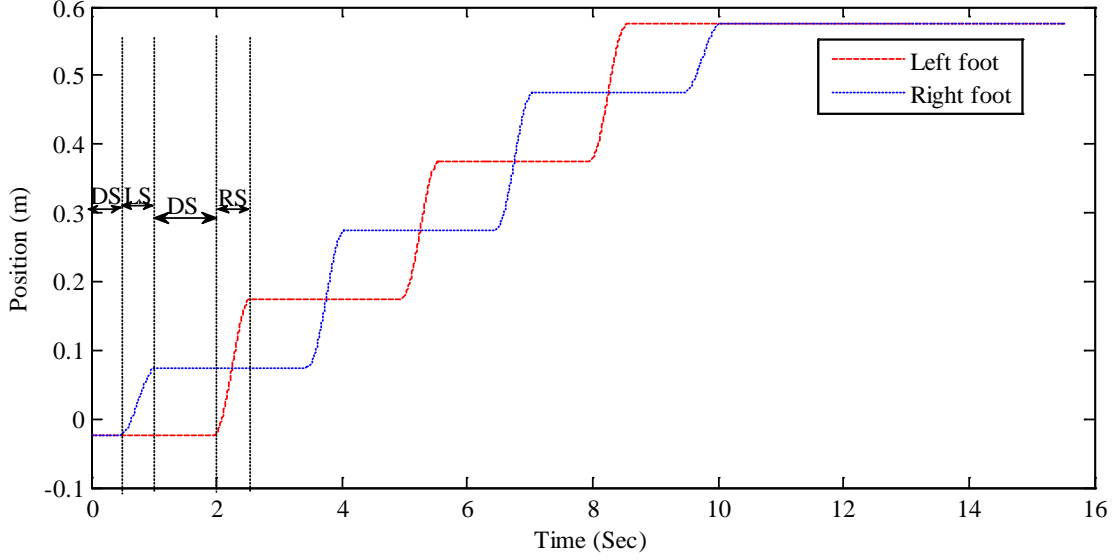


Figure 4.2: Foott walking trajectories, DS stands for the double support phase, LS stands for the left leg single support phase, and RS stands for the right leg single support phase.

#### 4.4.2 Joint friction generation in simulations

Here, the joint friction is generated using the nonlinear model [23]

$$\mathbf{u}_F = \gamma_1 \left( \tanh(\gamma_2 \dot{\boldsymbol{\theta}}) - \tanh(\gamma_3 \dot{\boldsymbol{\theta}}) \right) + \gamma_4 \tanh(\gamma_5 \dot{\boldsymbol{\theta}}) + \gamma_6 \dot{\boldsymbol{\theta}}, \quad (4.37)$$

where  $\gamma_i, i=1, \dots, 6$  are positive constants. The model has the viscous dissipation term  $\gamma_6 \dot{\boldsymbol{\theta}}$  and the Coulomb friction term  $\gamma_4 \tanh(\gamma_5 \dot{\boldsymbol{\theta}})$ . It captures the Stribeck effect by the term  $\tanh(\gamma_2 \dot{\boldsymbol{\theta}}) - \tanh(\gamma_3 \dot{\boldsymbol{\theta}})$ . The static coefficient of friction can be approximated by  $\gamma_1 + \gamma_4$ .

The parameters values of the friction model (4.37) for each joint of the leg are listed in Table 4.1. The corresponding generated true friction is shown Figure 4.3.

Table 4.1: True Friction model parameters for each joint of the leg

	$\theta_1$	$\theta_2$	$\theta_3$	$\theta_4$	$\theta_5$	$\theta_6$
$\gamma_1$	0.7	0.6	0.5	0.4	0.2	0.05
$\gamma_2$	100	100	100	100	100	100
$\gamma_3$	10	10	10	10	10	10
$\gamma_4$	0.6	0.5	0.4	0.3	0.02	0.01
$\gamma_5$	100	100	100	100	100	100
$\gamma_6$	0.9	0.9	0.9	0.9	0.9	0.9

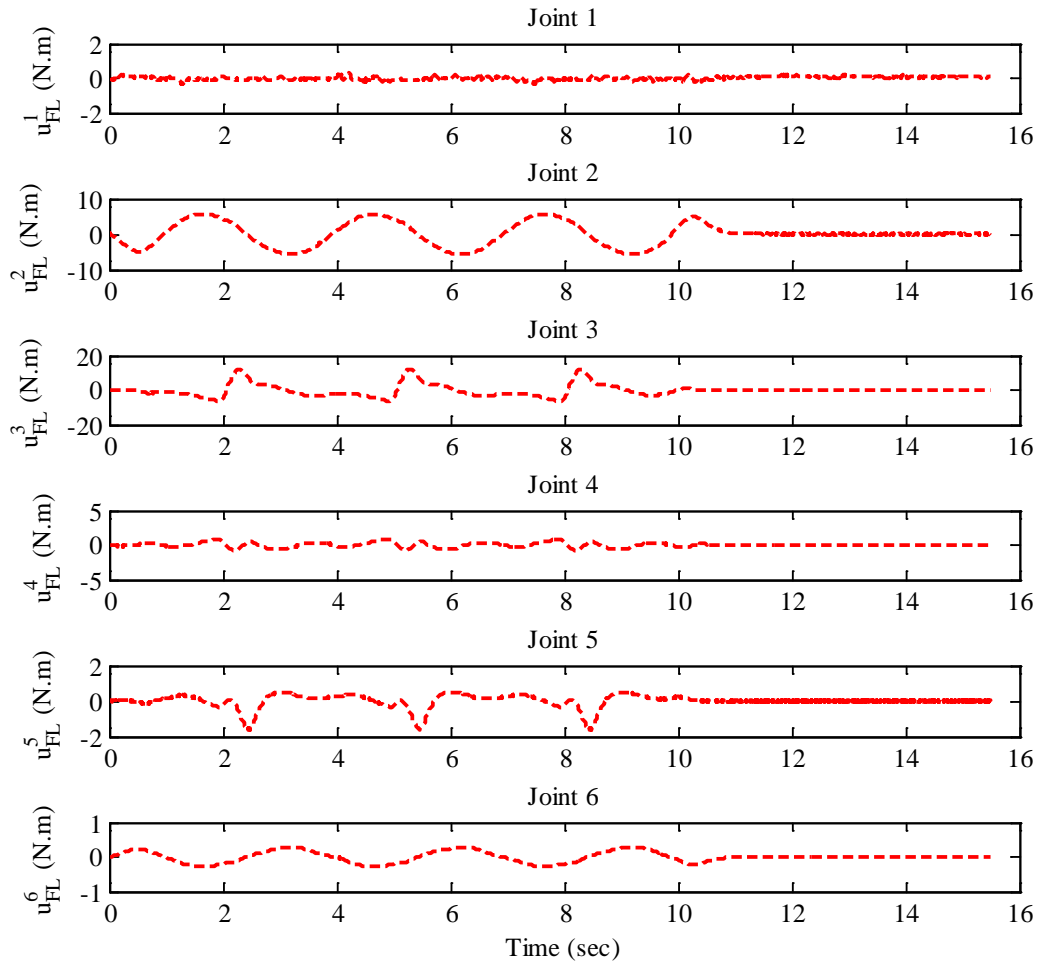


Figure 4.3: The true generated friction for the left leg joints

### 4.4.3 Joint friction estimation

To be more realistic, (4.37) is used solely for the generation of the joint friction. To estimate the friction, another model which differs from (4.37) is adopted. Here the adopted model is linear in its parameters. The Coulomb and viscous friction effects are considered. For the joint  $n$ , the model is written as

$$\hat{\mathbf{u}}_{\mathbf{F}_m}^n = F_c^n \operatorname{sgn}(\dot{\theta}_n) + \bar{F}_v^n \dot{\theta}_n, \quad (4.38)$$

or

$$\langle \hat{\mathbf{u}}_{\mathbf{F}_m}^n \rangle_{Z(s)} = F_c^n \operatorname{sgn}(\dot{\theta}_n) + \bar{F}_v^n \dot{\theta}_n, \quad (4.39)$$

where  $\bar{F}_v$  is the viscous friction coefficient and  $F_c$  the Coulomb friction. When the foot is in contact, the estimated friction  $\hat{\mathbf{u}}_{\mathbf{F}_m}$  from (4.18) or  $\langle \hat{\mathbf{u}}_{\mathbf{F}_m}^n \rangle_{Z(s)}$  from (4.34) is used in (4.38) or (4.39) respectively to estimate  $\bar{F}_v$  and  $F_c$  for each joint. Then when the leg is swinging, the estimated parameters  $\hat{\bar{F}}_v$  and  $\hat{F}_c$  are used to calculate the friction forces for each joint. (4.38) can be written in a matrix form that includes all the joint friction values for the leg  $\mathbf{m}$  as

$$\hat{\mathbf{u}}_{\mathbf{F}_m} = \Psi \Phi, \quad (4.40)$$

where

$$\Psi = \begin{bmatrix} \psi_1 & 0 & \cdots & 0 \\ 0 & \psi_2 & & \vdots \\ \vdots & & \ddots & 0 \\ 0 & \cdots & 0 & \psi_6 \end{bmatrix}_{6 \times 12}, \quad (4.41)$$

$$\Phi = \left[ F_c^1 \quad \bar{F}_v^1 \quad F_c^2 \quad \bar{F}_v^2 \quad \cdots \quad F_c^6 \quad \bar{F}_v^6 \right]_{1 \times 12}^T, \quad (4.42)$$

$$\psi_i = \left[ \operatorname{sgn}(\dot{\theta}_i) \quad \dot{\theta}_i \right], \quad (4.43)$$

and  $i = 1, 2, \dots, 6$ . The same goes for (4.39), where the equation can be written as

$$\left\langle \hat{\mathbf{u}}_{F_m} \right\rangle_{Z(s)} = \Psi \Phi . \quad (4.44)$$

The RLS method is used here for the estimation as a real time application with  $\mathbf{Y} = \hat{\mathbf{u}}_{F_m}$  or  $\mathbf{Y} = \left\langle \hat{\mathbf{u}}_{F_m} \right\rangle_{Z(s)}$ . The RLS algorithm was discussed in Section 2.2. The estimation initial values of the RLS algorithm are  $\Phi_0 = 0_{12 \times 1}$  and  $P_{RLS_0} = 10I_{12}$ .

The joint friction is computed simultaneously for all joints. The switching between the DS and the SS phases is time based. The two legs are assumed to have the same frictional models, the same number of joints and the same number of the ground contact points at each foot. The estimation process is as follows: In the DS phase, the friction compensation is model-free and the friction is estimated based on the force measurements. At the same time, the estimated friction is used to identify the friction model parameters  $\bar{F}_v$  and  $F_c$  for each joint in each leg. At the time instant  $t=0.5$  sec, the robot switches from the DS phase to the LS phase. At this instant, the friction models with the identified parameters  $\hat{\bar{F}}_v$  and  $\hat{F}_c$  are used to compute the friction for the right leg joints. For the left leg joints, the friction estimation is still model-free and the corresponding friction model parameters are still being identified. At the time instant  $t=1.1$  sec, the robot again switches to the DS phase. Again the friction estimation is model-free and the friction model parameters are being identified for both legs joints. Hence the friction model parameters are adaptively identified and corrected. At the time instant  $t=2$  sec, the robot switches from the DS phase to the RS phase. At this instant, the friction models with the identified parameters are used to compute the friction for the left leg joints. For the right leg, the friction estimation is still being carried on as a friction model-free. The corresponding friction model parameters are still being identified, and so forth.

#### 4.4.3.1 The estimated friction with non-slipping constraint

The estimated friction values for the left leg joints are shown in Figure 4.4 (solid blue line). The same goes for the right leg. When the foot is in contact with the ground, the

measurement-based online friction compensation is used. When the leg is swinging, the model (4.38) is used to estimate the joint friction. As depicted in Figure 4.4, the estimated joint friction tracks the true friction for all the friction cases. One observation is that when the foot is in contact, the estimated friction is noisy. This is due to the measured noisy forces. However, when it is swinging i.e. when the friction model is used, the friction is much smoother. In these simulations, small and large frictional forces are used to test the ability of the proposed method.

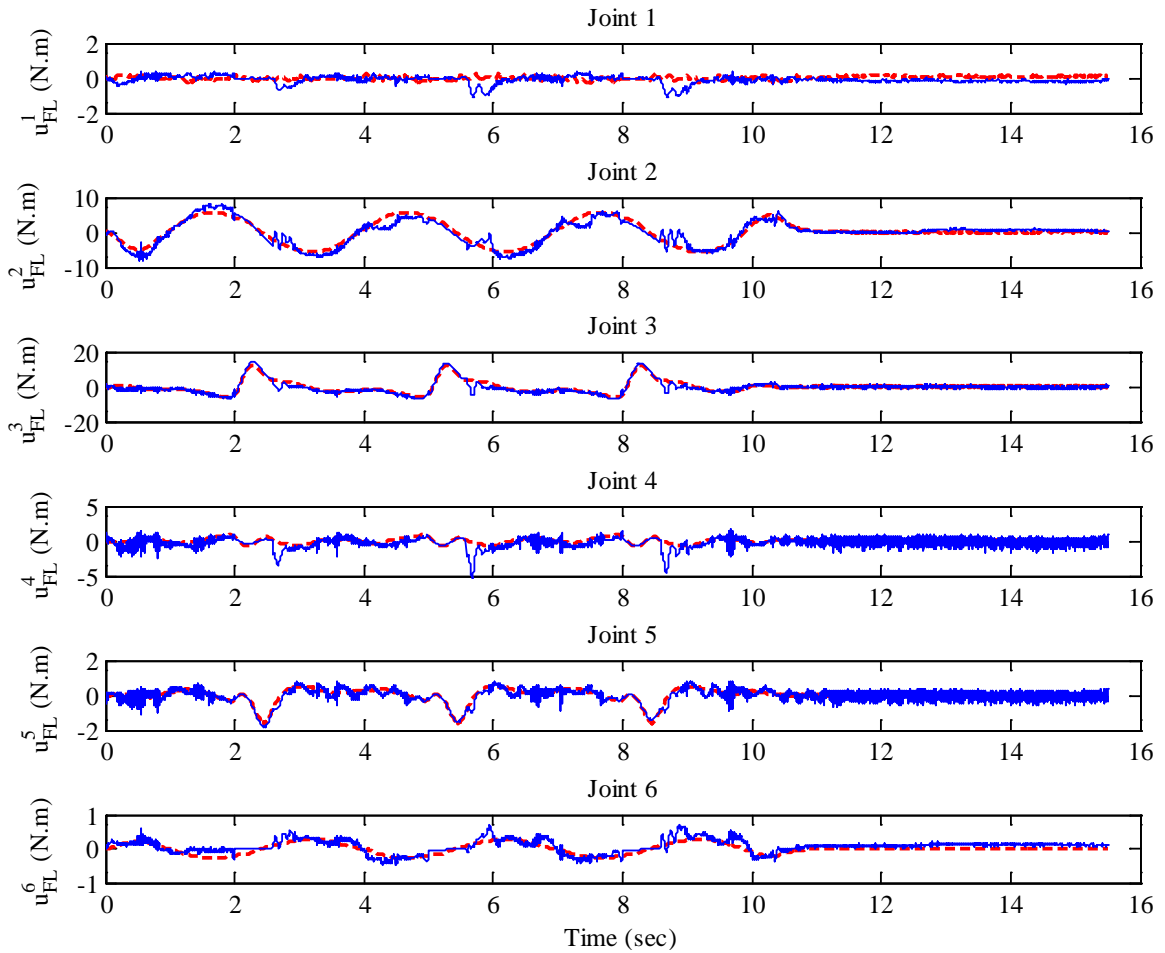


Figure 4.4: The estimated friction (solid blue line) and the true generated friction (dashed red line) for the left leg joints



#### 4.4.3.2 The estimated friction using the filtered dynamic model

The estimated friction parameters follow the same idea as mentioned before. The used filter constants are as listed in Table 4.2. These constant are user selected.

Table 4.2: Filter constants

	$\theta_1$	$\theta_2$	$\theta_3$	$\theta_4$	$\theta_5$	$\theta_6$
$K$	1	2	2	2	4	2
$\sigma$	1	1	1	2	4	2

The estimation results are shown here for the left leg in Figure 4.5. The dashed red line is the true friction trajectory that is generated using (4.37) with the parameters listed in Table 4.1. The estimated filtered friction is the solid blue line. When the leg is swinging, the estimated friction uses the model (4.39) with the identified parameters. From the figure, the estimated friction tracks the true friction for all the friction cases. In these simulations, small and large frictional forces are used to test the ability of the proposed method. The simulations indicate that it is able to track the friction forces in all cases.

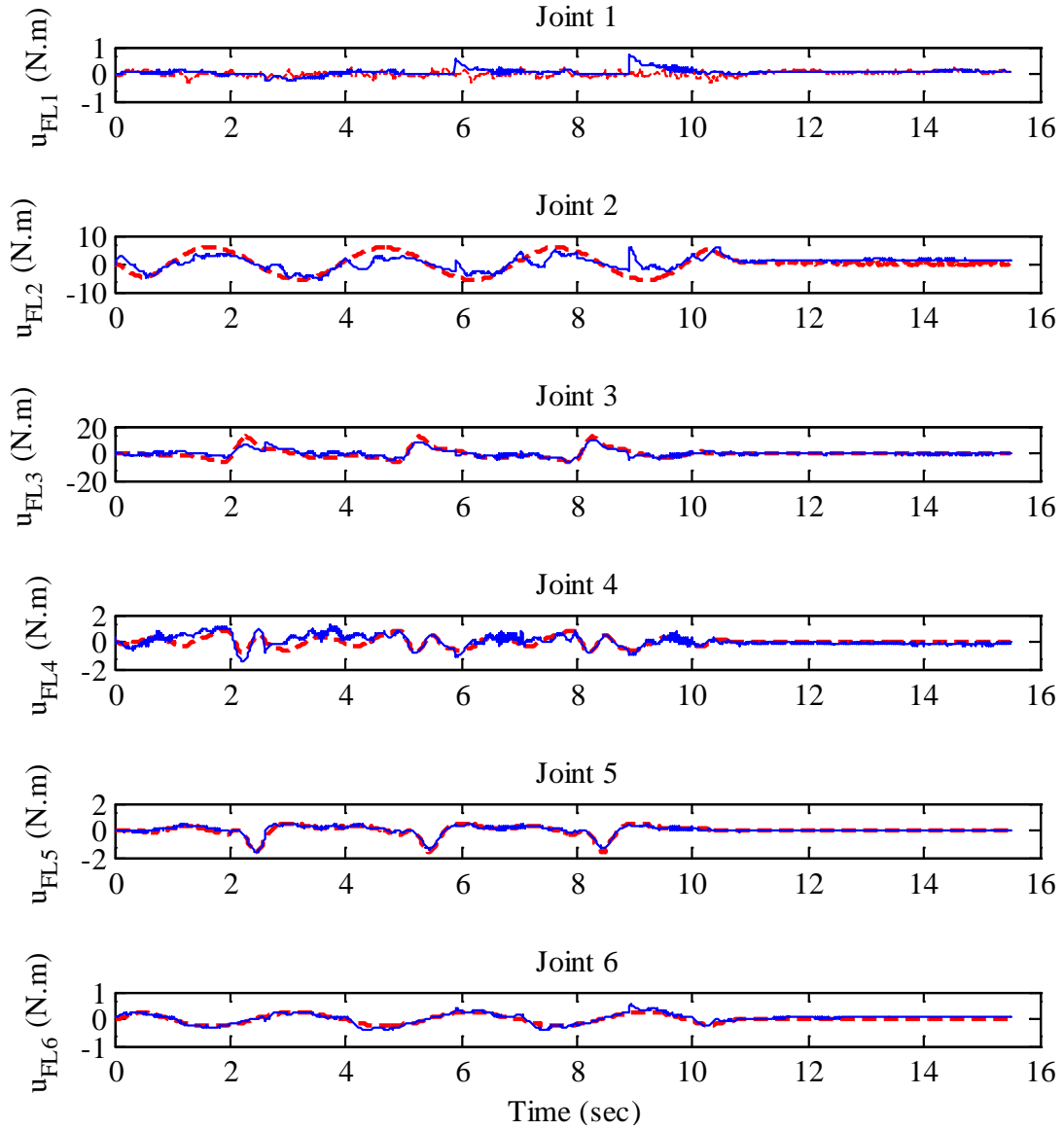


Figure 4.5: The estimated friction (solid blue line) and the true generated friction (dashed red line) for the left leg joints

#### 4.4.4 Joint friction compensation approach

To compensate for the joint friction, two control structures are used. The first one is shown in Figure 4.6. The position controller is a PD controller with proportional gain  $k_p$  and derivative gain  $k_d$ . The output of the PD controller  $\tau_{pos}$  is

$$\boldsymbol{\tau}_{pos} = \begin{bmatrix} k_p & 0 \\ 0 & k_p \end{bmatrix} (\boldsymbol{\theta}^{ref} - \boldsymbol{\theta}) + (\dot{\boldsymbol{\theta}}^{ref} - \dot{\boldsymbol{\theta}}), \quad (4.45)$$

where  $\boldsymbol{\theta}^{ref}$  and  $\dot{\boldsymbol{\theta}}^{ref}$  are the reference trajectories. Note that  $\boldsymbol{\theta}^{ref}$  is generated based on the desired CoM position  $\mathbf{c}^{des}$ . Therefore, we will compare the actual  $\mathbf{c}$  with  $\mathbf{c}^{des}$ . The torque controller output  $\boldsymbol{\tau}_{tor}$  is

$$\boldsymbol{\tau}_{tor} = \begin{bmatrix} k_i & 0 \\ 0 & k_i \end{bmatrix} \int_0^t (\boldsymbol{\tau}_{pos} - (\boldsymbol{\tau} - \hat{\mathbf{u}}_F)) d\tau, \quad (4.46)$$

where  $k_i$  is the integral gain.

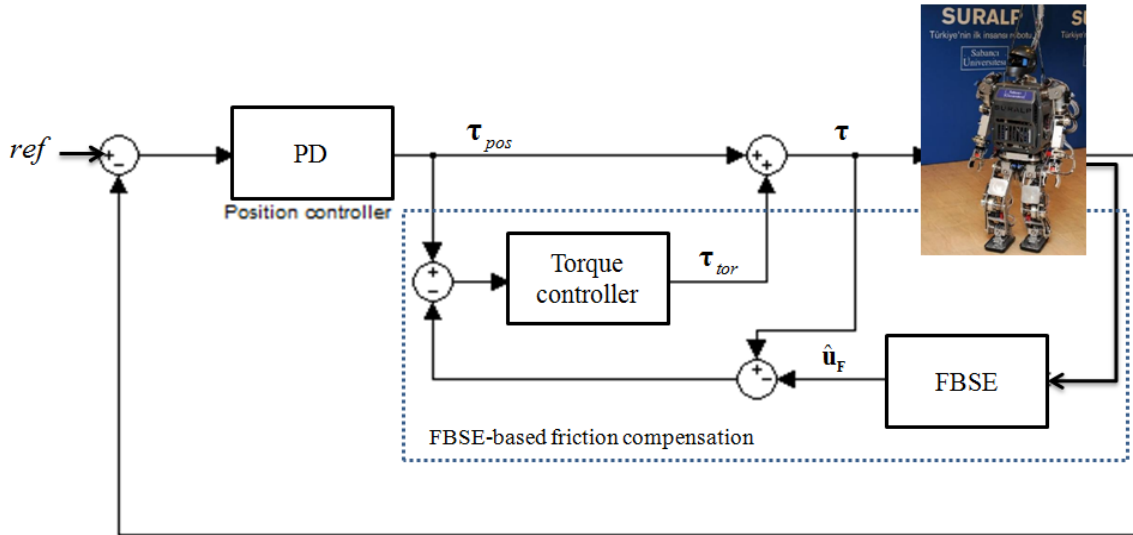


Figure 4.6: First control structure: Friction compensation using the proposed FBSE (Foot base sensor estimation) method

The root square error (RSE) is used as a performance measure of the response. The RSE is defined by

$$RSE = \sqrt{(\mathbf{c}^{des} - \mathbf{c})^2}. \quad (4.47)$$

The control parameters are: The derivative gain  $k_d = I_{12}$ , the proportional gain  $k_p = \text{diag}([6 \ 2 \ 2 \ 3 \ 3 \ 6] \times 10^3)$ , and the integral gain  $k_i = \text{diag}([2 \ 2 \ 1 \ 2 \ 2 \ 4])$ .

Figure 4.7 demonstrates the improvement due to the proposed method. First the conventional PD controller is used alone. Its response is compared with the response of the proposed FBSE method. As shown in Figure 4.7. b and c, the response error of the PD controller alone is higher than it when the PD controller is combined with the FBSE.

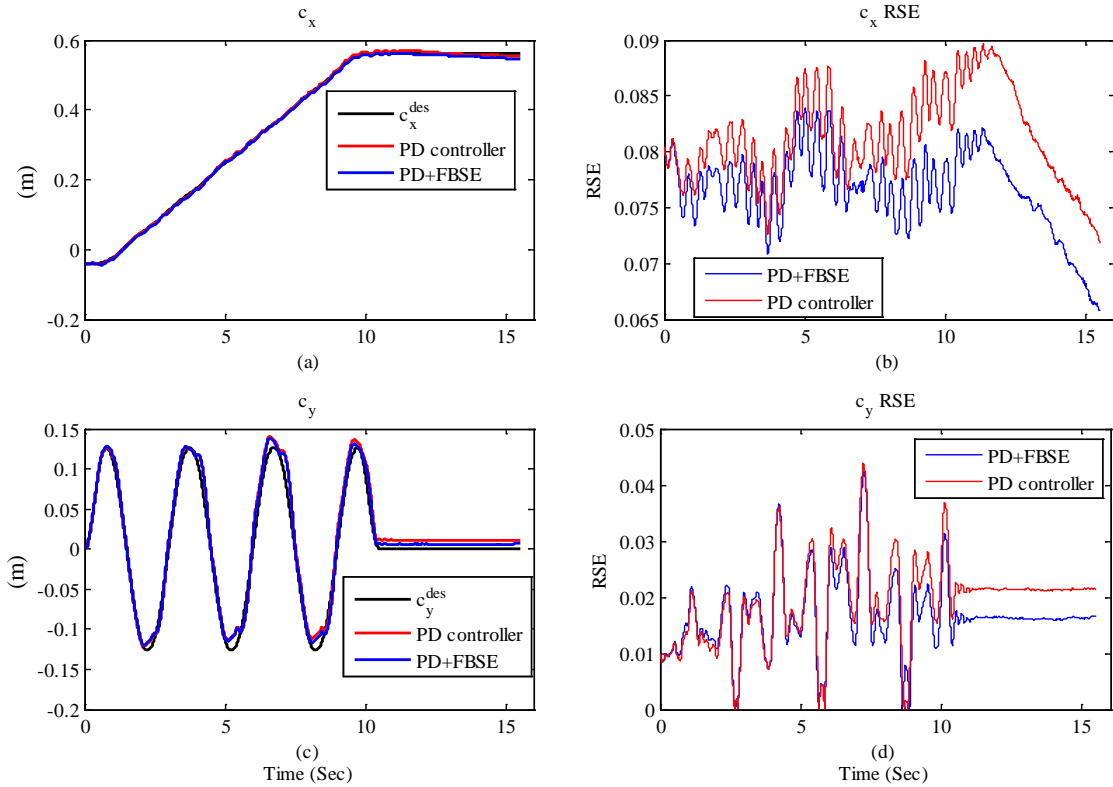


Figure 4.7: First control structure response. (a) CoM trajectory in the  $x$ –direction  $c_x$ , (b) RSE in  $c_x$ , (c) CoM trajectory in the  $y$ –direction  $c_y$ , and (d) RSE in  $c_y$ .

The second control structure is presented in Figure 4.8. The estimated friction is added to the control signal without torque controller. The position response of this structure is depicted in Figure 4.9. This control structure is simpler than the previous one, however the first structure has better performance.

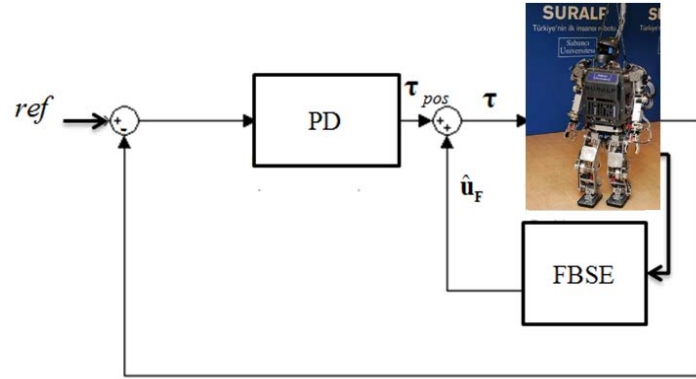


Figure 4.8: Second control structure: Friction compensation using the proposed FBSE method

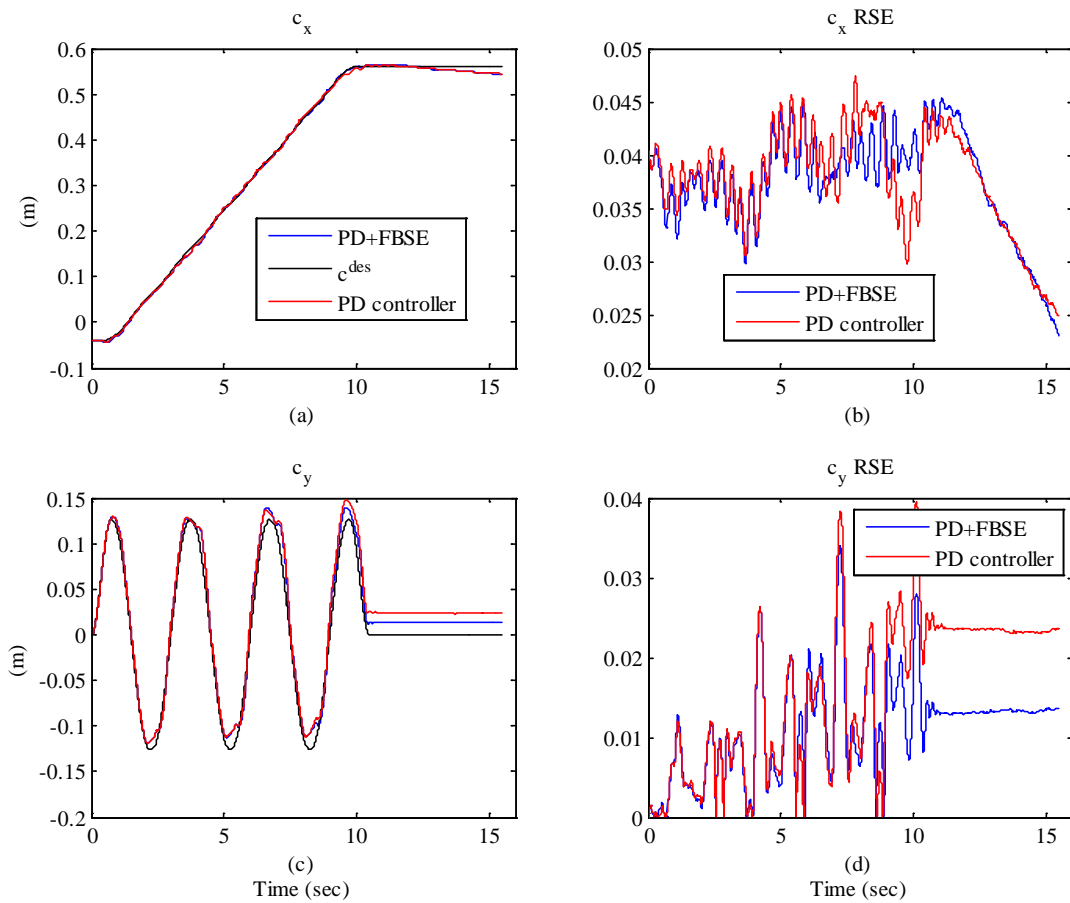


Figure 4.9: Second control structure response. (a) CoM trajectory in the  $x$ -direction  $c_x$ , (b) RSE in  $c_x$ , (c) CoM trajectory in the  $y$ -direction  $c_y$ , and (d) RSE in  $c_y$ .

## 4.5 Conclusion

A novel FBSE method for estimating the joint friction of walking bipeds is proposed. It utilizes the readings of IMU and foot contact reaction forces into a reduced model of the biped. It combines a measurement-based strategy with an adaptive model-based approach to estimate the joint friction. The measurement-based estimation is used when the feet are in contact, while the adaptive model-based friction is used when the leg is swinging. To achieve this estimation, the joint angular accelerations are either estimated online using the non-slipping foot constraint or their computation is avoided by filtering the model. This method requires the IMU, joint encoders and ground contact force measurements. It does not require joint torque sensors. The results show that the estimated friction tracks the true one. Furthermore, using the FBSE method in the feedback torque signal improves the position response.

## **Chapter 5**

### **5 Novel Method for Slip Prediction of Walking Biped Robots**

The robot foot, when it is in contact with the floor, is subjected to distributed reaction forces due to the interaction between the sole and floor surface. The horizontal components of these forces represent the friction forces. The friction forces are required so that the biped can walk. They determine the maximum allowable body acceleration the biped can have without slipping and the maximum allowable forces that can be applied on the biped. However determining these friction forces is a challenge. Several models were developed to represent the friction [36, 37]. Although using the walking surface coefficient of friction is widely used, it is not a solution since the surfaces change and the coefficient is not necessarily accurate.

In this thesis, based on the friction behavior, a measurement-based model-free online method is used to develop an algorithm to estimate the Coulomb friction. This algorithm updates the estimated friction online adaptively. The estimated friction is used to decide whether the foot is going to slip or not.

This chapter discusses the slip definition and detection, the slip prediction approach, parameter estimation and the results.

## 5.1 Slip definition and detection

Consider one of the robot feet as in Figure 5.1.a. The total force on the foot is  $F$ . Its tangential components in the  $x$ - and  $y$ - directions are  $F_{t_x}$  and  $F_{t_y}$ , respectively. The friction force components in the  $x$ - and  $y$ - directions are denoted by  $F_{f_x}$  and  $F_{f_y}$  respectively. The normal reaction force is  $F_N \geq 0$ . The slip is defined as the phenomenon when the friction force  $F_f$  between the foot and the contact surface is not satisfactory to make the relative velocity between them zero. In other words, it is the phenomenon when  $\|\mathbf{F}_t\| = \sqrt{F_{t_x}^2 + F_{t_y}^2} > \|\mathbf{F}_f\| = \sqrt{F_{f_x}^2 + F_{f_y}^2}$ , or in terms of components,  $F_{t_x} > F_{f_x}$  or/and  $F_{t_y} > F_{f_y}$ . This leads to generate a slip force  $F_{slip_x}$  in the  $x$ - direction or/and a slip force  $F_{slip_y}$  in the  $y$ - direction. The slip force vector  $\mathbf{F}_{slip} \equiv [F_{slip_x} \quad F_{slip_y}]^T$  can be obtained as

$$\mathbf{F}_{slip} = \mathbf{F}_t - \mathbf{F}_f, \quad (5.1)$$

with  $\mathbf{F}_t = [F_{t_x} \quad F_{t_y}]^T$  and  $\mathbf{F}_f = [F_{f_x} \quad F_{f_y}]^T$ .

The analysis for  $x$ - and  $y$ - directions is identical. Therefore, for convenience, the subscriptions  $x$  and  $y$  are dropped. According to (5.1)  $F_{slip} \geq 0$ , for the case when  $F_{slip} > 0$  the object is in motion as in Figure 5.1.b. When  $F_{slip} = 0$ , it indicates that the object is either moving in a constant speed as in Figure 5.1.c or the object is static as in Figure 5.1.d. The situation in Figure 5.1.c poses a problem which will be solved by assuming that the object was not initially moving at a constant speed.



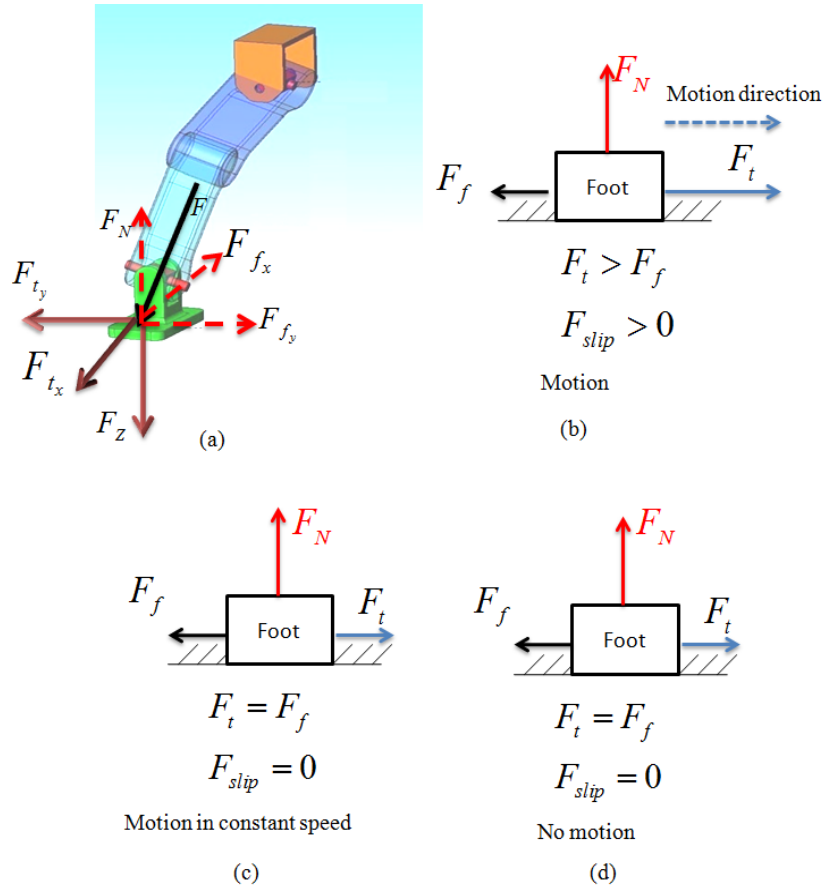


Figure 5.1: Slip force conditions

Accordingly, by referring to (5.1), the foot slips whenever it is subjected to a slip force  $F_{slip} > 0$ . Calculating  $F_{slip}$  depends on the available measurements. Here, three cases are discussed. The first case considers that the foot is equipped with force sensors located at the foot soles, hence the friction force is directly measured. The second case considers that the robot is equipped with a force/torque sensors located at the ankles and accelerometers located at the feet, hence  $\mathbf{F}_t$  is directly measured. The third case assumes that the foot is equipped with force sensors located at the foot soles and force/torque sensors located at the ankles.

### 5.1.1 Measured friction force

Referring to (5.1), the friction force is directly measured by the force sensors located at the foot sole.  $\mathbf{F}_t$  is unmeasured. However it can be calculated using the base link acceleration and angular velocity in addition to the legs joints angles.

Assume that there are  $l$  force sensors. These sensors are attached to known contact points at each foot with known positions relative to the foot frame. Their outputs are grouped in the force vector  $\mathbf{F}_E$  and defined as  $\mathbf{F}_E \equiv [\mathbf{F}_{E_R}^T \quad \mathbf{F}_{E_L}^T]^T$  with

$$\mathbf{F}_{E_m} = \begin{bmatrix} {}^m F_{f_x}^1 & {}^m F_{f_y}^1 & {}^m F_N^1 & {}^m F_{f_x}^2 & {}^m F_{f_y}^2 & {}^m F_N^2 & \dots & {}^m F_{f_x}^l & {}^m F_{f_y}^l & {}^m F_N^l \end{bmatrix}^T, \quad (5.2)$$

where  $\mathbf{F}_{E_m}$  is the force vector at the foot  $\mathbf{m}$ ,  ${}^m F_{f_j}^i$  the friction force component in the  $j = \{x \text{ or } y\}$  direction at contact point  $i = 1, 2, \dots, l$  of the foot  $\mathbf{m}$ .

The computed forces at the aforementioned contact points are grouped in the force vector  $\bar{\mathbf{F}}_E \equiv [\bar{\mathbf{F}}_{E_R}^T \quad \bar{\mathbf{F}}_{E_L}^T]^T$ .  $\bar{\mathbf{F}}_{E_m}$  represents the computed forces at the foot  $\mathbf{m}$  and is expressed as

$$\bar{\mathbf{F}}_{E_m} = \begin{bmatrix} {}^m F_{t_x}^1 & {}^m F_{t_y}^1 & {}^m \bar{F}_N^1 & {}^m F_{t_x}^2 & {}^m F_{t_y}^2 & {}^m \bar{F}_N^2 & \dots & {}^m F_{t_x}^l & {}^m F_{t_y}^l & {}^m \bar{F}_N^l \end{bmatrix}^T \quad (5.3)$$

where  ${}^m F_{t_j}^i$  and  ${}^m \bar{F}_N^i$  are the tangential and normal force components at contact point  $i = 1, 2, \dots, l$  of the  $\mathbf{m}$  foot. This force vector is related to  $\mathbf{u}_{E_1}$  in (4.2) using the Jacobian  $\mathbf{J}_{F_b}$  as

$$\mathbf{u}_{E_1} = \mathbf{J}_{F_b}^T \bar{\mathbf{F}}_E. \quad (5.4)$$

In terms of  $\bar{\mathbf{F}}_E$ , we can write

$$\bar{\mathbf{F}}_E = \mathbf{J}_{F_b}(\mathbf{x}) \left( \mathbf{J}_{F_b}^T(\mathbf{x}) \mathbf{J}_{F_b}(\mathbf{x}) \right)^{-1} \mathbf{u}_{E_1}. \quad (5.5)$$

The computation of the Jacobian  $\mathbf{J}_{F_b}$  depends on the robot geometry which is known. From the first row in (4.2), the net force effect of the reaction forces on the base  $\mathbf{u}_{E_1}$  is

$$\mathbf{u}_{E_1} = \mathbf{H}_F \begin{pmatrix} \dot{\mathbf{v}}_b \\ \dot{\boldsymbol{\omega}}_b \\ \ddot{\boldsymbol{\theta}}_L \\ \ddot{\boldsymbol{\theta}}_R \end{pmatrix} + \mathbf{b}_1, \quad (5.6)$$

with

$$\mathbf{H}_F = (H_{11} \quad H_{12} \quad H_{13} \quad H_{14}).$$

Substituting (5.4) and (5.5) into (5.6) we obtain

$$\bar{\mathbf{F}}_E = \mathbf{J}_{F_b}^\dagger \left( \mathbf{H}_F \begin{pmatrix} \dot{\mathbf{v}}_b \\ \dot{\boldsymbol{\omega}}_b \\ \ddot{\boldsymbol{\theta}}_L \\ \ddot{\boldsymbol{\theta}}_R \end{pmatrix} + \mathbf{b}_1 \right) \quad (5.7)$$

with  $\mathbf{J}_{F_b}^\dagger = \mathbf{J}_{F_b}(\mathbf{x})(\mathbf{J}_{F_b}^T(\mathbf{x})\mathbf{J}_{F_b}(\mathbf{x}))^{-1}$ . In (5.7), the bias  $\mathbf{b}_1$  depends on the same variables as in (4.7) i.e.  $\mathbf{b}_1 = \mathbf{f}_1(\mathbf{A}_b, \boldsymbol{\theta}, \boldsymbol{\omega}, \boldsymbol{\omega}_b, \mathbf{v}_b)$ . These variables are either measured or estimated.  $\mathbf{H}_F$  is also known. To find the angular accelerations, the same method as in Section 4.2.2 is used. The stable filter  $Z_F$  is used as

$$Z_F(s) = K_F \frac{1}{s + \lambda_F}, \quad (5.8)$$

with its impulse response

$$z_F(t) = \ell^{-1}(Z_F(s)) = K_F e^{-\lambda_F t}. \quad (5.9)$$

Equation (5.7) is composed of  $3 \times 2 \times l$  equations. Each of them is filtered by (5.8). Therefore, there will be  $3 \times 2 \times l$  filters with impulse responses as

$$\mathbf{z}_F(t) = \begin{bmatrix} K_{F_1} e^{-\lambda_{F_1} t} & & 0 \\ & \ddots & \\ 0 & & K_{F_{(3 \times 2 \times l)}} e^{-\lambda_{F_{(3 \times 2 \times l)}} t} \end{bmatrix}_{(3 \times 2 \times l) \times (3 \times 2 \times l)} \quad (5.10)$$

where  $K_{F_i}$  and  $\lambda_{F_i}$   $i=1, 2, \dots, 3 \times 2 \times l$  are the  $i^{\text{th}}$  equation filter constants. The multiplication in the frequency domain is equivalent to the convolution in time domain, thus the filtered version of (5.7) is

$$\begin{aligned}
\int_0^t \mathbf{z}_F(t-\tau) \bar{\mathbf{F}}_E d\tau &= \int_0^t \mathbf{z}_F(t-\tau) \mathbf{J}_{\mathbf{F}_b}^\dagger (H_{13} \ H_{14}) \begin{pmatrix} \ddot{\boldsymbol{\theta}}_L \\ \ddot{\boldsymbol{\theta}}_R \end{pmatrix} d\tau \\
&+ \int_0^t \mathbf{z}_F(t-\tau) \mathbf{J}_{\mathbf{F}_b}^\dagger \left( (H_{11} \ H_{12}) \begin{pmatrix} \dot{\mathbf{v}}_b \\ \dot{\boldsymbol{\omega}}_b \end{pmatrix} + \mathbf{b}_1 \right) d\tau
\end{aligned} \tag{5.11}$$

For simplification, the term  $\xi_F = \mathbf{J}_{\mathbf{F}_b}^\dagger (H_{13} \ H_{14})$  is introduced. The term

$\int_0^t \mathbf{z}_F(t-\tau) \xi_F \begin{pmatrix} \ddot{\boldsymbol{\theta}}_L \\ \ddot{\boldsymbol{\theta}}_R \end{pmatrix} d\tau$  can be integrated by parts with  $\dot{\boldsymbol{\theta}}_L(0) = \dot{\boldsymbol{\theta}}_R(0) = 0$  and

$$\mathbf{z}_F(0) = \mathbf{K}_F = \begin{bmatrix} K_{F,1} & & 0 \\ & \ddots & \\ 0 & & K_{F,3 \times 2 \times l} \end{bmatrix}$$

as

$$\begin{aligned}
\int_0^t \mathbf{z}_F(t-\tau) \xi_F \begin{pmatrix} \ddot{\boldsymbol{\theta}}_L \\ \ddot{\boldsymbol{\theta}}_R \end{pmatrix} d\tau &= \mathbf{K}_F \xi_F \begin{pmatrix} \dot{\boldsymbol{\theta}}_L \\ \dot{\boldsymbol{\theta}}_R \end{pmatrix} \\
&- \int_0^t \mathbf{z}_F(t-\tau) \dot{\xi}_F \begin{pmatrix} \dot{\boldsymbol{\theta}}_L \\ \dot{\boldsymbol{\theta}}_R \end{pmatrix} d\tau - \int_0^t \dot{\mathbf{z}}_F(t-\tau) \xi_F \begin{pmatrix} \dot{\boldsymbol{\theta}}_L \\ \dot{\boldsymbol{\theta}}_R \end{pmatrix} d\tau,
\end{aligned} \tag{5.12}$$

where

$$\dot{\xi}_F = \mathbf{J}_{\mathbf{F}_b}^\dagger (\dot{H}_{13} \ \dot{H}_{14}) + \dot{\mathbf{J}}_{\mathbf{F}_b}^\dagger (H_{13} \ H_{14}). \tag{5.13}$$

The filtered version of the force is

$$\begin{aligned}
\int_0^t \mathbf{z}_F(t-\tau) \bar{\mathbf{F}}_E d\tau &= \mathbf{K}_F \xi_F \begin{pmatrix} \dot{\boldsymbol{\theta}}_L \\ \dot{\boldsymbol{\theta}}_R \end{pmatrix} - \int_0^t \mathbf{z}_F(t-\tau) \dot{\xi}_F \begin{pmatrix} \dot{\boldsymbol{\theta}}_L \\ \dot{\boldsymbol{\theta}}_R \end{pmatrix} d\tau \\
&+ \int_0^t \mathbf{z}_F(t-\tau) \mathbf{J}_{\mathbf{F}_b}^\dagger \left( (H_{11} \ H_{12}) \begin{pmatrix} \dot{\mathbf{v}}_b \\ \dot{\boldsymbol{\omega}}_b \end{pmatrix} + \mathbf{b}_1 \right) d\tau. \\
&- \int_0^t \dot{\mathbf{z}}_F(t-\tau) \xi_F \begin{pmatrix} \dot{\boldsymbol{\theta}}_L \\ \dot{\boldsymbol{\theta}}_R \end{pmatrix} d\tau
\end{aligned} \tag{5.14}$$

All the terms are filtered using (5.8) except  $\int_0^t \dot{\mathbf{z}}_F(t-\tau) \xi_F \begin{pmatrix} \dot{\boldsymbol{\theta}}_L \\ \dot{\boldsymbol{\theta}}_R \end{pmatrix} d\tau$ . It is filtered by

$$Z_{F_2}(s) = \ell\{\dot{\mathbf{z}}_F(t)\} = \ell\{-K_F \lambda_F e^{-\lambda_F t}\} = -K_F \frac{\lambda_F}{s + \lambda_F} \tag{5.15}$$

or in matrix form, we can formulate

$$\mathbf{z}_{F_2}(t) = - \begin{bmatrix} K_{F_1} \lambda_{F_1} e^{-\lambda_{F_1} t} & & 0 \\ & \ddots & \\ 0 & & K_{F_{3 \times 2 \times l}} \lambda_{F_{3 \times 2 \times l}} e^{-\lambda_{F_{3 \times 2 \times l}} t} \end{bmatrix}_{(3 \times 2 \times l) \times (3 \times 2 \times l)} . \quad (5.16)$$

To write (5.14) in more compact form, the notation  $\langle \chi \rangle_\beta$  is introduced. This notation means the filtered version of the term  $\chi$  using the filter  $\beta$ . Accordingly, (5.14) is written as

$$\begin{aligned} \langle \bar{\mathbf{F}}_{\mathbf{E}} \rangle_{Z_F(s)} &= \mathbf{K}_F \xi_F \begin{pmatrix} \dot{\boldsymbol{\theta}}_{\mathbf{L}} \\ \dot{\boldsymbol{\theta}}_{\mathbf{R}} \end{pmatrix} - \left\langle \xi_F \begin{pmatrix} \dot{\boldsymbol{\theta}}_{\mathbf{L}} \\ \dot{\boldsymbol{\theta}}_{\mathbf{R}} \end{pmatrix} \right\rangle_{Z_F(s)} \\ &+ \left\langle \mathbf{J}_{F_b}^\dagger \left( (H_{11} \ H_{12}) \begin{pmatrix} \dot{\mathbf{v}}_b \\ \dot{\boldsymbol{\omega}}_b \end{pmatrix} + \mathbf{b}_1 \right) \right\rangle_{Z_F(s)} - \left\langle \xi_F \begin{pmatrix} \dot{\boldsymbol{\theta}}_{\mathbf{L}} \\ \dot{\boldsymbol{\theta}}_{\mathbf{R}} \end{pmatrix} \right\rangle_{Z_{F_2}(s)} . \end{aligned} \quad (5.17)$$

From the estimated filtered forces vector  $\langle \bar{\mathbf{F}}_{\mathbf{E}} \rangle_{Z_F(s)}$ , the filtered components are obtained from the vector  $\langle \bar{\mathbf{F}}_{\mathbf{E}} \rangle_{Z_F(s)} \equiv \left\langle \begin{bmatrix} \bar{\mathbf{F}}_{\mathbf{E}_R}^T & \bar{\mathbf{F}}_{\mathbf{E}_L}^T \end{bmatrix}^T \right\rangle_{Z_F(s)}$  and they are ordered as in (5.3). Out of these forces, the tangential components are used for the slip detection as in (5.1).

### 5.1.2 Measured foot acceleration

The slip force can be measured by mounting an accelerometer at the foot. Then, by using the foot mass  $m_f$  and the measured foot acceleration  $\ddot{\mathbf{p}} \equiv \begin{bmatrix} \ddot{p}_x & \ddot{p}_y \end{bmatrix}^T$ , the slip force is

$$\mathbf{F}_{slip} = m_f \ddot{\mathbf{p}} , \quad (5.18)$$

Hence, the foot slips whenever  $\ddot{p} > 0$ . Bearing in mind that the  $\mathbf{F}_t$  is measured using the force/torque sensor, the friction force is calculated from (5.1) and (5.18) as

$$\mathbf{F}_f = \mathbf{F}_t - m_f \ddot{\mathbf{p}} . \quad (5.19)$$

### 5.1.3 Measured friction and tangential forces

If the biped is equipped with contact force sensors at the foot soles and force/torque sensors at the ankles, then the measured  $\mathbf{F}_f$  and  $\mathbf{F}_t$  are used directly in (5.1) to detect the slip.

The obtained equations, i.e. (5.18) and (5.1), for the three discussed cases can be used for slip detection only. However, they can not be used alone to predict the slip due to the friction behavior. To overcome this challenge, a safety margin is introduced as shown later.

## 5.2 Slip prediction

The slip prediction is based on the friction behavior at the low speed. The friction behavior is explained in Section 2.1.1. For the non-slipping case,  $F_t$  must be in the static friction area where  $F_t < F_s$  as in Figure 5.2. Equivalently, the allowable force  $F_t$  such that the object is not slipping must be inside a cone with radius  $F_s$  and height  $F_N$  as in Figure 2.1.c.

However,  $F_s$  (or  $\mu_{static}$ ) changes with changing walking surfaces. Thus specifying a value for it limits the motion to one surface or to a limited number of surfaces. One more challenge originates from the friction behavior. Precisely, it is due to the fact that the kinetic friction is less than the static friction. This necessitates looking at the friction behavior in Figure 2.2. The main frictional components are the Coulomb friction  $F_c$ , Stribeck friction  $F_{st}$ , viscous friction  $F_v$  and  $F_s$ . Since the interest is in the slip prediction at low speed,  $F_v$  is out of scope. According to the friction behavior, the minimum friction force beyond which slip will be observed is  $F_c$ . This force is used in replace of  $F_s$  and thus overcome the aforementioned challenge. To cope with several surfaces,  $F_c$  is estimated online in an adaptive way. In this way the walking will not be limited to certain surfaces.

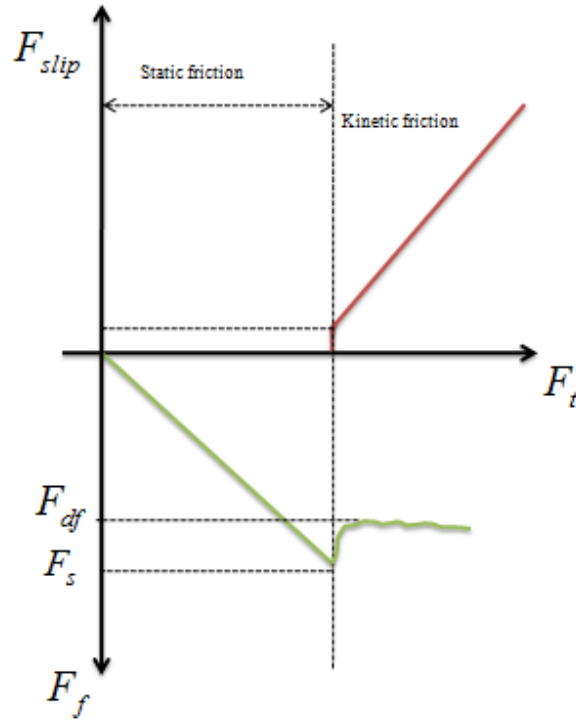


Figure 5.2: Static and kinetic friction

### 5.2.1 Slip prediction approach

The slip prediction approach for the two feet is the same. It is based on the estimated minimum friction value  $\hat{F}_c$  (or  $\hat{\mu}_c$ ) as a slip threshold. A safety margin with a value  $F_{ms}$  is introduced to design the slip predictor. Also, the proposed method defines a sufficient coefficient of friction  $\mu_{suf}$  with a sufficient friction force  $F_{suf} = \mu_{suf} F_N$  such that  $F_{suf} + F_{ms} \leq \hat{F}_c$ . Accordingly, the foot never slips if the inequality  $F_t \leq F_{suf}$  is satisfied as in Figure 5.3. The given safety margin leads to the simple slip prediction scheme: At each time instant  $k$ , if  $\mathbf{F}_{slip} = 0$  or  $\ddot{\mathbf{p}} = 0$ , then the object will not slip if  $F_t \leq F_{suf}$  or tends to slip if  $F_t \in (F_{suf}, \hat{F}_c = F_{suf} + F_{ms})$ , i.e.

$$\text{if } \begin{cases} F_{suf}(k) < F_t(k) < \hat{F}_c(k) & \text{tends to slip} \\ F_t(k) \leq F_{suf}(k) & \text{no slipping} \end{cases}, \quad (5.20)$$

However,  $\hat{F}_c$  still unknown. It is estimated online as discussed in the next section.

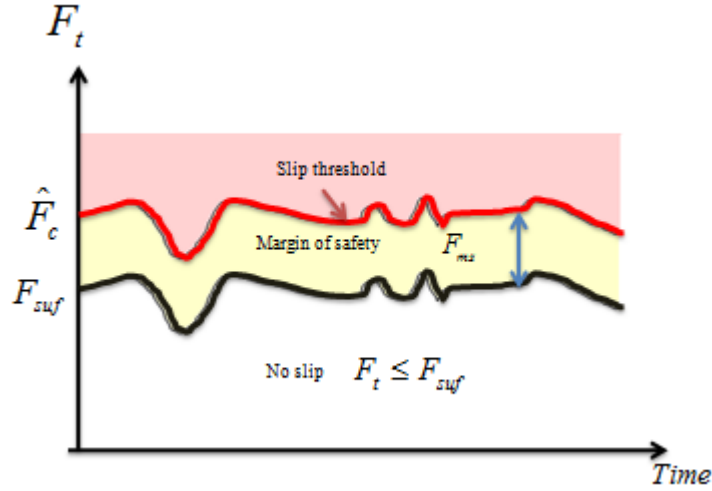


Figure 5.3: Slip prediction regions

### 5.2.2 Slip prediction threshold estimation

The threshold  $F_c$  estimation follows whether the foot is slipping or not based on (5.18) or  $\ddot{\mathbf{p}}=0$ . For the parameter estimation, we define  $\hat{F}_c$  and  $\hat{F}_s$  as the estimated variables. The estimation is done empirically without using models. The estimation steps are:

**Step 1:** Initialize  $F_s$ ,  $F_{st}$ ,  $F_{ms}$  and  $\hat{F}_c$

**Step 2:** Check whether the foot is in contact with the floor or not. If it is in contact go to step 3, else the variables are

$$\begin{aligned} \hat{F}_c(k) &= \hat{F}_c(k-1) \\ \hat{F}_s(k) &= \hat{F}_s(k-1) \\ \hat{F}_{st}(k) &= \hat{F}_{st}(k-1) \end{aligned} \quad (5.21)$$



**Step 3:** Check whether the foot is slipping or not.

**Step 4:** If it is not slipping, then the friction force is the same as the measured tangential force as in

$$F_f(k) = F_t(k), \quad (5.22)$$

and the estimated static friction  $\hat{F}_s$  is the maximum value of the friction. It is obtained by

$$\hat{F}_s(k) = \max\left(|F_f(k)|, |\hat{F}_s(k-1)|\right). \quad (5.23)$$

With the knowledge of  $\hat{F}_c(k-1)$ , the Coulomb friction is estimated as

$$\hat{F}_c(k) = \min\left(\hat{F}_s(k), \hat{F}_c(k-1)\right). \quad (5.24)$$

However, the friction force may exceed the threshold, i.e.  $|F_f(k)| > \hat{F}_c(k) + \hat{F}_{st}(k-1)$ . For this case, the Coulomb friction is calculated again as

$$\hat{F}_c(k) = \left| |F_f(k)| - \hat{F}_{st}(k-1) \right|. \quad (5.25)$$

The sufficient friction  $F_{suf}$  is calculated as

$$\begin{aligned} F_{suf}(k) &= \hat{F}_c(k) - F_{ms}, \\ F_{suf}(k) &\geq 0, \end{aligned} \quad (5.26)$$

**Step 5:** If the foot is slipping, then calculate  $\hat{F}_c$  as

$$\hat{F}_c(k) = \min\left(|F_f(k)|, |\hat{F}_c(k-1)|\right) \quad (5.27)$$

$\hat{F}_s$ ,  $\hat{F}_{st}$  and  $F_{suf}$  are obtained by

$$\hat{F}_s(k) = \hat{F}_s(k-1) \quad (5.28)$$

$$\begin{aligned} \hat{F}_{st}(k) &= \hat{F}_s(k-1) - \hat{F}_c(k), \\ \hat{F}_{st} &\geq 0 \end{aligned} \quad (5.29)$$

and

$$\begin{aligned} F_{suf}(k) &= \hat{F}_c(k) - F_{ms}, \\ F_{suf}(k) &\geq 0, \end{aligned} \quad (5.30)$$

respectively.

**Step 6:** Update the variables

$$\begin{aligned}
 \hat{F}_c(k-1) &= \hat{F}_c(k) \\
 \hat{F}_s(k-1) &= \hat{F}_s(k) \\
 \hat{F}_{st}(k-1) &= \hat{F}_{st}(k)
 \end{aligned} \tag{5.31}$$

**Step 7:** Go to step 2.

### 5.3 Experimental results

The proposed method is tested on SURALP. The results are shown for the right leg. The available measurements are from a six-axes force/torque sensor assembled at the ankle and from a three-axes accelerometer fixed at the foot. It is checked whether the foot is in contact with the ground or not using the measured normal force from the force/torque sensor.

As an implementation consideration, the accelerometer generates a reading even though the biped is not moving. Therefore, the slip is detected if the acceleration readings are larger than a threshold  $Tr$  (i.e. if  $\ddot{\mathbf{p}} \geq Tr$ ). This threshold depends on the initial accelerometer reading.

The estimated friction terms for the right foot in the  $x$ - direction are shown in Figure 5.4. This estimation is based on the experimentally observed  $Tr = 0.09$ . The repeated peaks pattern of the acceleration represents the leg when it is swinging, here there are four walking steps. The algorithm detects whether the foot is in contact or not and updates the variables accordingly. When the leg is swinging, the variables values are calculated as in (5.21). The estimated  $\hat{F}_s$  and  $\hat{F}_{st}$  are shown in Figure 5.4.c.  $\hat{F}_c$  and  $F_{suff}$  are presented in Figure 5.4.d. From the figure, the estimated friction terms are observed as:  $\hat{F}_s = 85N$ ,  $\hat{F}_{st} = 64N$ ,  $\hat{F}_c = 21N$  and  $F_{suff} = \hat{F}_c - 5 = 16N$  where  $F_{ms} = 5N$ .

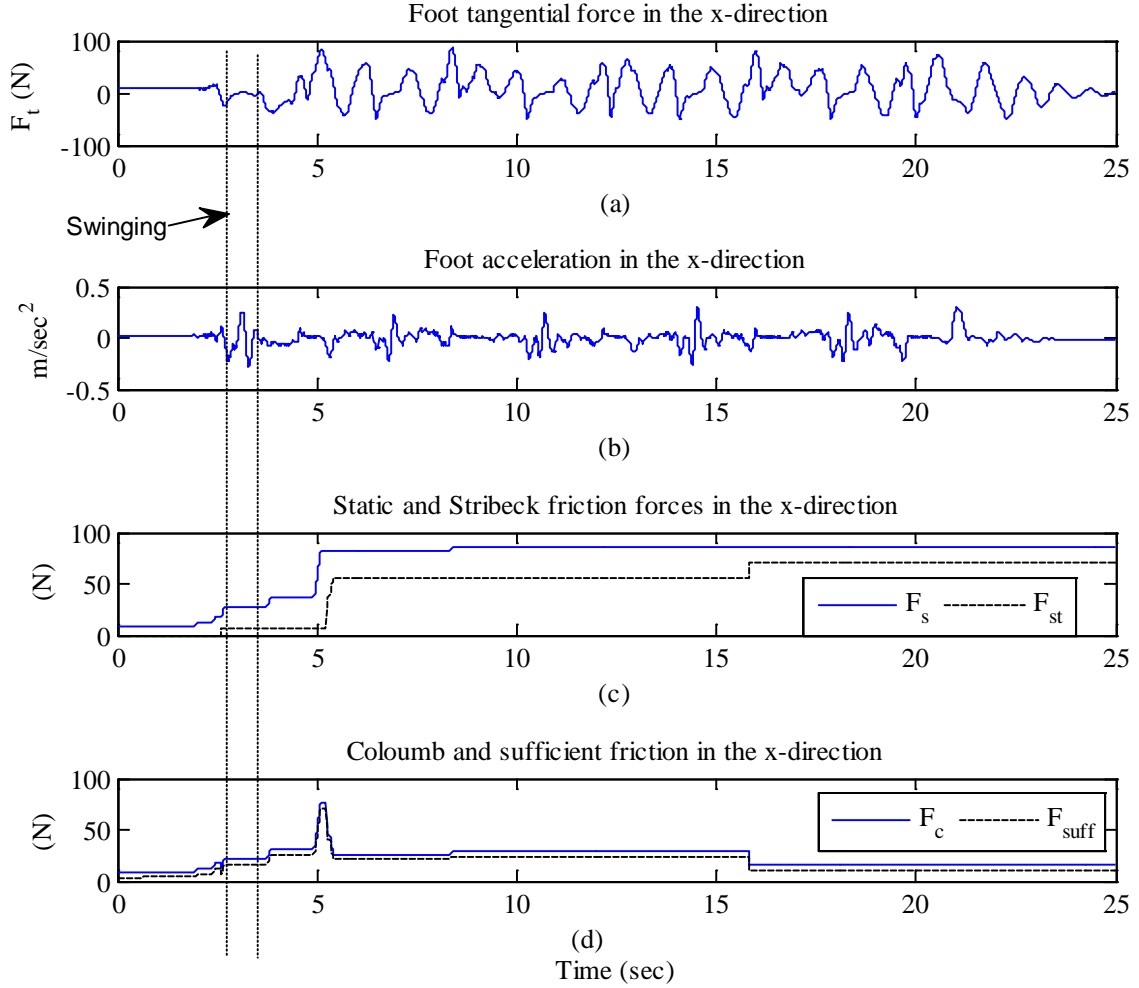


Figure 5.4: Friction parameter update in the  $x$  – direction

The estimated values are used for slip prediction. The test is carried on a new walk of SURALP, hence on new data. According to the algorithm and as shown in Figure 5.5.a, when  $|F_t| \geq |\hat{F}_c|$  then the foot is slipping, when  $|\hat{F}_{suff}| \leq |F_t| < |\hat{F}_c|$  then the foot tends to slip, and when  $|F_t| < |\hat{F}_{suff}|$  then the foot will not slip. The accelerometer is used to detect the actual slipping occurrence. The same  $Tr = 0.09$  is used as in Figure 5.5.b.

Slip prediction performance analysis:

- DS phase to LS phase: When the right foot starts leaving the ground so that the biped switches from DS to LS. At the transition period the algorithm detects the

slip. This is confirmed from the measured acceleration as shown in the beginning of swinging region in Figure 5.5.

- LS phase to DS phase: When the right foot starts landing so that the biped switches from LS to DS. At the transition period the algorithm detects the slip. This is confirmed from the measured acceleration as shown right after the swinging region in Figure 5.5.
- As observed from in Figure 5.5, the algorithm predicts and detects the slip. This is confirmed by the accelerometer readings. i.e. when the acceleration exceeds the threshold.
- False slip alarms: As mentioned before, the tangential force may exceed  $\hat{F}_c$  and still the foot is not slipping. Therefore, it is expected to have false slipping alarms. These alarms can be reduced by changing the threshold, i.e. use  $\hat{F}_c$  with a portion of  $\hat{F}_{st}$  instead of using  $\hat{F}_c$  alone. However, this may lead to false non slip deductions.
- The accuracy of the prediction depends on the accuracy of the measurements and thresholds. A very small acceleration threshold leads to a very small  $\hat{F}_c$  which will result in slip detection all time. On the other hand, a large acceleration threshold leads to missing the slip detection.
- A statistical summary of Figure 5.5 is listed in Table 3.
  - When the foot is slipping, the slip estimation accuracy is 74%. False non-slipping alarms and tending to slip condition have percentages of 5% and 21% respectively.
  - On the other hand, when the foot is not slipping, the algorithm accuracy is 59%. False non-slipping alarms and tending to slip condition have percentages of 37% and 4% respectively.
  - This work assumes that there will be a controller to prevent slipping and compensate for the slip occurrence. Accordingly, the controller utilization percentage is 54%.

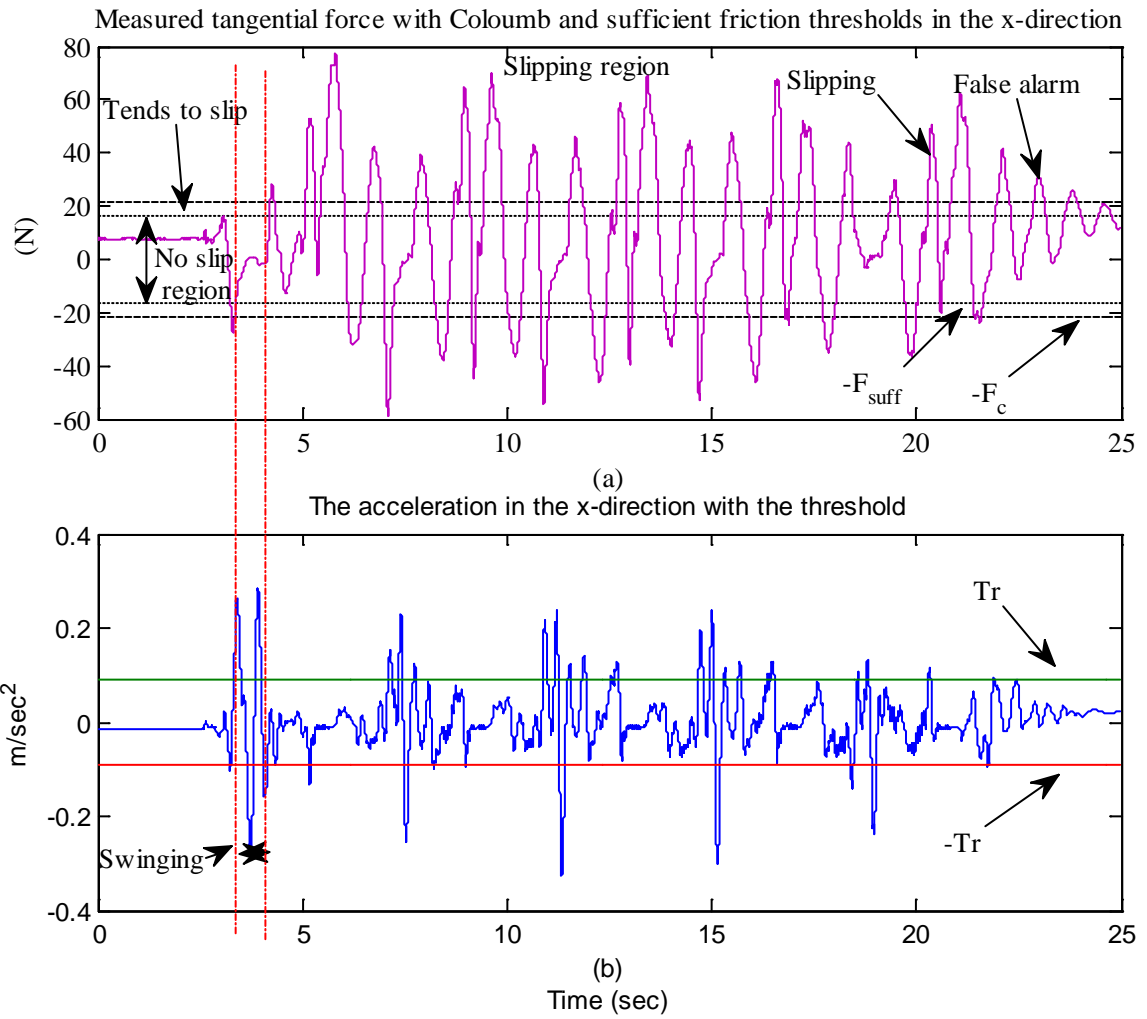


Figure 5.5: Slip prediction test in the  $x$  – direction

Table 3: A statistical summary of Figure 5.5

Estimated \ True	Non slipping	Slipping	Tends to slip
Non slipping	37	23	3
Slipping	1	14	4

## 5.4 Conclusion

A novel measurement-based method for online friction estimation is proposed. Based on the friction behavior, the Coulomb, Stribeck and static friction terms between the foot sole and the contact surface are estimated adaptively. The estimation is based on acceleration and force measurements. The Coulomb friction is used as a threshold for slip detection. To predict the slip occurrence, a margin of safety with Coulomb friction is considered. Whenever the measured force enters this margin, then the foot is going to slip. Experimental results demonstrate the applicability of the proposed method. The accuracy of the algorithm depends on the selected thresholds. Further, while low acceleration thresholds increase the false slipping alarms, high acceleration thresholds increase the false non-slipping alarms.

## Chapter 6

### 6 Conclusion and Future work

A method to estimate the center of mass CoM position and its derivative and the disturbance effects on a walking biped robot is proposed. The method utilizes the robot body acceleration and the reactions forces at the robot feet. An AKF is employed for the states estimation based on the Linear Inverted Pendulum Model LIPM.

The LIPM is written in two state space forms: Form 1 and form 2. The former is well known. The latter is introduced in this thesis to estimate the CoM variables in the presence of modeling errors, compensate for the modeling errors and estimate them. Two types of disturbances are estimated, modeling errors and external accelerations. The results show that Form 2 fails when there exists an external acceleration. On the other hand, form 1 fails when there are modeling errors in the measured  $\mathbf{p}_{ZMP}^{F_N}$ .

A Novel method (FBSE) for the joint friction estimation of non-slipping walking biped robots is proposed. The proposed approach combines a measurement-based strategy with an adaptive model-based approach to estimate the joint friction. The former is used to estimate the joint friction online when the foot is in contact with the ground, while the latter adopts a friction model to represent the joint friction when the leg is swinging. To achieve this estimation, the joint angular accelerations are either estimated online using the non-slipping foot constraint or their computation is avoided by filtering the model.

The measurement-based strategy utilizes the measured ground reaction forces and the readings of an inertial measurement unit IMU located at the robot body. Based on these measurements, the body attitude and velocity are estimated.

The aforementioned measurements and estimates are used in a reduced dynamical model of the biped. However, when the leg is swinging, this strategy is inapplicable. Therefore, a friction model is adopted. Its parameters are identified adaptively using the estimated online friction whenever the foot is in contact. The results show that the estimated friction tracks the true one. Furthermore, using the FBSE method in the feedback torque signal improves the position response.

A new measurement-based method for slip prediction of walking biped robots is proposed. This method is based on the foot acceleration and ankle force measurements. First, the aforementioned measurements are used for slip detection. Then, based on the friction behavior, an adaptive algorithm is developed to estimate the Coulomb, Stribeck and static friction terms between the foot sole and the contact surface adaptively. This algorithm updates the friction terms based on the measurements and whether slip is detected or not. According to the friction behavior, the minimum friction force beyond which slip will be observed is the Coulomb friction. Therefore, the estimated Coulomb friction is used as a threshold for slip detection. For slip prediction, a margin of safety is introduced in the negative vicinity of the estimated Coulomb friction. The estimation algorithm concludes that when the applied force enters the safety margin, then the foot tends to slip.

The accuracy of the algorithm depends on the selected thresholds. Further, while low acceleration thresholds increase the false slipping alarms, high acceleration thresholds increase the false non-slipping alarms.

The contributions of this thesis are:

- A new state space form for the LIPM is introduced where the measurements are force and acceleration. This form estimates the CoM variables in the presence of modeling errors, compensates for the modeling error and estimates it.
- A novel FBSE method for estimating the joint friction of walking bipeds is proposed. It utilizes the readings of an IMU and foot contact reaction forces into a reduced model



of the biped. It combines a measurement-based strategy with an adaptive model-based method to estimate the joint friction. Using the FBSE method in the control loop improves the position response.

- An adaptive measurement-based online algorithm for slip prediction is proposed. First, it estimates the friction between the feet and the contact surface. Then, the estimated Coulomb friction is used as a threshold for slip detection. Finally, this algorithm predicts the slip occurrence by introducing a safety margin in the negative vicinity of the estimated Coulomb friction to define a slip risk band. Hence, the foot will not slip whenever the force is below this band. If the applied force is within the safety margin, then the foot tends to slip

As a future work, the followings are suggested

- Design a control law that can handle the modeling errors in the *ZMP* and acceleration measurements. Further, an integration methodology of the two state space forms of the LIPM is required to overcome their drawbacks.
- In this thesis, the slip is predicted only. A control action is required in case of predicted slip. A controller has to be designed so that the applied force is within the safety region.
- The estimated CoM variables and the computed forces at the feet can be used to increase the redundancy of the position and force measurements. A fault-detection and isolation scheme would be necessary to detect the faulty sensors and compensate for the faults.

## 7 References

- [1] H. Hirukawa, "Walking biped humanoids that perform manual labour," *Philos Trans A Math Phys Eng Sci*, vol. 365, pp. 65-77, Jan 15 2007.
- [2] T. Nishiyama, H. Hoshino, K. Sawada, A. Baba, T. Sekine, W. Yamada, A. Terasawa, R. Nakajima, Y. Tokunaga, and M. Yoneda, "Communication agent embedded in humanoid robot," in *SICE Annual Conference*, 2003, pp. 1514-1519 Vol.2.
- [3] M. H. Raibert and E. R. Tello, "Legged Robots That Balance," *IEEE Expert*, vol. 1, pp. 89-89, 1986.
- [4] M. Koeda, Y. Uda, S. Sugiyama, and T. Yoshikawa, "Shuffle turn and translation of humanoid robots," in *IEEE International Conference on Robotics and Automation (ICRA)*, 2011, pp. 593-598.
- [5] K. Miura, S. Nakaoka, M. Morisawa, F. Kanehiro, K. Harada, and S. Kajita, "Analysis on a friction based "Twirl" for biped robots," in *IEEE International Conference on Robotics and Automation (ICRA)*, 2010, pp. 4249-4255.
- [6] S. Kajita, M. Morisawa, K. Miura, S. Nakaoka, K. Harada, K. Kaneko, F. Kanehiro, and K. Yokoi, "Biped walking stabilization based on linear inverted pendulum tracking," in *IEEE/RSJ International Conference on Intelligent Robots and Systems (IROS)*, 2010, pp. 4489-4496.
- [7] T. Liu, Y. Inoue, and K. Shibata, "A wearable ground reaction force sensor system and its application to the measurement of extrinsic gait variability," *Sensors*, vol. 10, pp. 10240-10255, 2010.

- [8] U. Seven, T. Akbas, K. Fidan, and K. Erbatur, "Bipedal robot walking control on inclined planes by fuzzy reference trajectory modification," *Soft Computing*, pp. 1-18, 2012.
- [9] S.-J. Yi, B.-T. Zhang, D. Hong, and D. D. Lee, "Practical bipedal walking control on uneven terrain using surface learning and push recovery," in *IEEE/RSJ International Conference on Intelligent Robots and Systems (IROS)*, 2011, pp. 3963-3968.
- [10] K. Yeoun-Jae, L. Joon-Yong, and L. Ju-Jang, "A balance control strategy of a walking biped robot in an externally applied force," in *International Conference on Information and Automation (ICIA)*, 2012, pp. 572-577.
- [11] J. P. Ferreira, M. M. Crisostomo, and A. P. Coimbra, "Human Gait Acquisition and Characterization," *IEEE Transactions on Instrumentation and Measurement*, vol. 58, pp. 2979-2988, 2009.
- [12] B. Siciliano and O. Khatib, *Springer Handbook of Robotics*: Springer-Verlag New York, Inc., 2007.
- [13] R. H. Hensen, M. Van de Molengraft, and M. Steinbuch, "Friction induced hunting limit cycles: A comparison between the LuGre and switch friction model," *Automatica*, vol. 39, pp. 2131-2137, 2003.
- [14] R. H. Hensen and M. J. van de Molengraft, "Friction induced hunting limit cycles: an event mapping approach," in *Proceedings of the American Control Conference*, 2002, pp. 2267-2272.
- [15] H. Olsson and K. J. Astrom, "Friction generated limit cycles," *IEEE Transactions on Control Systems Technology*, vol. 9, pp. 629-636, 2001.
- [16] B. Bona and M. Indri, "Friction Compensation in Robotics: an Overview," in *IEEE European Control Conference on Decision and Control*, 2005, pp. 4360-4367.
- [17] F. Jatta, R. Adamini, A. Visioli, and G. Legnani, "Hybrid force/velocity robot contour tracking: an experimental analysis of friction compensation strategies," in

- IEEE International Conference on Robotics and Automation*, 2002, pp. 1723-1728 vol.2.
- [18] K. Erbatur and O. Kurt, "Natural ZMP Trajectories for Biped Robot Reference Generation," *IEEE Transactions on Industrial Electronics*, vol. 56, pp. 835-845, Mar 2009.
- [19] M. Vukobratovi'c and B. Borovac, "Zero-moment point -thirty five years of its life," *International Journal of Humanoid Robotics (IJHR)*, vol. 01, pp. 157-173, 2004.
- [20] H. Hirukawa, S. Hattori, K. Harada, S. Kajita, K. Kaneko, F. Kanehiro, K. Fujiwara, and M. Morisawa, "A universal stability criterion of the foot contact of legged robots - adios ZMP," in *Proceedings of the IEEE International Conference on Robotics and Automation*, 2006, pp. 1976-1983.
- [21] B. J. Stephens and C. G. Atkeson, "Dynamic Balance Force Control for compliant humanoid robots," in *IEEE/RSJ International Conference on Intelligent Robots and Systems (IROS)*, 2010 pp. 1248-1255.
- [22] C. Yang and Q. Wu, "Effects of gravity and friction constraints on bipedal balance control," in *Control Applications, 2005. CCA 2005. Proceedings of 2005 IEEE Conference on*, 2005, pp. 1093-1098.
- [23] C. Makkar, W. E. Dixon, W. G. Sawyer, and G. Hu, "A new continuously differentiable friction model for control systems design," in *IEEE/ASME International Conference on Advanced Intelligent Mechatronics. Proceedings*, 2005, pp. 600-605.
- [24] D. Vischer and O. Khatib, "Design and development of high-performance torque-controlled joints," *IEEE Transactions on Robotics and Automation*, vol. 11, pp. 537-544, 1995.
- [25] L. E. Pfeiffer, O. Khatib, and J. Hake, "Joint torque sensory feedback in the control of a PUMA manipulator," *IEEE Transactions on Robotics and Automation*, vol. 5, pp. 418-425, 1989.

- [26] K. Erbatur, U. Seven, E. Taskiran, O. Koca, M. Yilmaz, M. Unel, G. Kiziltas, A. Sabanovic, and A. Onat, "SURALP: A New Full-Body Humanoid Robot Platform," in *IEEE-Rsj International Conference on Intelligent Robots and Systems*, New York, 2009, pp. 4949-4954.
- [27] B. Ugurlu, T. Kawasaki, M. Kawanishi, and T. Narikiyo, "Continuous and dynamically equilibrated one-legged running experiments: Motion generation and indirect force feedback control," in *Intelligent Robots and Systems (IROS), 2012 IEEE/RSJ International Conference on*, 2012, pp. 1846-1852.
- [28] B. Ugurlu, J. A. Saglia, N. G. Tsagarakis, S. Morfey, and D. G. Caldwell, "Bipedal Hopping Pattern Generation for Passively Compliant Humanoids: Exploiting the Resonance," *Industrial Electronics, IEEE Transactions on*, vol. 61, pp. 5431-5443, 2014.
- [29] K. Joohyung, K. Hoseong, L. Heekuk, S. Keehong, L. Bokman, L. Minhyung, L. Jusuk, and R. Kyungsik, "Balancing control of a biped robot," in *IEEE International Conference on Systems, Man, and Cybernetics (SMC)*, 2012, pp. 2756-2761.
- [30] T. Yoshikawa and O. Khatib, "Compliant humanoid robot control by the torque transformer," in *IEEE/RSJ International Conference on Intelligent Robots and Systems (IROS)*, 2009, pp. 3011-3018.
- [31] D. Xing, J. Su, Y. Liu, and J. Zhong, "Robust approach for humanoid joint control based on a disturbance observer," *Control Theory & Applications, IET*, vol. 5, pp. 1630-1636, 2011.
- [32] H. Yan, B. Vanderborght, R. Van Ham, W. Qining, M. Van Damme, X. Guangming, and D. Lefeber, "Step Length and Velocity Control of a Dynamic Bipedal Walking Robot With Adaptable Compliant Joints," *IEEE/ASME Transactions on Mechatronics*, vol. 18, pp. 598-611, 2013.
- [33] P. van Zutven, D. Kostic, and H. Nijmeijer, "Foot placement for planar bipeds with point feet," in *IEEE International Conference on Robotics and Automation (ICRA)*, 2012, pp. 983-988.

- [34] T. Hase, H. Qingjiu, and C. Xuedong, "Performance analysis of biped walking robot with circular feet using optimal trajectory planning method," in *IEEE International Conference on Robotics and Biomimetics*, 2009, pp. 143-148.
- [35] K. Miyahara, Y. Harada, D. N. Nenchev, and D. Sato, "Three-dimensional Limit Cycle Walking with joint actuation," in *IEEE/RSJ International Conference on Intelligent Robots and Systems (IROS)*, 2009, pp. 4445-4450.
- [36] B. Armstrong-Hélouvry, P. Dupont, and C. C. De Wit, "A survey of models, analysis tools and compensation methods for the control of machines with friction," *Automatica*, vol. 30, pp. 1083-1138, 1994.
- [37] R. H. A. Hellsen, G. Z. Angelis, M. J. G. van de Molengraft, A. G. de Jager, and J. J. Kok, "Grey-box Modeling of Friction: An Experimental Case-study," *European Journal of Control*, vol. 6, pp. 258-267, 2000.
- [38] W. Shang, S. Cong, and Y. Zhang, "Nonlinear friction compensation of a 2-DOF planar parallel manipulator," *Mechatronics*, vol. 18, pp. 340-346, 2008.
- [39] R. H. A. Hensen, M. J. G. Van de Molengraft, and M. Steinbuch, "Frequency domain identification of dynamic friction model parameters," *IEEE Transactions on Control Systems Technology*, vol. 10, pp. 191-196, 2002.
- [40] J. Moreno and R. Kelly, "Manipulator velocity field control with dynamic friction compensation," in *IEEE Conference on Decision and Control*, 2003, pp. 3834-3839 vol.4.
- [41] J. Moreno, R. Kelly, and R. Campa, "Manipulator velocity control using friction compensation," *IEE Proceedings- Control Theory and Applications*, vol. 150, pp. 119-126, 2003.
- [42] D. Kostic, B. de Jager, M. Steinbuch, and R. Hensen, "Modeling and identification for high-performance robot control: an RRR-robotic arm case study," *IEEE Transactions on Control Systems Technology*, vol. 12, pp. 904-919, 2004.

- [43] G. Morel, K. Iagnemma, and S. Dubowsky, "The precise control of manipulators with high joint-friction using base force/torque sensing," *Automatica*, vol. 36, pp. 931-941, 2000.
- [44] S. Grami and Y. Gharbia, "GMS friction compensation in robot manipulator," in *Conference of the IEEE on Industrial Electronics Society (IECON)*, 2013, pp. 3555-3560.
- [45] Z. Dongdong, N. Jing, R. Xuemei, G. Herrmann, and S. Longo, "Adaptive control of robotic servo system with friction compensation," in *IEEE Conference on Robotics, Automation and Mechatronics (RAM)*, 2011, pp. 285-290.
- [46] L. R. Ray, A. Ramasubramanian, and J. Townsend, "Adaptive friction compensation using extended Kalman–Bucy filter friction estimation," *Control Engineering Practice*, vol. 9, pp. 169-179, 2001.
- [47] P. Vedagarbha, D. M. Dawson, and M. Feemster, "Tracking control of mechanical systems in the presence of nonlinear dynamic friction effects," *IEEE Transactions on Control Systems Technology*, vol. 7, pp. 446-456, 1999.
- [48] B. Friedland and Y. J. Park, "On adaptive friction compensation," *IEEE Transactions on Automatic Control*, vol. 37, pp. 1609-1612, 1992.
- [49] A. Mohammadi, M. Tavakoli, H. J. Marquez, and F. Hashemzadeh, "Nonlinear disturbance observer design for robotic manipulators," *Control Engineering Practice*, vol. 21, pp. 253-267, 2013.
- [50] C. Wen-Hua, D. J. Ballance, P. J. Gawthrop, and J. O'Reilly, "A nonlinear disturbance observer for robotic manipulators," *IEEE Transactions on Industrial Electronics*, vol. 47, pp. 932-938, 2000.
- [51] J.-H. Ryu, J. Song, and D.-S. Kwon, "A nonlinear friction compensation method using adaptive control and its practical application to an in-parallel actuated 6-DOF manipulator," *Control Engineering Practice*, vol. 9, pp. 159-167, 2001.

- [52] B. Armstrong, D. Neevel, and T. Kusik, "New results in NPID control: Tracking, integral control, friction compensation and experimental results," *IEEE Transactions on Control Systems Technology*, vol. 9, pp. 399-406, 2001.
- [53] V. Lampaert, J. Swevers, and F. Al-Bender, "Comparison of model and non-model based friction compensation techniques in the neighbourhood of pre-sliding friction," in *Proceedings of the American Control Conference*, 2004, pp. 1121-1126 vol.2.
- [54] S. N. Huang, K. K. Tan, and T. H. Lee, "Adaptive friction compensation using neural network approximations," *IEEE Transactions on Systems, Man, and Cybernetics, Part C: Applications and Reviews*, vol. 30, pp. 551-557, 2000.
- [55] V. Vitiello and A. Tornambe, "Adaptive compensation of modeled friction using a RBF neural network approximation," in *IEEE Conference on Decision and Control*, 2007, pp. 4699-4704.
- [56] Y. H. Kim and F. L. Lewis, "Reinforcement adaptive learning neural network based friction compensation for high speed and precision," in *Proceedings of the IEEE Conference on Decision and Control*, 1998, pp. 1064-1069 vol.1.
- [57] G. L. Wang, Y. F. Li, and D. X. Bi, "Support Vector Networks in Adaptive Friction Compensation," *IEEE Transactions on Neural Networks*, vol. 18, pp. 1209-1219, 2007.
- [58] Y. F. Wang, D. H. Wang, and T. Y. Chai, "Modeling and control compensation of nonlinear friction using adaptive fuzzy systems," *Mechanical Systems and Signal Processing*, vol. 23, pp. 2445-2457, 2009.
- [59] L. Mostefai, M. Denai, S. Oh, and Y. Hori, "Optimal Control Design for Robust Fuzzy Friction Compensation in a Robot Joint," *IEEE Transactions on Industrial Electronics*, vol. 56, pp. 3832-3839, 2009.
- [60] W. Yongfu, W. Dianhui, and C. Tianyou, "Extraction and Adaptation of Fuzzy Rules for Friction Modeling and Control Compensation," *IEEE Transactions on Fuzzy Systems*, vol. 19, pp. 682-693, 2011.



- [61] D. Velez-Diaz and T. Yu, "Adaptive robust fuzzy control of nonlinear systems," *IEEE Transactions on Systems, Man, and Cybernetics, Part B: Cybernetics*, vol. 34, pp. 1596-1601, 2004.
- [62] M. A. Llama, R. Kelly, and V. Santibanez, "Stable computed-torque control of robot manipulators via fuzzy self-tuning," *IEEE Transactions on Systems, Man, and Cybernetics, Part B: Cybernetics*, vol. 30, pp. 143-150, 2000.
- [63] K. Shiev, N. Shakev, A. V. Topalov, and S. Ahmed, "Trajectory control of manipulators using type-2 fuzzy neural friction and disturbance compensator," in *IEEE International Conference Intelligent Systems (IS)*, 2012, pp. 324-329.
- [64] R. J. Patton, D. Putra, and S. Klinkhieo, "Friction compensation as a fault-tolerant control problem," *International Journal of Systems Science*, vol. 41, pp. 987-1001, 2010.
- [65] B. Stephens and C. Atkeson, "Modeling and control of periodic humanoid balance using the Linear Biped Model," in *IEEE-RAS International Conference on Humanoid Robots*, 2009, pp. 379-384.
- [66] G. Kinoshita, T. Kimura, and M. Shimojo, "Dynamic sensing experiments of reaction force distributions on the sole of a walking humanoid robot," in *Proceedings of International Conference on Intelligent Robots and Systems*, 2003, pp. 1413-1418.
- [67] K. Nishiwaki, Y. Murakami, S. Kagami, Y. Kuniyoshi, M. Inaba, and H. Inoue, "A six-axis force sensor with parallel support mechanism to measure the ground reaction force of humanoid robot," in *Proceedings of IEEE International Conference on Robotics and Automation*, 2002, pp. 2277-2282.
- [68] L. Sentis and O. Khatib, "A whole-body control framework for humanoids operating in human environments," in *Robotics and Automation, 2006. ICRA 2006. Proceedings 2006 IEEE International Conference on*, 2006, pp. 2641-2648.
- [69] S. Kajita, F. Kanehiro, K. Kaneko, K. Fujiwara, K. Harada, K. Yokoi, and H. Hirukawa, "Biped walking pattern generation by using preview control of zero-

- moment point," in *Proceedings of IEEE International Conference on Robotics and Automation ICRA*, 2003, pp. 1620-1626 vol.2.
- [70] B. Ugurlu, J. A. Saglia, N. G. Tsagarakis, and D. G. Caldwell, "Hopping at the resonance frequency: A trajectory generation technique for bipedal robots with elastic joints," in *Robotics and Automation (ICRA), 2012 IEEE International Conference on*, 2012, pp. 1436-1443.
- [71] P. B. Wieber, "Viability and predictive control for safe locomotion," in *Intelligent Robots and Systems, 2008. IROS 2008. IEEE/RSJ International Conference on*, 2008, pp. 1103-1108.
- [72] S. Kajita, K. Kaneko, K. Harada, F. Kanehiro, K. Fujiwara, and H. Hirukawa, "Biped walking on a low friction floor," in *Intelligent Robots and Systems, 2004.(IROS 2004). Proceedings. 2004 IEEE/RSJ International Conference on*, 2004, pp. 3546-3552.
- [73] C. A. Klein and S. Kittivatcharapong, "Optimal force distribution for the legs of a walking machine with friction cone constraints," *Robotics and Automation, IEEE Transactions on*, vol. 6, pp. 73-85, 1990.
- [74] C. Zhu and A. Kawamura, "What Is the Real Frictional Constraint in Biped Walking?-Discussion on Frictional Slip with Rotation," in *Intelligent Robots and Systems, 2006 IEEE/RSJ International Conference on*, 2006, pp. 5762-5768.
- [75] H. Yamamoto and K. Ohnishi, "An approach to stable walking on unknown slippery floor for biped robot," in *Industrial Electronics Society, 2001. IECON '01. The 27th Annual Conference of the IEEE*, 2001, pp. 1728-1733 vol.3.
- [76] K. Kaneko, F. Kanehiro, S. Kajita, M. Morisawa, K. Fujiwara, K. Harada, and H. Hirukawa, "Slip observer for walking on a low friction floor," in *Intelligent Robots and Systems, 2005. (IROS 2005). 2005 IEEE/RSJ International Conference on*, 2005, pp. 634-640.
- [77] H. Takemura, M. Deguchi, J. Ueda, Y. Matsumoto, and T. Ogasawara, "Slip-adaptive walk of quadruped robot," *Robotics and Autonomous Systems*, vol. 53, pp. 124-141, 11/30/ 2005.

- [78] H. Onodera, T. Yamaguchi, H. Yamanouchi, K. Nagamori, M. Yano, Y. Hirata, and K. Hokkirigawa, "Analysis of the slip-related falls and fall prevention with an intelligent shoe system," in *Biomedical Robotics and Biomechatronics (BioRob), 2010 3rd IEEE RAS and EMBS International Conference on*, 2010, pp. 616-620.
- [79] L. S. Lincoln and S. J. M. Bamberg, "Insole sensor system for real-time detection of biped slip," in *Engineering in Medicine and Biology Society (EMBC), 2010 Annual International Conference of the IEEE*, 2010, pp. 1449-1452.
- [80] F. Cordes, S. Bartsch, T. Birnschein, D. Kuehn, and F. Kirchner, "Towards an Intelligent Foot for Walking and Climbing Robots," in *Robotics (ISR), 2010 41st International Symposium on and 2010 6th German Conference on Robotics (ROBOTIK)*, 2010, pp. 1-8.
- [81] N. Okita and H. Sommer, "A novel foot slip detection algorithm using unscented Kalman filter innovation," in *American Control Conference (ACC), 2012*, pp. 5163-5168.
- [82] S. Roosen, "Ground-Contact Friction Estimation and Slip Prevention in Bipedal Robots," in *Mechanical Engineering*. vol. Master: UNIVERSITY OF MELBOURNE, 2012.
- [83] C. J. Tsaprounis and N. A. Aspragathos, "A linear differential formulation of friction forces for adaptive estimator algorithms," *Robotica*, vol. 19, pp. 407-421, 2001.
- [84] S. I. Han and K. S. Lee, "Robust friction state observer and recurrent fuzzy neural network design for dynamic friction compensation with backstepping control," *Mechatronics*, vol. 20, pp. 384-401, 2010.
- [85] S. Kajita and K. Tani, "Study of dynamic biped locomotion on rugged terrain-derivation and application of the linear inverted pendulum mode," in *Proceedings of IEEE International Conference on Robotics and Automation*, 1991, pp. 1405-1411 vol.2.
- [86] M. Van Damme, P. Beyl, B. Vanderborght, V. Grosu, R. Van Ham, I. Vanderniepen, A. Matthys, and D. Lefeber, "Estimating robot end-effector force

- from noisy actuator torque measurements," in *IEEE International Conference on Robotics and Automation (ICRA)*, 2011, pp. 1108-1113.
- [87] P. Dahl, "A solid friction model," DTIC Document1968.
- [88] C. C. de Wit, H. Olsson, K. J. Astrom, and P. Lischinsky, "A new model for control of systems with friction," *Automatic Control, IEEE Transactions on*, vol. 40, pp. 419-425, 1995.
- [89] J. Swevers, F. Al-Bender, C. G. Ganseman, and T. Projogo, "An integrated friction model structure with improved presliding behavior for accurate friction compensation," *Automatic Control, IEEE Transactions on*, vol. 45, pp. 675-686, 2000.
- [90] V. Lampaert, J. Swevers, and F. Al-Bender, "Modification of the Leuven integrated friction model structure," *IEEE Transactions on Automatic Control*, vol. 47, pp. 683-687, 2002.
- [91] L. Ljung, *System Identification: Theory for the User*, 2nd ed. Upper Saddle River, NJ: Prentice-Hall PTR, 1999.
- [92] G. Hughes-Hallett, McCallum et al., *Calculus single and multivariable*, 6th ed.: John Wiley & Sons, Inc, 2009.
- [93] M. S. Grewal and A. P. Andrews, *Kalman Filtering: Theory and Practice Using MATLAB*, 2nd ed. New York, NY, USA: John Wiley & Sons, 2001.
- [94] D. Simon, *Optimal State Estimation: Kalman, H Infinity, and Nonlinear Approaches*. Hoboken, New Jersey, USA: Wiley & Sons, 2006.
- [95] P. S. Maybeck, *Stochastic models, estimation and control* vol. 3. New York, NY, USA: Academic Press, 1982.
- [96] H. Heffes, "The effect of erroneous models on the Kalman filter response," *IEEE Transactions on Automatic Control*, vol. 11, pp. 541-543, 1966.
- [97] R. J. Fitzgerald, "Divergence of the Kalman filter," *IEEE Transactions on Automatic Control*, vol. 16, pp. 736-747, 1971.

- [98] M. Karasalo and X. Hu, "An optimization approach to adaptive Kalman filtering," *Automatica*, vol. 47, pp. 1785-1793, 2011.
- [99] I. Hashlamon and K. Erbatur, "An improved real-time adaptive Kalman filter with recursive noise covariance updating rules," *Turkish journal of electrical engineering & computer sciences*, accepted, 2013.
- [100] I. Hashlamon and K. Erbatur, "Experimental verification of an orientation estimation technique for autonomous robotic platforms." vol. Master degree thesis Istanbul: Sabanci University, 2010.
- [101] K. Erbatur and U. Seven, "Humanoid gait synthesis with moving single support ZMP trajectories," in *Proceedings of the 13th Iasted International Conference on Robotics and Applications/Proceedings of the Iasted International Conference on Telematics*, K. Schilling, Ed. Anaheim: Acta Press Anaheim, 2007, pp. 95-100.
- [102] I. Hur, Y. Matsuki, N. Tomokuni, J. Huang, and T. Yabuta, "Standing Stability of Surfing Robot without Force Sensor," in *the 25th Annual Conference of the Robotics Society of Japan, 3H11*, 2007.
- [103] B. J. Stephens, "State estimation for force-controlled humanoid balance using simple models in the presence of modeling error," in *IEEE International Conference on Robotics and Automation*, 2011, pp. 3994-3999.
- [104] I. Hashlamon and K. Erbatur, "Center of Mass States and Disturbance Estimation for a Walking Biped " in *IEEE International Conference on Mechatronics, ICM 2013*, Vicenza (ITALY) . 2013, pp. 248-253.
- [105] K. Erbatur and A. Kawamura, "A new penalty based contact modeling and dynamics simulation method as applied to biped walking robots," in *Proc. FIRA World Congress*, Vienna, Austria, 2003.
- [106] P. Hsu, M. Bodson, S. Sastry, and B. Paden, "Adaptive identification and control for manipulators without using joint accelerations," in *Proceedings IEEE International Conference on Robotics and Automation*, 1987, pp. 1210-1215.

- [107] V. van Geffen, "A study of friction models and friction Compensation," *DCT*, vol. 118, p. 24.